(12) LEVEL III

AD

AD-E400 301

AD A068504

CONTRACTOR REPORT ARLCD-CR-79004

BLAST CAPACITY EVALUATION OF PRE-ENGINEERED BUILDING

WILLIAM STEA
NORVAL DOBBS
SAMUEL WEISSMAN
AMMANN AND WHITNEY
NEW YORK, N. Y.

PAUL PRICE, PROJECT LEADER
JOSEPH CALTAGIRONE, PROJECT ENGINEER
ARRADCOM, DOVER, N. J.

MARCH 1979

US ARMY ARMAMENT RESEARCH AND DEVELOPMENT COMMAND
LARGE CALIBER
WEAPON SYSTEMS LABORATORY
DOVER, NEW JERSEY

The views, opinions, and/or findings contained in this report are those of the author(s) and should not be construed as an official Department of the Army position, policy or decision, unless so designated by other documentation.

Destroy this report when no longer needed. Do not return to the originator.

The citation in this report of the names of commercial firms or commercially available products or services does not constitute official endorsement or approval of such commercial firms, products, or services by the United States Government.

UNCLASSIFIED
SECURITY CLASSIFICATION OF THIS PAGE (When Data Entered)

REPORT DOCUMENTATION PAGE

READ INSTRUCTIONS BEFORE COMPLETING FORM

1. REPORT NUMBER: Contractor Report ARLCD-CR-79004
2. GOVT ACCESSION NO.:
3. RECIPIENT'S CATALOG NUMBER:

4. TITLE (and Subtitle): BLAST CAPACITY EVALUATION OF PRE-ENGINEERED BUILDING
5. TYPE OF REPORT & PERIOD COVERED: Final Report
6. PERFORMING ORG. REPORT NUMBER:

7. AUTHOR(s): William Stea, Norval Dobbs, and Samuel Weissman
Ammann and Whitney
Paul Price, Project Leader, ARRADCOM
Joseph Caltagirone, Project Engineer, ARRADCOM
8. CONTRACT OR GRANT NUMBER(s): DAAK-10-77-C-0134

9. PERFORMING ORGANIZATION NAME AND ADDRESS:
Ammann and Whitney, Consulting Engineers
Two World Trade Center
New York, NY 10048
10. PROGRAM ELEMENT, PROJECT, TASK AREA & WORK UNIT NUMBERS: MMT-5774291

11. CONTROLLING OFFICE NAME AND ADDRESS:
ARRADCOM, TSD
ATTN: STINFO (DRDAR-TSS)
Dover, NJ 07801
12. REPORT DATE: March 1979
13. NUMBER OF PAGES: 142

14. MONITORING AGENCY NAME & ADDRESS (if different from Controlling Office):
ARRADCOM, LCWSL
ATTN: MTD (DRDAR-LCM-SP)
Dover, NJ 07801
15. SECURITY CLASS. (of this report): Unclassified
15a. DECLASSIFICATION/DOWNGRADING SCHEDULE:

16. DISTRIBUTION STATEMENT (of this Report)

Approved for public release; distribution unlimited.

17. DISTRIBUTION STATEMENT (of the abstract entered in Block 20, if different from Report)

18. SUPPLEMENTARY NOTES
This project was accomplished as part of the U.S. Army's Manufacturing Methods and Technology Program. The primary objective of this program is to develop, on a timely basis, manufacturing processes, techniques, and equipment for use in production of Army materiel.

19. KEY WORDS (Continue on reverse side if necessary and identify by block number)
Blast overpressures
Pre-engineered building
Inhabited building distance
Personnel protection
MMT, blast effects

20. ABSTRACT (Continue on reverse side if necessary and identify by block number)

A series of dynamic tests was performed to evaluate the blast resistant capacity of pre-engineered buildings for use in Army Ammunition Plants. Test results indicated that conventional pre-engineered buildings can resist approximately 3.4 kPa (0.5 psi) of blast overpressures, while modified pre-engineered buildings can economically be strengthened to resist blast over-pressures as large as 13.8 kPa (2 psi).

DD FORM 1 JAN 73 1473 EDITION OF 1 NOV 65 IS OBSOLETE

UNCLASSIFIED
SECURITY CLASSIFICATION OF THIS PAGE (When Data Entered)

ACKNOWLEDGEMENTS

The authors wish to express their sincere appreciation to the following persons for their assistance and guidance during the past program and/or report preparation: Messrs. Philip Miller and Charles Warneke of the U.S. Army Dugway Proving Ground, Utah; Messrs. David Kossover, Robert Langan, George Pecone, Michael Dede, Mark Dobbs and Ram Arya of Ammann & Whitney, Consulting Engineers, New York, N.Y.

TABLE OF CONTENTS

FIGURES

SUMMARY

The U.S. Army, under the direction of the Project Manager for Production Base Modernization and Expansion, is currently engaged in a multi-billion dollar program to modernize and expand its ammunition production capability. In support of this program, the Manufacturing Technology Division of the Large Caliber Weapons Systems Laboratory, ARRADCOM, with the assistance of Ammann & Whitney, Consulting Engineers, has, for the past several years, been engaged in a broad base program to improve explosive safety at these facilities. One segment of this program deals with the development of design criteria for explosion-resistant protective structures.

Development of these design criteria has, in the past, been primarily concerned with structures located in the high pressure region close to an explosion. The basic document to evolve from this effort is the tri-service manual, TM 5-1300, "Structures to Resist the Effects of Accidental Explosions" (Ref 3). This manual contains comprehensive information on the principles of protective design, the calculation of blast loadings, dynamic analyses, and detailed procedures for designing reinforced concrete protective structures.

It is common practice in the explosives industry for process buildings associated with the same line to be separated by "intraline distances" which are meant to provide a high degree of protection against the propagation of explosions from building to building. Similarly, the minimum distance permitted between an inhabited building, not associated with the line in question, and an explosives location is the "inhabited building distance". These distances are published in the DARCOM Safety Manual (DRCR 385-100) and are based on the cubic root scaling of the explosive weight which defines areas of equal pressure. In all cases, however, the blast overpressures that an acceptor structure would experience in the event of an explosion in the "building next door" would be greater than the overpressures a conventional structure is designed to withstand, and serious injury to personnel within it is likely.

In this regard, explosive tests have been conducted to evaluate the blast capacity of pre-engineered buildings. The results of these tests, which are described below, have been used to verify and refine data contained in the ARRADCOM technical reports pertaining to the design of acceptor structures (Refs 1 and 2).

The structure consisted of a modified version of the STR4 Series produced by the Star Manufacturing Company. It originally consisted of five structural steel frames, each spaced 6.1 m (20 ft) on center. Each frame was 6.1 m (20 ft) long by 3.7 m (12 ft) high. Adjoining frames were connected by girts at the 2.4-m (8-ft) level and by six roof girts. All secondary members were zee-shapes. Roof and siding for the building consisted of 24-gage cold-formed steel panels. To increase the overall blast capacity of the structure, the number of girts was increased from one on each side to two per side. Also, the sizes of both the girts and purlins were increased. Since the test was primarily concerned with the steel portion of the structure, a footing design somewhat heavier than that required for conventional loads was used.

Instrumentation consisted of electronic deflection gages to record the movement of the structure, pressure gages to measure the blast loads acting on the building as well as free-field, accelerometers also to measure deflections, and strain gages to measure support reaction. Also photographic coverage, including both still photographs and motion pictures, was used to document both pre-shot construction and post-shot test results.

A total of six tests were performed, each of which utilized approximately 900 kg (2,000 lb) of nitro-carbo-nitrate as the explosive source. The recorded peak free-field pressure for each test was 1.86 kPa (0.27 psi), 3.86 kPa (0.56 psi), 5.10 kPa (0.74 psi), 6.96 kPa (1.01 psi), 8.62 kPa (1.25 psi) and 8.96 kPa (1.30 psi). Damage incurred by the structure during the first two tests was minimal, consisting essentially of enlargement of screw holes and some loosening of the screws. A significant pressure build-up was recorded within the structure in each test. Motion picture coverage showed that the door opened during the second test. However, the pressure build-up within the building during the second test was proportionally no greater than in the first test. The major portion of the pressure build-up within the building was attributed to leakage between the seams of the siding and roofing

More extensive structural damage occurred in Test No. 3. The blastward wall panels were kinked where they were attache to the girts and a portion of the panel was disengaged where it was attached to the foundation slab. In addition, the heads of some of the screws were pulled through the paneling. The major structural damage which occurred during this test consisted of bending of one of the column anchor bolts and twisting of several of the girt angle connections to the columns. The door was also found ajar after the test.

The damage that occurred in Tests Nos. 4 and 5 was similar to that in the previous tests but was somewhat more severe. The increased loading produced tearing of several of the girt connections as well as enlargement of some of the bolt holes. The connection of the blastward wall panel to the foundation slab completely failed. The damage in Test No. 6 was essentially the same as in Tests Nos. 4 and 5, except that the damage was sustained by the opposite wall which, in this test, served as the blastward wall.

Pressure measurements on the front of the building were consistent with theory; that is, the blast pressure acting on the front wall varied from approximately 2.3 to 2.8 times the incident free-field pressure at the bottom to about 1.2 to 1.4 times the incident pressure at the top. The pressure on the roof was slightly larger than the free-field pressure. On the other hand, leeward pressures were only approximately 50 to 60 percent of the incident pressures.

Test data provided by the deflection gages was quite extensive and was more than adequate to analyze the test results. However, the data obtained from either the accelerometers or strain gages was too limited to be useful.

Based upon the overall results of the tests, the following observations can be made:

1. Pre-engineered buildings can be used as protective structures.

2. For incident blast pressures in the order of approximately 3.45 kPa (0.5 psi), conventional pre-engineered buildings will not require any modifications.

3. Certain modifications to pre-engineered buildings can be made to increase their blast-resistant capacity to overpressures in the order of 13.8 kPa (2 psi). The cost of reinforcing these buildings will generally be in the order of approximately 20 percent of the basic building cost.

INTRODUCTION

Background

Acceptor structures are generally related to those buildings located at pressure ranges of 10 psi or less. If these buildings contain personnel and/or valuable equipment, sufficient protection must be provided by the buildings against the effects of blast and fragment output of an accidental explosion. Steel buildings used for protective structures can range from pre-engineered buildings for low overpressures of about 7 kPa (1 psi) to strengthened steel buildings for high overpressures. One disadvantage of steel structure designs at the higher overpressures is that they provide little protection against fragment penetrations. However, at the lower overpressures where pre-engineered buildings can sustain the blast overpressures, fragments are not usually a major concern.

Except for the rigid frames, most components of pre-engineered buildings are formed from cold-formed steel and utilize unsymmetrical shapes such as a "zee" section for purlins and girts. Also, the rigid frames themselves are usually fabricated from built-up sections and, therefore, vary in section modulus. Because of these differences, the response of pre-engineered structures was unpredictable and their use for protective structures was questionable.

In order to more fully define the blast capacity of pre-engineered buildings, a series of tests were undertaken by the Manufacturing Technology Division of the Large Caliber Weapons Systems Laboratory, ARRADCOM, as part of its overall Safety Engineering Support Program for the Project Manager for Production Base Modernization and Expansion. This report, which was prepared with the assistance of Ammann & Whitney, Consulting Engineers, summarizes and evaluates the results and presents recommended changes to more fully develop the blast capacity of pre-engineered buildings.

Purpose and Objectives

The overall purpose of the test program was to evaluate the usefulness of pre-engineered buildings as protective structures at Army Ammunition Plants and to provide recommended changes whereby the full blast capacity of these structures could be achieved. The objectives of the test program and related analyses are summarized below:

1. To evaluate the blast capacity of pre-engineered building components when tested as a unit as compared to component testing.

2. To establish those parameters of pre-engineered buildings which should be changed to increase their overall blast capacity, and

3. To evaluate computer programs and methods of analyses as presented in References 1 and 2 to determine their usefulness for pre-engineered building design.

Format and Scope of Report

The following two sections describe the test program, including the test procedures and results. These sections are followed by a section which evaluates the results and provide recommended changes for the specific building tested. The next section presents the results of an analytical evaluation of the structure. Appendix A contains reproductions of a comparison of actual blast loads and theoretical blast loads as computed from the design manual "Structures to Resist the Effects of Accidental Explosions" (TM 5-1300) (Ref 3). The second appendix contains reproductions of the engineering drawings used for the tests.

Since future standards of measurement in the United States will be based upon the SI Units (International System of Units) rather than the United States System now in use, all measurements presented in this report will conform to those of the SI System. However, for those persons not fully familiar with the SI Units, United States equivalent units of the particular test data are presented in parentheses adjacent to the SI Units.

TEST DESCRIPTION

General

Blast tests of a pre-engineered building were performed at Dugway Proving Ground (DPG), Dugway, Utah, during the weeks of 31 January and 7 February 1977. A total of six tests were performed with only minimal repairs required between tests. In each test, the structure was subjected to the blast pressures produced by the detonation of 900 kilograms (2,000 pounds) of high explosive material. The structure was subjected to progressively higher pressures in successive tests by moving the explosive closer to its blastward wall. Free-field pressures measured in the vicinity of the building ranged from 1.86 kPa (0.27 psi) in the first test to 8.96 kPa (1.30 psi) in the sixth test.

Instrumentation, to record the structural response of the building, consisted of electronic self-recording deflection gages, pressure gages, accelerometers and strain gages. In addition, both still and motion picture coverage were used to record both pre- and post-shot damage as well as to view the structural response during the event.

Description of Test Structure

The structure tested was a modified version of the STR4 Series produced by the Star Manufacturing Company of Oklahoma City, Oklahoma. Overall dimensions of the building were 24.4 m (80 ft) long by 6.1 m (20 ft) wide by 3.7 m (12 ft) high. The building was oriented such that its long side faced the explosion. The selection of the basic pre-engineered building design was based on the following conventional loads:

Live Load	1.44 kPa (30 psf)
Wind Load	1.20 kPa (25 psf)
Dead Load	0.14 kPa (3 psf).

Figure 1 shows the building during the construction phase; Figure 2 is a view of one end of the building after construction has been completed. Engineering drawings showing the plans and sections of the test structure are provided in Appendix B (Drawing No. 131, Sheets 1 and 2). As may be noted, an access door was positioned in one of the side walls and, therefore, was

subjected to the incident overpressures. The door withstood the blast loads in all tests.

Figures 3 and 4 show the framing plan of the building. The building was subdivided into four bays in the longitudinal direction, each of which was approximately 6.1 m (20 ft) wide. The primary structural framework in the transverse direction consisted of three interior rigid frames, an exterior rigid frame at one end which was identical to an interior frame, and a "post and beam" frame at the other end. The columns and girders of the rigid frames were fabricated of plate stock having a minimum static yield stress of 380,000 kPa (50,000 psi). The flanges and webs of these members were joined by a minimum of 50 percent web penetration fillet weld on one side of the web. The post and beam frame was constructed of cold-formed channel members. Figure 5 shows a typical rigid frame together with a post and beam frame.

The frames used in the test structure were the same as those used in conventional construction of pre-engineered buildings. However, conventional design of pre-engineered buildings generally utilizes post and beam frames as the end frames. The sidesway resistance of a post and beam frame is developed by the interaction between the frame itself and the wall panels, which transmit the loads by diaphragm action. Loads acting on the frame members are sheared into the wall panels by the metal screws used to fasten the panels to frame and secondary members. The substitution of a rigid frame at one end of the building was made to evaluate the structural response of a post and beam frame relative to the structural response of a rigid frame.

Since the building was rigidly framed in the transverse direction only, lateral bracing was provided in the longitudinal direction. However, no tests were performed to measure the longitudinal structural response of the building.

The walls and roof of the building consisted of 24-gage cold-formed steel panels having a minimum static yield stress of 551,000 kPa (80,000 psi). The panel profile is shown in Figure 6. Normally, a building of this size is furnished with 26-gage panels. However, pre-shot dynamic analyses indicated that the blast resistance of the 26-gage panels was much less than the blast resistance of the main frames. Hence, to preclude premature failure of these components, the panel thickness was increased to 24 gage. The panels, which were furnished in 0.91-m (3-ft) wide sections, were attached to the primary and secondary framing with #12 self-drilling screws. The screws were spaced at 0.13 - 0.18 m (5 - 7 in) along primary frame members and 0.3 m

(1.0 ft) along secondary framing members. Laps of adjacent sections were fastened together with self-drilling screws spaced at 0.61 m (2.0 ft). At the base of the walls, the panels were fastened to tubular members cast into the concrete foundation.

The secondary framing (girts, purlins) of the walls and roof consisted of cold-formed Z-shaped members which spanned between the building frames. The minimum static yield stress of the material used to fabricate these members was 380,000 kPa (55,000 psi). Like the wall and roof panels, the blast capacity of the girts and purlins was shown, by pre-test dynamic analyses, to be less than that of the main frames. Therefore, the following modificaitons were required to equalize the blast resistance of both primary and secondary framing:

1. The number of girts was increased from one each side to two per side. The girt located at the 2.4-m (8-ft) level was that which is furnished with the building. The added girt was located at 1.2 m (3 ft - 11 in) above the foundation slab.

2. The size of each girt was increased from a [0.20 m (8 in) x 0.08 m (3 in) x 1.63 mm (0.064 in)]Z to [0.25 m (9.75 in) x 0.10 m (4 in) x 3.42 mm (0.1345 in)]Z.

3. The size of each roof purlin was changed from [0.20 m (8 in) x 0.07 m (3 in) x 1.63 mm (0.064 in)]Z to [0.20 m (8 in) x 0.07 m (3 in) x 2.13 mm (0.084 in)]Z in the interior bays and [0.20 m (8 in) x 0.07 m (3 in) x 2.44 mm (0.096 in)]Z in the end bays.

The cost of the above modifications was estimated at approximately 20 percent of the basic building costs (excluding the foundation).

The steel framework was supported on a 0.91-m (3-ft) deep continuous reinforced concrete footing [f'_c = 21,000 kPa (3,000 psi)] which formed the periphery of a 0.15-m (6-in) thick foundation slab. Figure 7 shows a typical cross-section of the foundation. The design of the continuous footing was based on the maximum column axial loads determined from pre-test dynamic analyses of the main frames performed using the DYNFA Computer Program (Ref 2). The resulting footing design was somewhat heavier than that required for conventional loads. The steel framework was attached to the footing using 22.2-mm (0.875-in) diameter anchor bolts cast into the concrete.

Instrumentation

Deflection Gages

The test structure was provided with 13 deflection gages which were located as shown in Figure 8. All of the gages were linear displacement transducers which operated on the principle of change in inductance in the coils of a linear differential transformer with change in position of the core. The deflection gages measured the deflection time histories of both end frames, the center frame, two girts and a wall panel. A deflection gage schedule is provided in Table 1. Each end frame was provided with three gages. Two of these gages measured the horizontal deflections of the blastward column and the third measured the vertical deflection at the midspan of the girders. The center frame was instrumented in a similar manner and also provided with a fourth deflection gage to measure the horizontal deflections at a point on the leeward column (D4 in Figure 8). In addition, deflection gages were provided to measure the horizontal deflections at the midspan of a lower girt (D11 in Figure 8), an upper girt (D12 in Figure 8) and the section of wall panel spanning between upper and lower girts (D13 in Figure 8). As shown in Figure 8, Gages D11, D12 and D13 were located such that the relative midspan deflections of the wall panel could be determined from the measurements recorded by the three gages. The deflection gages used to measure horizontal frame displacements had a 0.25-m (10-in) stroke; vertical deflections were measured with gages having a 0.15-m (6-in) stroke and the horizontal deflections of the girts and wall panel were measured with gages having a 0.30-m (1-ft) stroke.

The gages were mounted to steel support frames which were welded to base plates cast into the foundation slab. Figure 9 shows a typical gage mount and Drawing No. 131, Sheet 4 (Section F) of Appendix B shows the details of the gage support frames. The deflection rods (cores) were connected to steel rods (Fig 9) which were attached to the structure. Since the building was subjected to horizontal deflections in only one direction, the steel rods for all horizontal gages were rigidly attached to the structure as shown in Figure 10a. Such a connection could not be used for the vertical deflection gages because the horizontal deflections of the structure would have produced bending in the steel rods as they moved downward, thereby inhibiting the motion of the rod and possibly damaging the rod, the connection of the rod to the structure and the support framework. Therefore, the sliding connection shown in Figure 10b was used for all vertical deflection gages.

Pressure Gages

Pressure gages were used to record the blast loads acting on the exterior surfaces of the building, as well as the blast pressure leakage into the building and the free-field pressures. A total of 17 pressure gages were located as shown on Figures 11 and 12. Nine gages (P4 through P12, Fig 11) were located on the center frame; three on the blastward and leeward walls and three on the roof. One gage was located on each sidewall (P13 and P14, Fig 12) and three gages for measuring pressure leakage into the building were located on the centerline of the building at each interior frame line (P15, P16, P17, Fig 11). In addition, three gages (P1, P2, P3, Fig 11) were provided for measuring the free-field pressures in the vicinity of the building. Two of these gages were located 6.1 m (20 ft) from the side of the building containing the access door, with one gage placed in line with the blastward wall and the other one placed in line with the leeward wall. The third gage was placed 6.1 m (20 ft) from the opposite end of the building.

Figure 13 shows a typical detail of the method utilized to attach a pressure gage to the building and Figure 14 shows three pressure gages fastened to an exterior wall.

Accelerometers

Accelerometers were attached to two frames and a girt. A total of four were utilized in the test. The accelerometers were included to determine if reliable deflection versus time histories could be determined by double integration of measured acceleration records. If this method proved accurate, then accelerometers would be used more extensively in future tests.

Strain Gages

Two strain gages were attached at the centerline of the web of the blastward column of the center frame. The purpose of these gages was to determine the axial forces developed in the column.

Photographic Documentation

Motion picture camera coverage of the test was used to observe the test structure during each detonation and for documentary purposes. Three high-speed cameras were used to photograph the exterior of the building during detonation. Two cameras had a speed of 400 frames per second, while the third camera had a speed of 3,000 frames per second. The positioning

of the cameras is illustrated in Figure 15. In addition, two interior cameras, with a speed of 250 frames per second, were utilized. Still photographs were taken to record the pre-test setup in terms of general arrangement, construction details and instrumentation.

A hand motion picture camera was also used to make a documentary film of the pre- and post-shot phases of each test, and record the various phases of the construction. Post-shot still photographs were taken to record the general condition of the structure after each test, as well as close-ups of damage to the structure. Photographs depicting failures, permanent deformations, plus details of special interest, were taken.

Hand Measurements and Observations

Pre- and post-shot measurements were made to determine permanent deflections of all frames, girts, purlins, wall panels, and roof panels. In addition, observations of damage and general structural behavior were noted.

Explosives

The explosives used in this test program were nitro-carbo-nitrate as the primary charge and Composition C-4 as the booster charge. The combined weight of the primary charge and booster in each test was approximately 900 kg (2,000 lb) with the booster weighing approximately 23 kg (50 lb). The nitro-carbo-nitrate explosive, consisting of 94.5 percent by weight of ammonium nitrate and 5.5 percent by weight of No. 2 fuel oil, was in the form of small pellets which were shipped to the site in 23-kg (50-lb) bags.

The total explosive charge was held in a cylindrical aluminum container (Fig 16). Each charge was formed by pouring 39 bags of nitro-carbo-nitrate pellets into a container after which a series of C-4 blocks, each weighing approximately 0.6 kg (1-1/4 lb), were placed on top of the nitro-carbo-nitrate pellets and arranged to form a cubical shape. The Composition C-4 booster was primed with two electric detonators which initiated detonation of the entire charge.

Test Setup

A total of six tests were performed. The explosive charge was located in two orientations (Fig 15). In the first five tests, the charge was centered on one long side of the building. In the sixth test, the charge was centered on the opposite side

of the building. The distances from the charges to the building were calculated to produce progressively higher overpressures on the structure in successive tests. It was assumed that the explosive mixture had a TNT equivalency of 1.0. However, it was observed in several of the initial tests that, for a given selected scaled distance, the actual incident overpressure produced at the building was approximately 10 percent less than that anticipated, indicating that the explosive mixture had a TNT equivalency slightly less than one. Hence, to account for this difference, in later tests, the distance that would ordinarily be used to predict a given incident overpressure was reduced, thereby producing good agreement between predicted and actual incident overpressures obtained.

After each detonation, the test structure was inspected for damage. Still photographs were taken to document the damage. Preparation of the test structure for each subsequent test included repairing damaged components to insure the structural integrity of the building, and checking and calibrating the measuring instruments.

TEST RESULTS

General

Photographs of structural damage, and displacement and pressure measurements are used to present the test results. Table 2 summarizes the test results and includes free-field pressures; frame, girt and panel displacements; and a brief description of typical damage for each test. Strain and acceleration measurements are not included because the instruments for measuring these quantities did not yield acceptable test data.

Structural Damage

Test No. 1

A minimal amount of damage was incurred in Test No. 1 which consisted primarily of the enlargement of the side wall panel screw holes along the laps (seams) of adjacent sections of panel. Some of the screws were found loose after the test. This damage was attributed primarily to the diaphragm behavior of the side wall. The lap fasteners tie the individual wall panel sections together to produce composite diaphragm action of the entire wall. Thus, shear forces are transmitted from one section of panel to another through the lap fasteners. These forces produced bearing overstresses in the panel thereby resulting in the enlargement of screw holes. In addition, the angle clip (Fig 5) which connects the girder to the column of the "post and beam" frame was slightly bent.

Small gaps were observed to have formed between the screws of roof panel seams. Although similar gaps were not apparent in the wall panel seams after the test, motion pictures taken from the interior of the structure indicated that these seams did open and close repeatedly, yet remained closed after the shock wave passed. It is theorized that the vibrational motions of the panels (both roof and walls) at their seams were the major source of the pressure build-up measured within the structure. The magnitude of this internal pressure increase was approximately 40 percent of the free-field pressure.

Test No. 2

The damage incurred in Test No. 2 was similar to that observed after Test No. 1. In addition to the roof gaps, small permanent gaps were formed at the panel seams of the leeward wall. These gaps were similar to those shown in Figure 17, but

with the openings somewhat smaller. The screw hole enlargements formed in the first test were further enlarged. Motion picture coverage showed the opening of the door during the test. The door was not locked during this test, and resistance to opening was provided solely by the hinges and striker. The pressure build-up in the second test was proportionally no greater than that of Test No. 1, although the door did not open in the first test. This is a further indication that the primary source of pressure leakage into the building is through the gaps formed at the seams. Sections of the corner flashings were ajar and some tearing of the panel at the corner of the door opening was observed. The base of the leeward column of the "post and beam" frame was deformed, as was the angle clip which connects the column to the foundation.

Test No. 3

More extensive structural damage was formed in Test No. 3. The blastward wall panel kinked (buckled) at points where it was supported on the girts. In some places, the panel was slightly disengaged where it was fastened to the foundation (Fig 18). This damage was attributed to the inadequacy of the detail used for attaching the wall panels to the foundation slab. In this case, small (19.1 mm x 19.1 mm) (3/4 in x 3/4 in) tubular members were embedded into the corners of the foundation slab. They were anchored by a series of "pig tails" welded to the tubes and embedded in the concrete. The base of the wall panels was fastened to these tubes by self-drilling screws. The pig tails failed, thereby permitting the rebounding panels to separate from the concrete. An improved detail, probably using steel angles attached to the concrete by anchor straps, is required for blast-resistant design. In addition, the heads of some of the screws were pulled through the paneling. This situation was modified by providing washers (Fig 19) for those screws which were disengaged. The use of washers during construction would probably have eliminated this condition. Also, the corner flashings suffered additional damage, and the tear in the panel at the corner of the door opening had increased several inches in length.

The major structural damage which occurred in Test No. 3 consisted of the bending of one of the column anchor bolts and the twisting of several of the girt angle connections to the columns. One of the clip angles was ripped and had to be welded. The twisting is principally attributed to the panel attachment to the girts which produced eccentric loads on them. As with the previous test, the door was opened by the rebound and negative overpressures. Also, the door was partially bent. In this case, the lock had been engaged and was not damaged upon opening the

door. This was an indication that the movement between the door and door frame was of sufficient magnitude to permit the door to be released. Further opening of the door during a test was prevented by the mechanism shown in Figure 2.

Test No. 4

The damage that occurred in Test No. 4 was similar to that of the previous test but somewhat more severe. The increased loading produced tearing of several of the girt angle connections to the columns as well as failure of several of the girt connection bolts (Fig 20) and enlargement of some bolt holes (Fig 21). The connection failures did not cause any girts to collapse and was remedied by replacing the standard bolts supplied with the building by high-strength bolts and by welding torn clip angles. The stronger bolts did cause enlargement of some bolt holes in subsequent tests.

Damage to the base support of the blastward wall panel was more severe, especially in those areas damaged in the previous test. Disengagement of the base tube from the concrete had progressed further along the base of the wall. Additional kinking of the blastward wall panel had occurred and plastic deformations of the girts were observed.

Test No. 5

The resulting damage in Test No. 5 was similar to that in the previous tests. Further twisting of the girts occurred; some enlargement of the bolt holes at several girt/column connections occurred where high-strength bolts had been used. The blastward wall anchorage failed completely (Fig 22). Sandbags were required to hold the base of the wall in place for the subsequent test. Kinking of the blastward wall panel occurred at each girt and between girts. In addition, many screws pulled through the wall panels at the girts in areas that had not sustained panel connection damage in previous tests. Permanent deformations of the main frames, girts and paneling were observed. A push rod connecting a deflection gage to a lower girt broke as the member twisted under the action of the blast.

Test No. 6

The damage observed after Test No. 6 was essentially the same as that which occurred in Test No. 5. However, the major damage occurred to the opposite side of the building which, in this test, was the side facing the explosion. In addition, buckling was observed on some of the roof purlin webs and frame

girder flanges. Permanent frame deflections produced in prior tests were reduced in Test No. 6 since the building deformed plastically in the opposite direction.

Pressure Measurements

Table 3 summarizes the peak pressures recorded by the various pressure gages. Figures 23 through 25 present several typical free-field pressure versus time measurements. In general, good agreement was obtained between predicted and measured incident overpressures. Figures 26 through 31 contain the pressure versus time plots recorded on the blastward wall in several of the tests. In all of the tests, the peak reflected pressures varied over the height of the blastward wall. The measurements in Table 3 indicate that the peak pressures recorded near the base of the wall (Gage P4) were approximately twice the incident pressure; whereas the peak pressures at the mid-height of the wall (Gage P5) varied from 2.3 to 2.8 times the incident pressure and the peak pressure measured near the top of the wall (Gage P6) ranged from 1.2 to 1.5 times the incident pressure. However, the average of the peak pressures recorded by the three gages (P4, P5 and P6) was approximately twice the incident pressure in Tests Nos. 2 through 4. In Test No. 1, the average was somewhat lower, approximately 1.75 times the incident pressure.

Of the three pressure gages located on the roof of the building (Gages P7, P8 and P9), only one, Gage P7, yielded acceptable test data. The measurements recorded by Gage P7 in Tests Nos. 3 through 5 indicate that the peak pressure on the blastward slope of the roof was approximately 10 to 20 percent greater than the incident pressure measured in the free-field. This increase over the incident pressure appears to be consistent with the data provided in Figure 4-6 of Reference 3. The referenced data indicate a reflected pressure of approximately 1.15 times the incident pressure for an angle of incidence of 87.6 degrees between the direction of propagation of the blast and the sloping roof. However, similar results were observed in Test No. 6, in which Gage P7 was located on the leeward slope of the roof. Hence, it is probable that the measured increase over the incident pressure was caused by an overshoot in the accelerating pressure gage.

Typical pressure versus time measurements for the leeward wall are provided in Figures 26 through 31. The figures and the measurements tabulated in Table 3 indicate that the peak pressures on the leeward wall were significantly less than incident pressure. The peak leeward wall pressures varied from

50 to 65 percent of the peak incident pressure in Tests Nos. 1 and 2 to approximately 80 percent of the peak incident pressure in the remaining tests. The pressure gages on the side wall yielded peak measurements that varied from 0.9 to 1.0 times the peak incident pressure.

Significant pressure levels were recorded inside of the building in all of the tests. Pressures within the structure attained peaks of approximately 40 percent of the measured free-field pressure at all pressure levels. It is generally believed that the repeated opening and closing of the roof and wall panel seams during each test was the major source of the internal pressure build-up. The effects of the internal pressures were to reduce the deflections of the individual structural components of the building (wall and roof panels, girts and purlins) and thereby increase their capacities to resist the exterior loads.

Deflection Measurements

Table 2 summarizes the peak displacements of some of the structural components (center frame, blastward wall girts and panels) of the building. A summary of the maximum deflections recorded by Gages D1 through D10 is provided in Table 4. The measurements recorded by Deflection Gages D11 through D13 are not included in Table 4 since they represent the absolute displacements of the girts and wall panel and, therefore, by themselves are meaningless. Typical side-sway deflection-time histories are provided in Figures 26 through 31 for the center frame of the building, in Figure 32 for the rigid end frame (Column Line 5) and in Figure 33 for the "post and beam" frame (Column Line 1). In addition, typical deflection-time histories are provided in Figure 34 for the vertical deflection at the mid-span of the center frame girder and in Figure 35 for the relative horizontal displacement at the mid-span of the blastward wall girts.

The test data provided by the deflection gages was quite extensive and was more than adequate to analyze the results. In general, the horizontal deflection gages gave higher quality deflection records than the vertical deflection gages. Among the horizontal deflection gages, those measuring frame displacements (Gages D1, D2, D4, D5, D6, D8 and D9) gave excellent displacement versus time histories for almost one second of response time, as illustrated in Figures 32 and 33. The excellent quality of these displacement records is attributed to the low frequency character of the responses measured by these gages and to the fact that these gages recorded absolute displacements.

The remaining horizontal deflection gages (namely, Gages D11, D12 and D13) measured the absolute mid-span displacement-time histories of an upper and lower girt, and a section of wall panel. The relative girt displacement at any given time was determined by subtracting the displacement at the end of the girt (where it is attached to a main frame) from the absolute displacement at the mid-span of the girt. Each girt monitored was located in an interior bay (between Column Lines 3 and 4) and, therefore, it was assumed that the frames at each end of the member had identical displacement-time histories. Based on this assumption, the horizontal deflections on the blastward column of the center frame were taken as the girt end displacements and the relative girt displacement-time histories were determined using the measurements recorded by Gages D1, D2, D11 and D12 as follows:

1. Lower girt: Gage D11 displacements minus corresponding displacements from Gage D1.

2. Upper girt: Gage D12 displacements minus corresponding displacements from Gage D2.

In this manner, good quality displacement records, such as the ones shown in Figure 35, were determined. The deflection records for the section of wall panel were determined in a similar manner using the measurements from Gages D11, D12 and D13. Gage D13 measured the absolute displacement of a section of wall panel between upper and lower girts. Hence, at any given time, the relative panel displacement was determined by subtracting the average of the values recorded by Gages D11 and D12 from the value recorded by Gage D13. This procedure did not yield acceptable results for the panel, principally because of the high frequency nature of the panel response and, in the early tests (Tests Nos. 1 through 3), the magnitudes of the panel displacements. The fundamental panel frequency was nearly 100 cycles per second, which was five times the fundamental frequency of a girt. In addition, based on analyses of both panels and girts for the pressure levels in Tests Nos. 1 through 3, the panel displacements should be approximately 10 to 20 percent of the peak girt displacements. Hence, small errors in the displacement measurements recorded by the three gages can result in large errors when the numbers are subtracted. In the later tests (Tests Nos. 4 through 6), excessive damage to the panels altered their support conditions, thereby leaving no means to correlate measurements with analyses. In future tests, the gages for measuring wall and roof panel deflections should be mounted

to frames which are attached to the members (purlins, girts) supporting the panel. In this manner, a direct measurement of the relative panel displacement will be achieved.

The vertical deflection gages (D3, D7, and D10) were attached to the underside of frame girders. The test data provided by these gages was generally inferior to that provided by the horizontal gages. In some cases, the gages did not record any meaningful data. At other times, only one-half to one cycle of response was recorded. The displacement records shown in Figure 34 are of the best quality achieved in the vertical direction. The deficiencies in the vertical deflection measurements are generally attributed to the high frequency nature of the responses being recorded combined with the lateral motions of the structure. The rapid motions of the vertical deflection rods in and out of the cores coupled with the lateral motion of both core and rod (as the building deflected horizontally) could have conceivably caused the rod to bind or hang up in the core, thus producing a gage malfunction. In future tests, the use of electro-optical displacement followers should be considered for measuring the vertical deflections.

EVALUATION OF TEST RESULTS

General

This section discusses the test results in terms of the measured deflection responses and observed damage levels of the main frames, blastward wall girts and blastward wall panels. An assessment is made of factors affecting the structural response and building performance under the blast loads. In addition, recommended design changes are suggested for the specific building tested. Additional evaluation on the basis of dynamic analyses is discussed in the next section.

Main Frames

Factors Affecting Frame Response

Several factors affected the frame responses. The most significant of these factors was found to be the negative phase of the pressure loadings. It is interesting to note the displacement versus time response and its relationship to the blast pressure loading. Figures 26 through 31 present plots of front wall pressure, rear wall pressure, and center frame side-sway displacement versus time for Test No. 1 (1.86 kPa), Test No. 3 (5.1 kPa), Test No. 4 (6.96 kPa) and Test No. 5 (8.55 kPa). The displacement curves for Tests Nos. 1 through 4 show the side-sway build-up due to the loading followed by a significant negative (rebound) displacement, and the peak positive displacement occurring in the second cycle after all the blast loading was off the structure. This behavior can be explained by the phasing of the blast loading as follows: The first positive peak is a result of the net positive loading on the building walls (front wall minus rear wall pressure). As the frame starts to rebound, the negative pressure on the front wall and positive pressure on the rear wall are both acting in the same direction and in phase with the rebound. This combination of events produced a peak negative displacement which is greater than the positive displacement. A second positive displacement, which is greater than the first positive displacement, is produced by the rebound of the structure from the negative displacement combined with the negative phase of the loading on the rear walls. At the higher pressure levels (Tests Nos. 5 and 6), the negative displacements were nearly equal to the positive displacement, as shown in Figures 30 and 31 (for Test Nos. 5 and 6). This is due to the plastic deformation in the frame.

Other factors which affected the frame responses are the build-up of internal pressures, resulting from leakage through the seams of the paneling and the responses of the secondary members (purlins, girts, wall and roof panels) relative to those of the frames. The impact of these factors can only be assessed by analytical methods, as will be discussed in the next section. Another factor which affected the frame responses was the connection damage suffered by both the girts and wall panels. This effect was greatest in the later tests (Tests Nos. 4, 5 and 6) where the damage was most severe. As discussed in the previous section, in these tests there were several instances of either girt clip angles twisting or tearing, bolt failures, and enlargement of bolt holes caused by bearing overstresses. In addition, panel attachment screws pulled through the panels, and the lower panel supports failed completely. The net effect of these failures was to relieve the loading on the frames, thereby reducing their responses. The post-shot frame analyses tend to support this. Good correlation between analytical and test results was obtained for Tests Nos. 1 and 3, whereas the analytical and test results for Tests Nos. 4 and 5 did not compare as well.

Comparison of Responses for "Post and Beam" and Rigid End Frames

Normally, a building of this type would utilize "post and beam" frames as the end frames. These systems utilize the diaphragm action of the wall panels to resist lateral loads. However, as discussed in Reference 2, blast-resistant design discounts diaphgragm action and utilizes rigid end frames instead. Therefore, to evaluate the structural response of a post and beam frame relative to that of a rigid frame, a rigid frame was substituted at one end of the building in place of the conventional "post and beam" frame. The results of the test program indicate that the post and beam frame withstood the blast loading as well as the rigid end frame. This conclusion is partially based on the absence of any indication, in the post-shot reports and photographs, that the post and beam end frame had sustained any extraordinary damage compared to the damage levels observed for the other frames.

A comparison of the side-sway responses of both end frames tends to reinforce the conclusion stated above. Figure 32 shows the side-sway response for the rigid end frame for Tests Nos. 3, 4 and 5 and Figure 33 shows the side-sway response of the post and beam frame for the same tests. It is interesting to note that the character of the response records for both frames is similar and resembles closely the character of the center frame

response records shown in Figures 26 through 31. The peak side-sway deflections of the post and beam frame are 40 to 70 percent less than the corresponding values for the rigid end frame, thereby indicating that the post and beam frame is a stiffer system.

Blastward Wall Girts

The blastward wall girts spanned 6.1 m (20 ft) between frames. The member, which was simply supported, had an ultimate flexural resistance of 73.7 kN (16.6 kips) and a dynamic yield deflection at mid-span of 86.4 mm (3.4 in). The computation of these values was based on the section properties of the member as provided by the Star Corporation and the design criteria for cold-formed members specified in Reference 1.

The peak girt displacements given in Table 2 are relative to the girt support displacement at the frame columns, as discussed in the previous section. The ductility ratios and rotations associated with these displacements have been compared to the design criteria presented in Reference 1 as follows:

1. The 76.2-mm (3.14-in) deflection for Test No. 3 is within the elastic range and represents a rotation of 1.4^{o} which is between the reusable criteria of 0.9^{o} and the non-reusable criteria of 1.8^{o}. The limited damage to the girt for Test No. 3 is consistent with this criteria.

2. The 119.4-mm (4.7-in) deflection for Test No. 4 corresponds to a ductility ratio of 1.4 which compares to the reusable criteria value of 1.25 and is less than the nonreusable criteria of 1.75. However, the rotation is 2.2^{o} which exceeds the non-reusable criteria rotation of 1.8^{o}. Since twisting of the girts and failures of the girt clip angles occurred, the girt would not be reusable and the limiting rotation value of 1.8 appears to be reasonable. In this case, the member is controlled by rotation rather than ductility.

3. The 121.9-mm (4.8-in) deflection for Test No. 5 corresponds to a ductility ratio of 1.4 which is between the reusable (1.25) and non-resuable (1.75) criteria values. Here again, extensive twisting of the girts and damage to the girt clip angles occurred, which would render the member non-reusable. This is consistent with the actual rotation of 2.3^{o} compared to the criteria value of 1.8^{o}.

Wall Panels

The peak panel displacements given in Table 2 were measured relative to the girts. The measurements are for a section of panel spanning between girts which is assumed to behave more or less as as fixed supported beam. On the basis of the measured response records for the panel and post-shot dynamic analyses, it was concluded that the panel measurements recorded were not accurate. As explained in the previous section, this was attributed to the manner in which the panel displacements were measured (i.e., subtraction of absolute measurements of girt and panel deflections), the high frequency nature of the panel response and, in the early tests (Tests Nos. 1, 2 and 3), and in the later tests (Tests Nos. 4, 5 and 6), the excessive damage to the panels which made correlation between measurements and analysis impossible.

Recommended Design Changes

On the basis of the discussion in this and the preceding sections, the following design changes are recommended to insure that the full blast capacity of this structure, and similar pre-engineered structures, is developed and to insure the safety of occupants in inhabited buildings:

1. Use symmetrical sections for girts or purlins in lieu of Z-shaped members. If cold-formed sections are desirable, perhaps back-to-back channels or hat sections could be used, If available as pre-engineered building components, standard structural steel shapes (hot-rolled) could be used.

2. Use high-strength bolts (A-325) in place of standard unfinished bolts. In addition, use clip angles of sufficient thickness to preclude tearing or bearing overstresses.

3. Increase the sizes of anchor bolts to be consistent with the blast capacity of the structure.

4. Provide washers or other means to prevent heads of screws from pulling through metal panels and roofing.

5. Use more lap fasteners to limit the pressure leakage in the building. In addition, use a backing strip at the laps (on the inside of the panel) to prevent the threaded end of the lap screws from pulling through the panel.

6. Strengthen the connection of the wall panels at the foundation. Use a structural angle rigidly attached to the foundation by steel anchor straps welded to the fillet of the angle and anchored at least 0.30 m (1 ft) into the concrete with a 90° bend at the embedded end.

7. Provide a reversal mechanism on the door consistent with the blast capacity to insure that the door does not fly open when subjected to the blast effects of an HE explosion.

In addition, on the basis of the test results, conventional "post and beam" frames could be used as the end frames of pre-engineered buildings in lieu of rigid frames. However, the following precautions should be taken to preclude a premature failure of the system:

1. The panel should be capable of resisting the peak-applied shears (i.e., the maximum blastward wall girt reactions) without suffering shear buckling.

2. A sufficient number of fasteners must be utilized to fasten the panel to the girts, the columns and girder of the post and beam frame and the panel support at the foundation.

3. The diaphragm wall girts should be designed to remain elastic under the blast loads to insure that they will be able to transmit the blastward wall girt reactions to the sidewall panels.

ANALYTICAL EVALUATION OF STRUCTURE

Introduction

A series of dynamic analyses were performed on the main frames, blastward wall girts, roof purlins and the blastward wall panel. The objective of these analyses was to evaluate the analytical and design methods provided in References 1 and 2 with a view towards establishing the applicability of these procedures for the design of blast-resistant pre-engineered buildings.

Most of the analyses utilized multi-degree-of-freedom models to represent the structural systems. These analyses were performed using the DYNFA Computer Program (Ref 2). In addition, several analyses were performed on single-degree-of-freedom models of individual members (girts, purlins, panels) utilizing elementary numerical integration methods.

The structure responded primarily in the elastic response range in Tests Nos. 1 and 2. Plastic deformations in the structure commenced in Test No. 3 and greatly increased in Tests Nos. 4, 5 and 6. Analytical evaluations were performed for Tests Nos. 1, 3, 4 and 5. There were no analyses for Test No. 2 because the results of such analyses, except for the magnitudes of the displacements, would have closely resembled the analytical results obtained for Test No. 1; hence, an analytical evaluation for Test No. 2 would have provided little additional information on the response of the structure. No analyses were performed for Test No. 6 because of the limited pressure data available for the analyses (due to the failures of many of the pressure gages on the structure) and the extensive damage suffered by the structure.

Evaluation of Frame Analysis

General

The basic objective of this evaluation was to determine if the dynamic analysis, based on the methods and procedures given in Reference 2, provided a reasonable estimate of the response of a rigid frame in a multi-framed pre-engineered building. To meet this objective, a series of parametric studies were performed to assess the impact of several factors on the frame response.

The first of these factors to be considered was the yield stresses of the materials used in the fabrication of the

structure. As stated in Reference 1, the design of blast-resistant structures is based on the minimum specified yield stress of the materials used in their fabrication. However, in some cases, the actual materials delivered may have a yield stress in excess of the specified minimum. In addition, in pre-engineered buildings, the columns and girders of the rigid frames are usually fabricated from built-up sections composed of plates from different lots of material; therefore, the yield stress may vary between the webs and flanges of the member. Consequently, the actual axial load and bending moment capacities of the members may not be the same as the capacity computed using the specified minimum yield stresses of the materials. Therefore, tensile tests were performed to determine the actual yield stress of the materials used to fabricate the test structure. These tests were performed by the Pittsburgh Testing Laboratory of Salt Lake City, Utah. The report furnished by the test laboratory is given in Figures 36 and 37. Specimens taken from frame members are listed below:

Lab Specimen Designation	Member
18-in Sample 76-2238 (-1)	Upper inner flanges of columns
18-in Sample 76-2238 (-2)	Upper inner flanges of columns
18-in Sample 76-2238 (-3)	Upper inner flanges of columns
18-in Sample 76-2238 (-7)	Lower inner flanges of columns
18-in Sample 76-2238 (-8)	Lower inner flanges of columns
18-in Sample 76-2238 (-9)	Lower inner flanges of columns
18-in Sample 76-2238 (-10)	Girder flanges
18-in Sample 76-2238 (-11)	Girder flanges
18-in Sample 76-2238 (-12)	Girder flanges
18-in Sample 76-2238 (-13)	Girder flanges
18-in Sample 76-2238 (-14)	Girder flanges
18-in Sample 76-2238 (-15)	Girder flanges
18-in Sample 76-2238 (-16)	Outer flange of columns
18-in Sample 76-2238 (-17)	Outer flange of columns

Lab Specimen Designation	Member
18-in Sample 76-2238 (-18)	Outer flange of columns
18-in Sample 76-2238 (-19)	Column web

The laboratory report indicates that, in general, the yield stress of these materials exceeds the specified minimum yield stress of 345,000 kPa (50,000 psi). However, the material used for the outer column flanges [Samples (-16), (-17) and (-18)] has a measured yield stress of 333,000 kPa (48,000 psi), which is slightly less than the specified minimum yield stress. Since the inner and outer column flanges differed in thickness, yielding of the member commences in the thinner flange (in this case, the outer flange), and progresses inward in the web. If the flanges differ greatly in thickness, the thinner flange will suffer large plastic strains before the thicker flange yields, thereby yielding a non-linear moment curvative diagram for the member which does not have a well defined yield point (Fig 38a). Exact analyses of members having such moment-curvature relationships are difficult and also beyond the scope of the methods in References 1 and 2. The methods referred to assume the moment-curvative relationship to be elastic - perfectly plastic. This assumption, though resonable for the design of hot-rolled sections (Fig 38b), is not suitable for the design of built-up members such as the columns of the test structure. However, for design purposes, the desired behavior can be approximated by selecting, for the analysis, the moment capacity which is expected to yield the desired amount of plastic action (ductility ratio μ). This process, which is basically trial and error by nature, is illustratred in Fig 38a. Such a procedure was required to determine the moment capacities of the columns for the evaluation analyses. The girder, on the other hand, had a symmetrical cross-section; therefore, its axial load and bending moment capacities at various sections were computed directly using the appropriate areas and section moduli. The yield stress for the girder was taken as the average of the values determined by tensile tests of the specimens of the girder flange material. Finally, the test report indicated that the thicknesses of the plates used to fabricate the frame members were slightly larger than the nominal sizes specified by the building manufacturer. To increase the accuracy of the analyses, the section properties of all frame members were computed using the actual thickness of the stock used to fabricate them.

Another important factor affecting the frame response was the negative phase of the blast loading. The procedures given in Reference 2 consider only the positive phase of the loading; the

negative phase loading is not included in the blast loadings. However, as shown in Figures 23 through 31, significant peak negative pressures were measured for all pressure levels tested; therefore, analyses were required to assess the negative phase of the loading. This was accomplished using average pressure waveforms derived from the actual measured pressure records.

The third factor to be evaluated was the effect of the pressure build-up inside the building. As indicated previously, significant internal pressures were recorded in each test. Insulated wall construction, normally utilized, would tend to provide a more effective seal against pressure leakage into the building. However, these pressures had to be considered in the case of the test structure in order to fully assess the adequacy of the frame analysis. Exact measurements of the internal pressures acting on the various surfaces (walls, roof) are not available since all of the interior pressure gages were located at the centerline of the building (as shown in Fig 11). Hence, the internal pressures measured included leakage from the walls as well as the roof, with the leakage from each surface adding to the total. A typical internal pressure record was characterized by two pronounced spikes. The first of these, which occurred when the wave reached the centerline of the building, built up to approximately 50 percent of the peak pressure recorded by the gage and then decayed rapidly. The second spike usually occurred when the wave reached the leeward wall. This spike built up to the peak recorded by the gage. On the basis of these measurements, in the analyses, the internal pressure acting on any surface (wall, roof) was taken to be one-half of the peak internal pressure recorded for the test. These values were subtracted from the peak pressure of each pressure waveform used in the analysis.

The fourth factor to be considered in the analytical evaluation was the interaction between the responses of the secondary members (girts, purlins) and main frames. The methods in Reference 2 provide for the design of the main building frames on the basis of analyses on a basic frame model, such as the one shown in Figure 39. However, in pre-engineered buildings, there are large disparities between the blast capacities of the secondary members (girts, purlins) and the main frames. Hence, analyses were performed to determine if the responses of the secondary members would in any way affect the response of the main frames. These analyses were performed on the revised frame model shown in Figure 40. In this model, the girts and purlins were represented by a series of single-degree-of-freedom (SDOF) models (spring with mass constrained to motion in one direction). The spring constants and masses for these models were computed

using the methods of Reference 4. The SDOF models were connected to the basic model at the exact locations where the girts and purlins are attached to the frame. In these analyses, the blast loadings were applied directly to the SDOF models of the girts and purlins. Hence, the direct loading on the frame members consisted of the girt and purlin reactions.

Table 5 summarizes the frame analyses performed for the various tests and indicates which of the above factors were considered in each test. In addition, a series of pre-shot analyses were performed to predict the performance of the structure during the tests. These analyses were based on the methods and procedures of Reference 2 and, therefore, are included in the subsequent discussions to provide a basis for evaluating the applicability of current blast design procedures for designing pre-engineered buildings.

Effect of Actual Strength of Building Materials

In general, the axial load and bending moment capacities computed using the actual material yield stresses and thicknesses were larger than those capacities utilized for the pre-shot analyses. The largest increases occurred at the ends and mid-span of the girder where the capacities increased 14 and 22 percent, respectively. The large increase at the girder mid-span was due to the use of an average capacity for the tapered member in the pre-shot analyses. Modest increases were computed for the column capacities. The capacities for the lower section increased 7 percent and those for the upper section increased by a modest 2 percent. Since the girder capacities far exceeded the column capacities, most of the plastic behavior occurred in the columns. Hence, the minimal increases in the column capacities had little effect on the overall frame response when compared to the other factors which influence the response.

Effect of Actual versus Design Pressure Waveforms

The results of the analyses indicated that the negative phase of the blast loadings had a significant effect on the side-sway response of the frame. Figures 41 through 44 compare the computed side-sway response of the frame with the measurements recorded for Tests Nos. 1, 3, 4 and 5, respectively. It is seen that an excellent correlation of the first positive and negative peak displacements was made for Test No. 1 (Fig 41). It is interesting to note that the measured displacement record appears to be "damping out", whereas in the corresponding analysis, the displacement record implies an undamped free vibration of the structure. The measured and calculated

displacement records for Test No. 3 (Fig 42) compare favorably for one and one-half cycles of response (first two positive peaks and first negative peak), and then diverge noticeably. In Test No. 4 (Fig 43), the measured and calculated side-sway records diverge markedly after one-half cycle of response and in Test No. 5 (Fig 44) divergence between measurements and analyses is apparent over the entire response range plotted. It is believed that the differences between the analytical and test results for Tests Nos. 4 and 5 were caused by the failures of some of the blastward wall panel and girt connections. Such failures would have tended to relieve the loading on the main frames. Closer inspection of the DYNFA Program results revealed the occurrence of plastic behavior in all phases of the frame response. Such behavior would account for the seemingly erratic side-sway responses computed for Tests Nos. 4 and 5. The absence of this erratic behavior in the measured side-sway displacement records tends to indicate that the plastic deformations in the actual structure were much less severe than those computed by the analyses.

To further evaluate the impact of the negative phase of the blast loadings, tabulations of the significant response parameters, as computed by the DYNFA analyses, are provided in Tables 6 and 7 for both pre- and post-shot center frame analyses, respectively. Note that the peak side-sway displacements and ductility ratios are significantly less when the negative phase of the blast loading is considered in the analysis. The pre-shot analyses predicted a reusable design capacity of 3.45 kPa (0.50 psi) and a non-reusable design capacity of 5.51 kPa (0.80 psi) for the center frame, whereas the corresponding design capacities predicted by the post-shot analyses are 5.1 kPa (0.74 psi) (reusable) and 6.96 kPa (1.00 psi) (non-reusable).

Effect of Pressure Build-Up Within Structure

Analyses to evaluate the effect of the internal pressure on the frame responses were performed for Tests Nos. 1, 3 and 5. In general, inclusion of the internal pressures in the analyses decreased the side-sway responses of the frames as well as the plastic deformations of the frame members. In Tests Nos. 1 and 3, the interior pressure reduced the side-sway displacement of the frame by approximately 11 percent. In Test No. 3, the peak ductility on the blastward column was reduced by 25 percent when the internal pressure was subtracted from the loading. In Test No. 5, inclusion of interior pressure effects decreased the first positive peak side-sway displacement but increased the first negative peak side-sway displacement (Fig 45). In addition, the significant peak ductility ratios throughout the frame were

reduced by an average of 22 percent, with the largest reductions (nearly 30 percent) occurring on the blastward column. The larger decreases in the blastward column ductility ratios account for the behavior exhibited in Figure 45. With less energy expended in the plastic deformations of the column, more energy is available for the elastic rebound of the frame. Thus, the frame rebounds to a larger side-sway displacement.

It is seen from the frame analyses, that the interior pressures have a greater effect on the plastic deformations of the frame members than on the overall side-sway responses of the frame. This appears reasonable when one considers that the plastic deformations in the frame occur in local bending modes of the individual members. Since these modes have small periods of vibration, they are extremely sensitive to the peak pressure. On the other hand, the side-sway response of the frame is low frequency in nature and, therefore, is more dependent on the total impulse of the loading rather than on the peak pressure.

It is conceivable that the interior pressures, in the immediate vicinity of the walls and roof, were much larger than those recorded by the pressure gages located at the centerline of the building. If this were the case, then significant reductions would have occurred in the responses of the wall and roof panels, girts and purlins, as well as the local bending reponses of the frame members. This statement is partially verified in subsequent evaluations of the girt responses.

Effect of Interactions Between Responses of Secondary Members and Main Frames

The interactions between the secondary members (girts, purlins) were considered in analyses for Tests Nos. 3, 4 and 5. The results of these analyses are given in Figures 46 through 48 in terms of horizontal side-sway versus time curves for the center frame. The curves show that the responses of the secondary members did not significantly alter the first half-cycle of the side-sway response. However, the rebound of the frame was significantly diminished in all three analyses. It was concluded that this occurred because of the large amount of energy absorbed by the plastic deformations of the girts. However, in some cases, the peak girt displacements computed by these responses were far in excess of the measured girt respones. Hence, in the actual structure, significantly less energy was absorbed by the plastic behavior of the girts. Thus, the energy not absorbed by the girts was transferred to the frame, thereby resulting in elastic rebound of the frame.

The effect of the secondary member responses on the plastic deformations of the frame was also studied. In all three analyses, the responses of the blastward wall girts reduced the peak ductility ratios computed near the mid-span of the blastward column. However, these reductions were offset by increased ductility ratios at the upper end of the column and in other locations on the frame. In general, plastic deformations resulting from the side-sway of the frame were increased, whereas plastic deformations resulting from local bending responses of individual members decreased. Consequently, in terms of plastic deformations, the blast capacity of the frame was the same as that computed using the basic frame model.

Evaluation of Analyses of Blastward Wall Girts

Analyses were performed to evaluate the responses of the blastward wall girts. A variety of analytical models were utilized to compute the responses of these members. The models utilized included:

1. Single-degree-of-freedom (SDOF) models of the individual members.

2. Combined secondary member/frame interaction model (Fig 40).

3. Combined wall panel/girt interaction model (Fig 49).

These analyses were performed using average pressure waveforms derived from the actual pressure measurements recorded during the tests. The actual yield strength of the material used to fabricate the girts and panels was not determined by tensile testing and, therefore, the analyses were based on the minimum specified yield stresses for the material used to fabricate these components of the building.

The spring constant for the single-degree-of-freedom model of the wall panel (shown in Figure 49) was computed using the equations provided in Section 3.7.2 of Reference 1. The referenced material specifies an effective moment of inertia of $0.75I_{20}$ [where I_{20} is the effective moment of inertia at a service stress of 130,000 kPa (20 ksi)] for use in the blast-resistant design of cold-formed members. This approximation is intended to account for the markedly non-linear load deflection curves for thin-metal cold-formed sections subject to local instabilities at high stress levels. Such an approximation is generally applicable to decking and wall paneling where width-thickness ratios (w/t) in excess of 40 are

common for the compression flange of the cross-section. However, the w/t ratio for the flange of the girt is 24. Section 2.3.1.1 of Reference 5 provides data which indicate that for a w/t of 24, the compression flange of the girt can be taken as fully effective for computing the deflections of the member. Hence, the full moment of inertia of the cross-section of the girt was used in the analyses.

Plots of the results of these analyses are shown in Figures 50 and 51 for Tests Nos. 3 and 4, respectively. The plots indicate that the single-degree-of-freedom model produces a conservative estimate of the girt response. On the other hand, the combined secondary member/frame model and the combined wall panel/girt model yield responses that compare more favorably with the test results. It is also apparent that it was appropriate to use the full moment of inertia of the girt, as the use of $0.75I_{20}$ in the analyses would have yielded peak deflections approximately 33 percent greater than those shown in Figures 50 and 51. In future designs, the effects of local instabilities (namely, local buckling of the compression flanges) should be considered when computing the effective section modulus and moment of inertia of cold-formed members with compression flanges having width-thickness ratios less than 40. This can be accomplished by applying the provision of Section 2.3.1.1 of Reference 5 to compute the effective width of the compressive flange, when it is subjected to the dynamic design stress of the material. If the effective w/t ratio of the flange, when it is subjected to the dynamic design stress, is markedly less than the actual w/t ratio, then an average value of the effective w/t ratio should be determined using the effective w/t ratios for several stress levels up to the dynamic design stress.

It is interesting to note that the girt rebound, as computed by the secondary member/frame model (Figs 50 and 51), is much less than the measured rebound. In the combined secondary member/frame analyses, the maximum dynamic flexural resistance was used for both load and rebound phases of the girt and purlin responses. Therefore, the comparison between analytical and measured girt responses suggests that the actual flexural resistance of the member in rebound is much less than its flexural resistance for the loading phase of the response. It was concluded that the low rebound resistance of the girts is caused by the effects of local instabilities.

A review of the applicable provisions of Reference 5 leads to the conclusion that the dominant instability effects were those associated with lateral torsional buckling of the compression zone of the member. Inspection of the drawings in

Appendix B reveals that the outer flange of the girt is securely fastened to the wall panels, whereas the inner flange is unbraced. Section 3.3.6 of Reference 1 states that the connection of the compression flange to steel siding constitutes adequate lateral bracing in most cases involving blast-resistant design; hence, for the loading phase of the girt response, there is no reduction in flexural resistance due to lateral torsional buckling. However, in rebound, the inner flange is in compression. Since this flange is unbraced, the provisions of Section 3.3 of Reference 6 dictate that, to prevent lateral torsional buckling, the maximum allowable compressive stress is 139,000 kPa (20.1 ksi). This value is much less than the dynamic design yield stress of the material and, when used to compute the flexural resistance of the member, yields a rebound resistance which is approximately 33 percent of the maximum flexural resistance of the member.

In order to assess the impact of lateral torsional buckling effects on the girt responses, the analyses of the secondary member/frame interaction model were repeated for Tests Nos. 3 and 4. In these analyses, the rebound flexural resistances of the girts and purlins were computed using the maximum allowable compressive stress to prevent lateral torsional buckling instead of the dynamic yield stress of the material. The results of these analyses are presented in terms of mid-span girt deflection versus time-response curves in Figures 52 and 53. The curves labeled "SECONDARY MEMBER/FRAME MODEL W/LTB" in the figures are the results of these latter analyses. Note the excellent correlation between the measured and computed rebound displacements.

With these latter results in hand, the measured girt displacements, as reported on page 22, are re-evaluated with a view towards the effects of lateral torsional buckling on the rebound phase of the response. The re-evaluation of the measured girt responses, which follows below, is based on a dynamic yield deflection at mid-span of 64.8 mm (2.56 in) for the loading phase (inward deflection of girt), and 21.5 mm (0.85 in) for the rebound phase (outward deflection of girt). These values were computed for the full moment of inertia of the section.

1. For Test No. 3, the 80-mm (3.15-in) inward deflection corresponds to a ductility ratio of 1.23; whereas the rebound displacement of 76.5 mm (3.0 in) corresponds to a ductility ratio of 4.22. Note that the total rebound displacement equals the absolute negative displacement of 76.5 mm (3.0 in) plus a plastic deformation of 15 mm (0.59 in) produced in the loading phase.

2. The 119.4-mm (4.7-in) deflection for the loading cycle of the lower girt in Test No. 4 corresponds to a ductility ratio of 1.84 which slightly exceeds the non-reusable criteria value of 1.75. The 99.1-mm (3.9-in) rebound displacement for this member corresponds to a ductility ratio of 7.1, which greatly exceeds the criteria value. For the upper girt, the ductility ratios for the loading and rebound phases of the response are 1.82 and 7.9, respectively.

3. For Test No. 5, the peak deflection of 108 mm (4.25 in) for the initial loading phase corresponds to a ductility ratio of 1.66; while the peak rebound deflection of 127 mm (5.0 in) corresponds to a ductility ratio of 7.9, which is greatly in excess of the non-reusable criteria of 1.75.

It is seen from the above that the largest plastic deformations of the girts occurred in the rebound phase of the response due to the effects of lateral torsional buckling on the unbraced compression zone of these members. It is conceivable that the large rebound deflections of the girts contributed to the failures of the anchorage at the base of the wall panels. Consequently, on the basis of the above observations and analytical results, the effects of lateral torsional buckling must be considered in the design of the secondary members of pre-engineered buildings. This can be accomplished by providing bracing for the inner flanges, which negates the effects of lateral torsional buckling. Another approach is to increase the size of the section in order to increase the permissible stresses on the unbraced flanges. However, in some cases, this may require the use of standard hot-rolled sections which may not be economical for use in pre-engineered building construction.

Evaluation of Analyses of Roof Purlins

Analyses were performed to evaluate the roof purlin responses computed by both single-degree-of-freedom analyses and the secondary member/frame interaction analyses. The yield strength of the material used to fabricate the purlins was taken to be 370,000 kPa (53,690 psi). This value was obtained by tensile testing of a specimen [8-inch sample - 76-2238(A) in Fig 36] of the material used to fabricate the purlins. The value recorded is probably a lower bound on the actual yield stress since the effects of cold-working, which generally increases the material yield stress by 10 to 20 percent, would not be apparent on a piece of flat, unworked stock. The full moment of inertia was used for the analyses of these members. Initially, the

maximum dynamic flexural resistance was used for both the loading and rebound phases of the response. Additional analyses were performed for Tests Nos. 3 and 4, which included a reduction in the rebound resistance due to the effects of lateral torsional buckling.

A typical comparison of the results from the various analyses is shown in Figure 54. In general, the single-degree-of-freedom response predicts a much greater purlin response. For Tests Nos. 4 and 5, the single-degree-of-freedom prediction of peak purlin displacement is twice the value predicted by the secondary member/frame interaction model. The analyses which included the effects of lateral torsional buckling produced rebound displacements of the purlins which exceeded those computed in the initial series of analyses. Therefore, as in the case of the girts, consideration should be given to the effects of lateral torsional buckling in the design of these members for pre-engineered buildings. Since no displacement gages were furnished for measuring purlin responses, there are no measurements available for comparison with the analytical results.

Evaluation of Analyses of Blastward Wall Panel

The blastward wall panel reponse was evaluated on the basis of analyses of single-degree-of-freedom models of the panel and a combined panel/girt interaction model. Typical panel responses computed by these analyses are shown in Figure 55 for Test No. 3. The measured panel response for Test No. 3 is included in the plot. It is seen that the measured girt displacement records show large positive and negative peaks (greatly in excess of those computed). In addition, the character of the measured record resembles neither of the computed records. Similar disparities were noted for Tests Nos. 4 and 5. On the basis of these differences, it was concluded that measured panel responses were inaccurate and, therefore, these records were discontinued in the evaluation.

The plots in Figure 55 indicate that the single-degree-of-freedom analysis predicts a much greater panel response than the analysis of the combined panel/girt model. Similar results were obtained for Tests Nos. 4 and 5.

CONCLUSIONS AND RECOMMENDATIONS

Conclusions

On the basis of the test results and analytical evaluations, it was seen that pre-engineered buildings fabricated with standard pre-engineered components can withstand blast pressures greatly in excess of their static load capacities. The test program and subsequent evaluations indicate that the structure tested has a reusable design capacity of 5.1 kPa (0.74 psi) and a non-reusable design capacity of approximately 6.9 kPa (1.0 psi). In addition, the test results indicate that post and beam frames can be used as the end frames of pre-engineered buildings. Also, the blast capacity of the structure tested could have been increased by reducing the spacing of the girts, purlins and main frames. Furthermore, it is concluded that the methods and procedures of References 1 and 2, when applied to the design of pre-engineered building components, yield conservative estimates of the structural response and required member sizes.

Recommendations

It is recommended that the methods and procedures of References 1 and 2 be extended for the design of pre-engineered buildings to include the following:

1. The negative phase of the blast loading.

2. The increase in the yield strengths of cold-formed members due to the effects of cold working.

3. The computation of the section moduli and moments of inertia of cold-formed members using the effective width-thickness ratios of the compression flanges of flexural members as computed using the equations in Section 2.3.1.1 of Reference 5 (in lieu of the values given in Reference 1).

4. The effects of lateral torsional buckling on the rebound phase on the responses of the secondary members (purlins, girts).

5. The interaction between the secondary member (girts, purlins) responses and the frame responses.

6. The interactions between the panel responses and the secondary member responses.

It is also recommended that dynamic tests, at higher pressure levels be performed on a steel structure designed according to the methods and procedures provided in References 1 and 2. It is believed that certain factors, which tended to relieve the responses of pre-engineered building components, will not have as much effect on a more rigid structure designed for higher pressures. Furthermore, it is recommended that all information developed on the blast capacities of steel structures and components be included in one design manual.

REFERENCES

1. HEALEY, J.J., et al., "Design of Steel Structures to Resist the Effects of HE Explosions", Technical Report 4837, prepared by Ammann & Whitney, Consulting Engineers, New York, N.Y., for Picatinny Arsenal, Dover, N.J., 1975.

2. STEA, W., et al., "Non-Linear Analysis of Frame Structures Subjected to Blast Overpressures", Report ARLCD-CR-77008, U.S. Army Armament Research and Development Command, Dover, N.J., May 1977.

3. Department of the Army, "Structures to Resist the Effects of Accidental Explosions (with Addenda)", Technical Manual TM 5-1300, Washington, D.C., June 1969.

4. BIGGS, J.M., Introduction to Structural Dynamics, McGraw-Hill Book Company, New York, N.Y., 1964.

5. "Specification for the Design of Cold-Formed Steel Structural Members" and "Commentary", and "Supplementary Information" thereon, American Iron and Steel Institute, Washington, D.C., 1968.

6. KINGERY, C.N., "Air Blast Parameters Versus Distance for Hemispherical TNT Surface Burst", BRL Report No. 1344, U.S. Army Materiel Command Ballistic Research Laboratories, Aberdeen Proving Ground, Maryland, September 1966.

7. GRANSTROM, S.A., "Loading Characteristics of Air Blasts from Detonating Charges", Report No. 100, Transactions of the Royal Institute of Technology, Stockholm, Sweden, 1956.

Table 1

Deflection gage schedule

Gage No.	Measurement Description		Measurement Location	
	Member	Direction	Column Line	Height above Foundation m (ft)
D1	Column	Horizontal	3-A	1.52 (5'-0")
D2	Column	Horizontal	3-A	2.95 (9'-8")
D3	Girder	Vertical	3-℄	3.20 (10'-6")
D4	Column	Horizontal	3-F	1.52 (5'-0")
D5	Column	Horizontal	5-A	1.52 (5'-8")
D6	Column	Horizontal	5-A	2.95 (9'-8")
D7	Girder	Vertical	5-℄	3.20 (10'-6")
D8	Column	Horizontal	1-A	1.52 (5'-0")
D9	Column	Horizontal	1-A	2.95 (9'-8")
D10	Girder	Vertical	1-℄	3.20 (10'-6")
D11	Girt	Horizontal	-	1.19 (3'-11')
D12	Girt	Horizontal	-	2.44 (8'-0")
D13	Panel	Horizontal	-	1.83 (6'-0")

Table 2

Summary of pre-engineered building test results

Test No.	Free-Field Pressure (kPa) (psi)	Peak Horizontal Displacement[a] Center Frame mm (in)	Girt[b] mm (in)	Panel mm (in)	Damage
1	1.86 (0.27)	43.2 (1.70)	20.3 (0.79) c	12.2 (0.60)	(1) Enlargement of side wall panel screw holes. (2) Small gaps between screws of roof panel seams.
2	3.86 (0.56)	53.3 (2.09)	c	c 60.9 (2.40)	(1) Further enlargement of side wall panel screw holes. (2) Small gaps between screws of back wall panel seams. (3) Door opened outward.
3	5.10 (0.74)	78.5 (3.09)	63.5 (2.50) 80.0 (3.14)	27.9 (1.10)	(1) Bent anchor bolt. (2) Front wall panel kinked along lower girt and pulled out at base at a few points. (3) Screw heads pulled through front wall panel at columns. (4) Some twisting of girt clip angles. (5) Door opened outward.

[a]Absolute displacements given for center frame; relative displacements given for girts and panel.
[b]Values are given for upper and lower girts.
[c]No measurements were made.

Table 2

Summary of pre-engineered building test results (continued)

Test No.	Free-Field Pressure (kPa) (psi)	Peak Horizontal Displacement[a] Center Frame mm (in)	Girt[b] mm (in)	Panel mm (in)	Damage
4	6.96 (1.01)	96.5 (3.79)	119.4 (4.70) 104.1 (4.09)	60.9 (2.39)	(1) Further twisting and tearing of girt clip angles. (2) Shearing of some girt connection bolts without collapse. (3) Twisting of girts. (4) Front wall panel anchorage pulled out. (5) Further kinking of front wall panel. (6) Plastic deformation of girts.
5	8.62 (1.25)	102.6 (4.04)	[c] 121.9 (4.79)	96.5 (3.79)	(1) Further twisting of girts. (2) Kinking of front wall panel at each girt and between girts. (3) Front wall panel anchorage completely pulled out. (4) Panel screw holes pulled through at girts. (5) Plastic deformations of frame, girts, and front wall panel.

[a]Absolute displacements given for center frame; relative displacements given for girts and panel.
[b]Values are given for upper and lower girts.
[c]No measurements were made.

Table 2

Summary of pre-engineered building test results
(concluded)

Test No.	Free-Field Pressure (kPa) (psi)	Peak Horizontal Displacement[a] Center Frame mm (in)	Girt[b] mm (in)	Panel mm (in)	Damage
6	8.96 (1.30)	125.5 (4.94)	124.5 (4.90) [c]	185.4[d] (7.30)	(1) Damage to front wall panel and girts similar to Test 5. (2) Buckling of roof purlin webs. (3) Some buckling of frame girder flange. (4) Plastic deformations of frame, girts and front wall panel.

[a]Absolute displacements given for center frame; relative displacements given for girts and panel.
[b]Values are given for upper and lower girts.
[c]No measurements were made.
[d]Questionable value.

Table 3

Summary of pressure measurements

Gage No.	Location	Test No. 1 kPa	(psi)	Test No. 2 kPa	(psi)	Test No. 3 kPa	(psi)	Test No. 4 kPa	(psi)	Test No. 5 kPa	(psi)	Test No. 6* kPa	(psi)
P1	Free-Field	1.76	(0.26)	3.45	(0.50)	5.10	(0.74)	6.96	(1.01)	8.62	(1.25)	8.20	(1.19)
P2	Free-Field	1.86	(0.27)	3.59	(0.52)	4.82	(0.70)	6.96	(1.01)	8.55	(1.24)	8.96	(1.30)
P3	Free-Field	1.86	(0.27)	3.86	(0.56)	4.96	(0.72)	7.17	(1.04)	8.14	(1.18)	9.38	(1.36)
P4	Blastward Wall	3.24	(0.47)	7.03	(1.02)	9.92	(1.44)	14.20	(2.06)	17.24	(2.50)	-	-
P5	Blastward Wall	4.20	(0.61)	9.85	(1.43)	14.50	(2.10)	19.30	(2.80)	21.20	(3.08)	6.69	(0.97)
P6	Blastward Wall	2.13	(0.31)	4.69	(0.68)	7.74	(1.12)	9.92	(1.44)	-	-	-	-
P7	Roof	-	-	-	-	6.14	(0.89)	8.14	(1.18)	9.65	(1.40)	9.99	(1.45)
P8	Roof	-	-	-	-	-	-	-	-	-	-	-	-
P9	Roof	-	-	-	-	-	-	-	-	-	-	-	-
P10	Leeward Wall	1.10	(0.16)	2.48	(0.36)	-	-	-	-	-	-	-	-
P11	Leeward Wall	0.90	(0.13)	2.34	(0.34)	3.93	(0.57)	5.58	(0.81)	6.48	(0.94)	16.75	(2.43)
P12	Leeward Wall	-	-	-	-	-	-	-	-	-	-	-	-
P13	Side Wall	1.31	(0.19)	3.24	(0.47)	4.21	(0.61)	6.48	(0.94)	8.20	(1.19)	-	-
P14	Side Wall	1.72	(0.25)	3.24	(0.47)	5.44	(0.79)	6.20	(0.90)	7.24	(1.05)	7.17	(1.04)
P15	Interior	0.69	(0.10)	1.38	(0.20)	2.21	(0.32)	2.90	(0.42)	3.38	(0.49)	3.65	(0.53)
P16	Interior	0.69	(0.10)	0.97	(0.14)	-	-	2.83	(0.41)	3.31	(0.48)	2.90	(0.42)
P17	Interior	0.69	(0.10)	-	-	1.86	(0.27)	3.10	(0.45)	3.24	(0.47)	3.93	(0.57)

* Charge centered on opposite side of building in Test No. 6; therefore, Gages P4 through P6 measured pressures on leeward wall and Gages P10 through P12 measured pressures on blastward wall.

Table 4

Partial summary of deflection measurements

Gage	Test No. 1 mm (in)	Test No. 2 mm (in)	Test No. 3 mm (in)	Test No. 4 mm (in)	Test No. 5 mm (in)	Test No. 6 mm (in)
D1	26.9 (1.06)	- -	47.0 (1.85)	64.3 (2.53)	69.1 (2.72)	75.2 (2.96)
D2	43.2 (1.70)	53.3 (2.10)	78.5 (3.09)	96.5 (3.80)	102.6 (4.04)	125.5 (4.94)
D3	7.6 (0.30)	16.8 (0.66)	23.1 (0.91)	- -	- -	- -
D4	28.2 (1.11)	43.9 (1.73)	49.5 (1.95)	54.4 (2.14)	64.3 (2.53)	67.8 (2.67)
D5	11.9 (0.47)	35.1 (1.38)	43.9 (1.73)	52.3 (2.06)	40.9 (1.61)	35.1 (1.38)
D6	18.5 (0.73)	46.5 (1.83)	63.5 (2.50)	71.1 (2.80)	65.5 (2.58)	73.4 (2.89)
D7	- -	4.6 (0.18)	7.6 (0.30)	10.9 (0.43)	14.0 (0.55)	12.2 (0.48)
D8	7.4 (0.29)	16.5 (0.65)	23.9 (0.94)	40.4 (1.59)	51.3 (2.02)	- -
D9	11.2 (0.44)	29.9 (1.18)	24.9 (0.98)	33.0 (1.30)	35.6 (1.40)	- -
D10	3.6 (0.14)	- -	- -	- -	14.0 (0.55)	- -

Table 5

Rigid frame analyses matrix

Factor considered	Parameter variations	Center Frame														End Frame		
		Test No. 1				Test No.2	Test No. 3				Test No. 4			Test No. 5				fest No.1	Test No.3	Test No.5
Strength of material	Min yield stresses	*	•	•		*	*				*			*				*		
	Measured yield stresses	•				•	•	•	•	•	•	•	•	•	•	•	•	•	•	•
Pressure loadings	Design waveforms (Ref 2)	•				•	•				•			•						
	Measured waveforms		•	•				•	•	•		•	•		•	•	•	•	•	•
Pressure leakage	With interior pressure		•					•	•			•	•			•	•		•	•
	Without interior pressure	•		•		•	•				•			•	•			•		
Type of frame Model	Basic model	•	•	•		•	•	•	•		•	•		•	•	•		•	•	•
	Model including girts and purlins									•			•				•			

Note: Each column beneath a "Test No." designates one analysis; the dots in the column denote the parameter considered in the analysis. Columns containing asterisks denote pre-shot analyses, remainder are post-shot analyses.

Table 6

Summary of results of pre-shot frame analyses

Test No.	P_{so} (kPa)	P_{so} (psi)	δ (mm)	δ (in)	Plastic Behavior μ	Plastic Behavior Member	Plastic Behavior Location	Comments
1	2.41	(0.34)	+47.6 -39.4	(1.87) -(1.55)	-	-	-	Elastic response.
2	3,45	(0.50)	71.9	(2.83)	1.1 2.3 2.0	Blastward column Girder Leeward column	Near mid-span Leeward end Upper end	a) $\delta/H \sim 50$ limit of re-usable design criteria. b) μ of 2.3 on girder; 2.0 on column limit of reusable design criteria.
3	5.51	(0.80)	92.5	(3.64)	3.3 2.1 5.1 3.8	Blastward column Girder Girder Leeward column	Near mid-span Blastward end Leeward end Upper end	a) $\delta/H = 36$. b) μ on columns and girder approach non-reusable design limit.
4	6.89	(1.00)	153.4	(6.04)	6.4 4.4 5.9 5.1	Blastward column Girder Girder Leeward column	Near mid-span Blastward end Leeward end Upper end	a) $\delta/H = 22$ exceeds non-reusable design criteria. b) μ on columns and girder exceed non-reusable design criteria.
5	8.27	(1.20)	176.3	(6.94)	10.4 6.2 8.0 4.1 9.1 11.1	Blastward column Blastward column Girder Girder Girder Leeward column	Near mid-span Upper end Blastward end Mid-span Leeward end Upper end	Frame severely damaged.

Note: P_{so} = Free-field pressures; values given are pre-shot predictions.
δ = Maximum side-sway deflection of frame.
μ = Maximum ductility ratio computed by DYNFA frame analysis.
H = Height of frame.

Table 7

Summary of results of post-shot frame analyses[a]

Test No.	P^b_{so} kPa	(psi)	δ^b mm	(in)	Plastic Behavior μ^b	Member	Location	Comments
1	1.86	(0.27)	+49.5 -49.3	(1.94) -(1.94)	-	-	-	Elastic response.
3	5.10	(0.74)	72.4	(2.85)	1.9 1.9	Blastward column Leeward column	Near mid-span Upper end	a) $\delta/H \sim 50$ limit of reusable criteria. b) μ on blastward column approach limit of reusable criteria.
4	6.96	(1.01)	129.0	(5.08)	3.9 5.4 3.0 2.8	Blastward column Girder Girder Leeward column	Near mid-span Blastward end Leeward end Upper end	a) $\delta/H \sim 25$ limit of non-reusable design criteria. b) μ on columns and girder approach non-reusable design criteria.
5	8.62	(1.25)	135.9	(5.35)	6.2 4.8 4.9 2.4	Blastward column Blastward column Girder Leeward column	Near mid-span Upper end Blastward end Leeward end	δ/H, μ on blastward column exceed non-reusable design criteria.

[a] Analyses included actual pressure waveforms, yield stresses of materials and internal pressure build-up.
[b] For definitions of nomenclature, see bottom of Table 6.

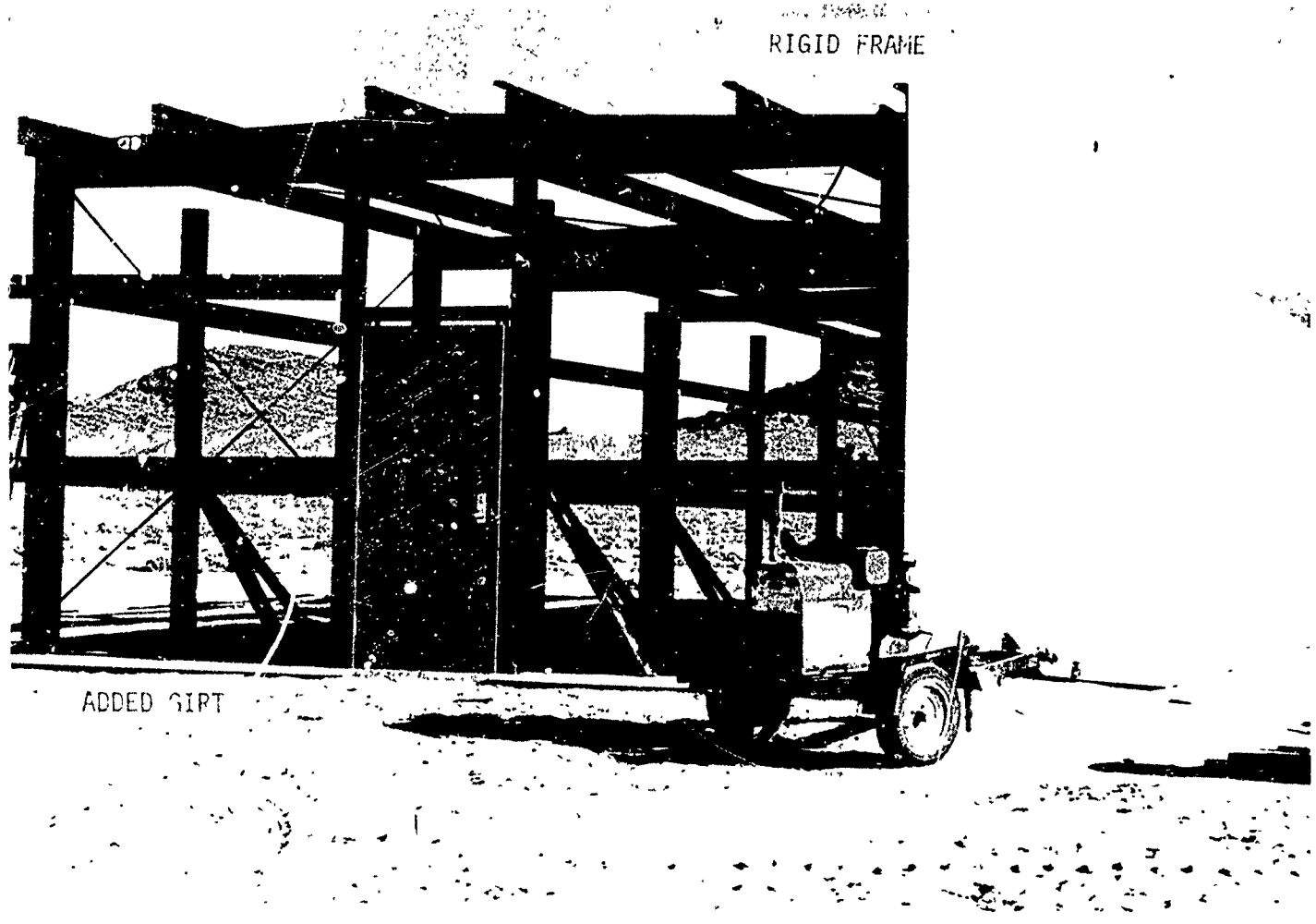

Fig 1 Pre-engineered building under construction

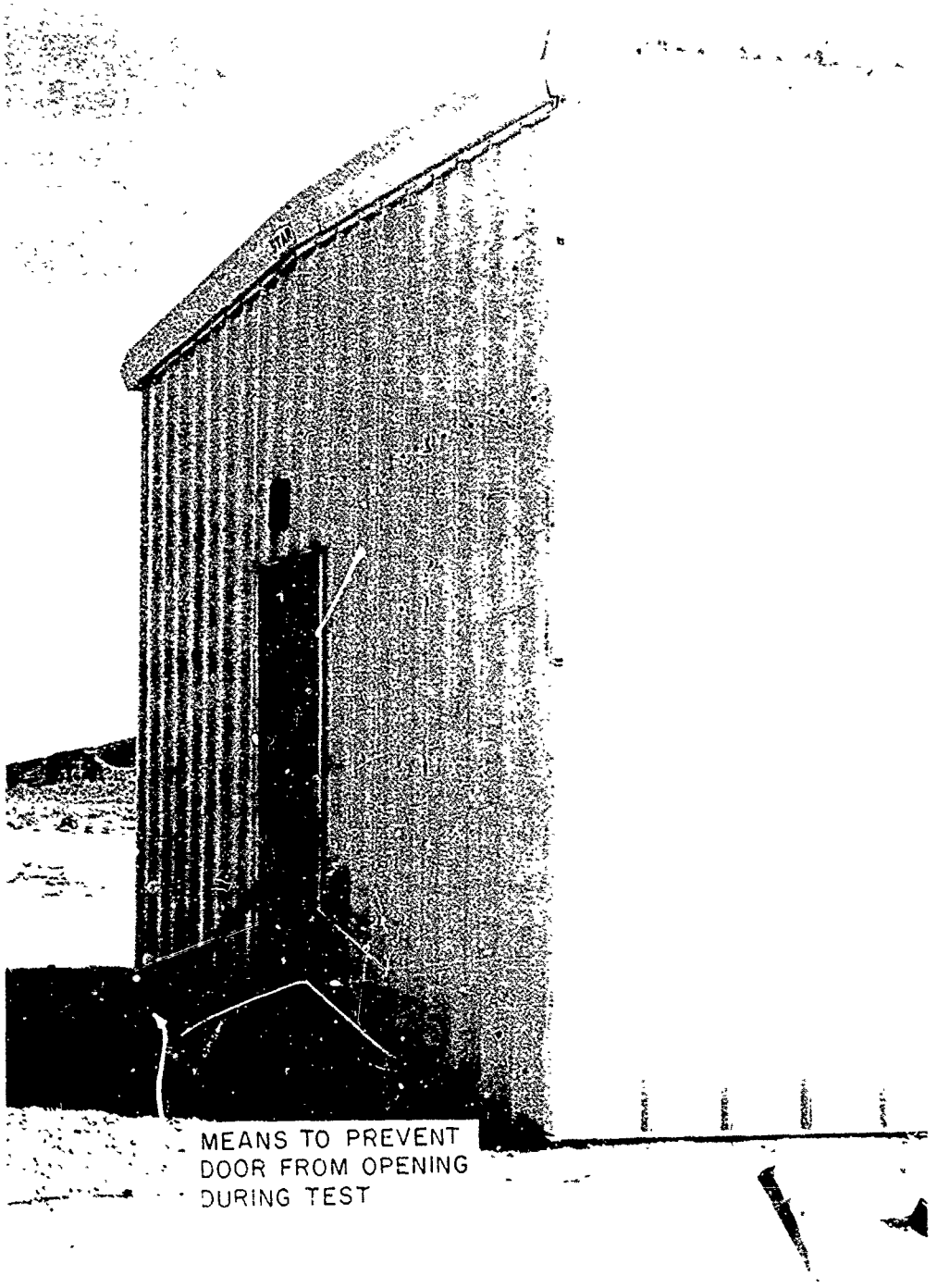

Fig 2 Exterior view of completed building

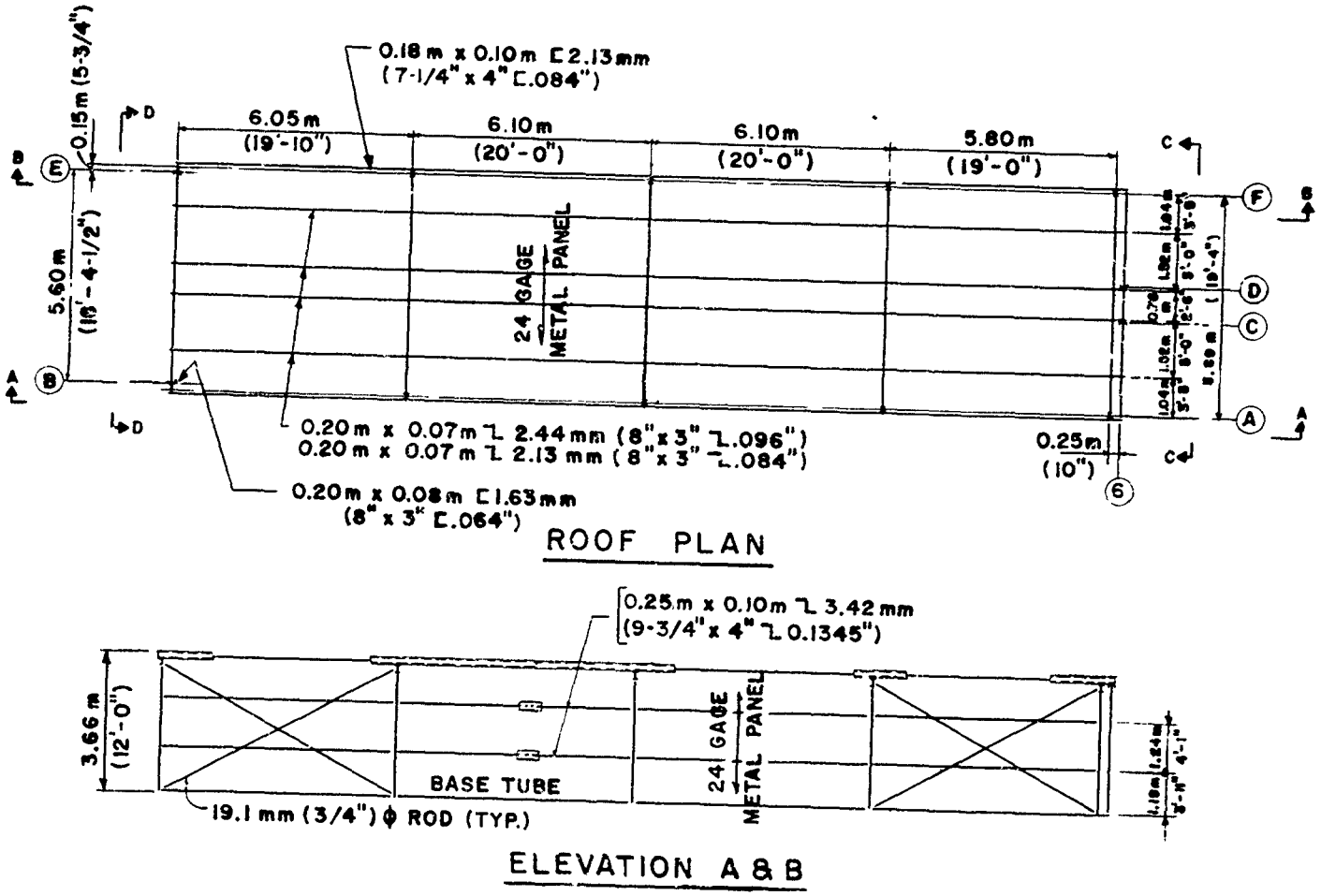

Fig 3 Framing of roof, and front and rear walls of test structure

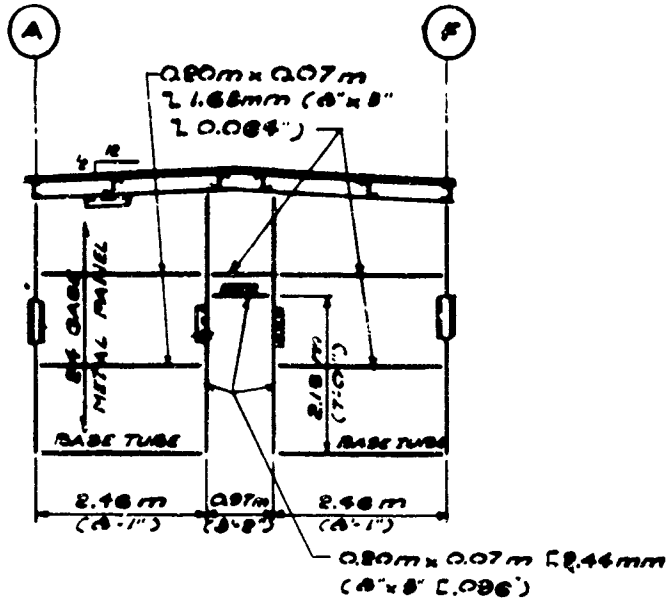

ELEVATION C

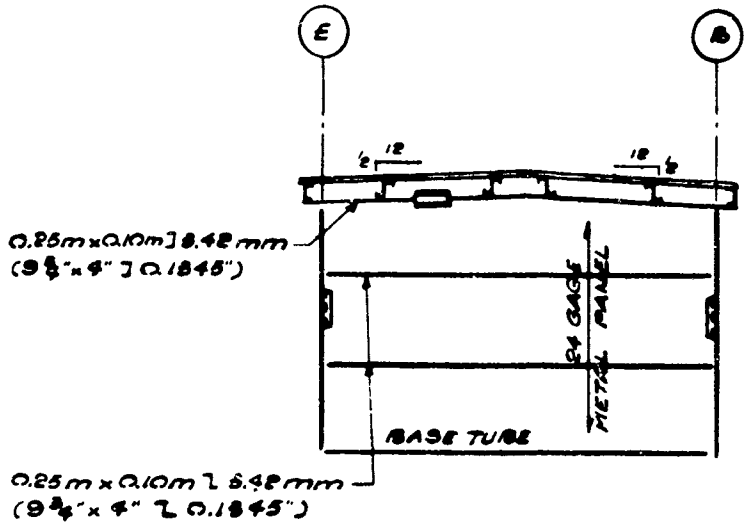

ELEVATION D

Fig 4 Framing of side walls of test structure

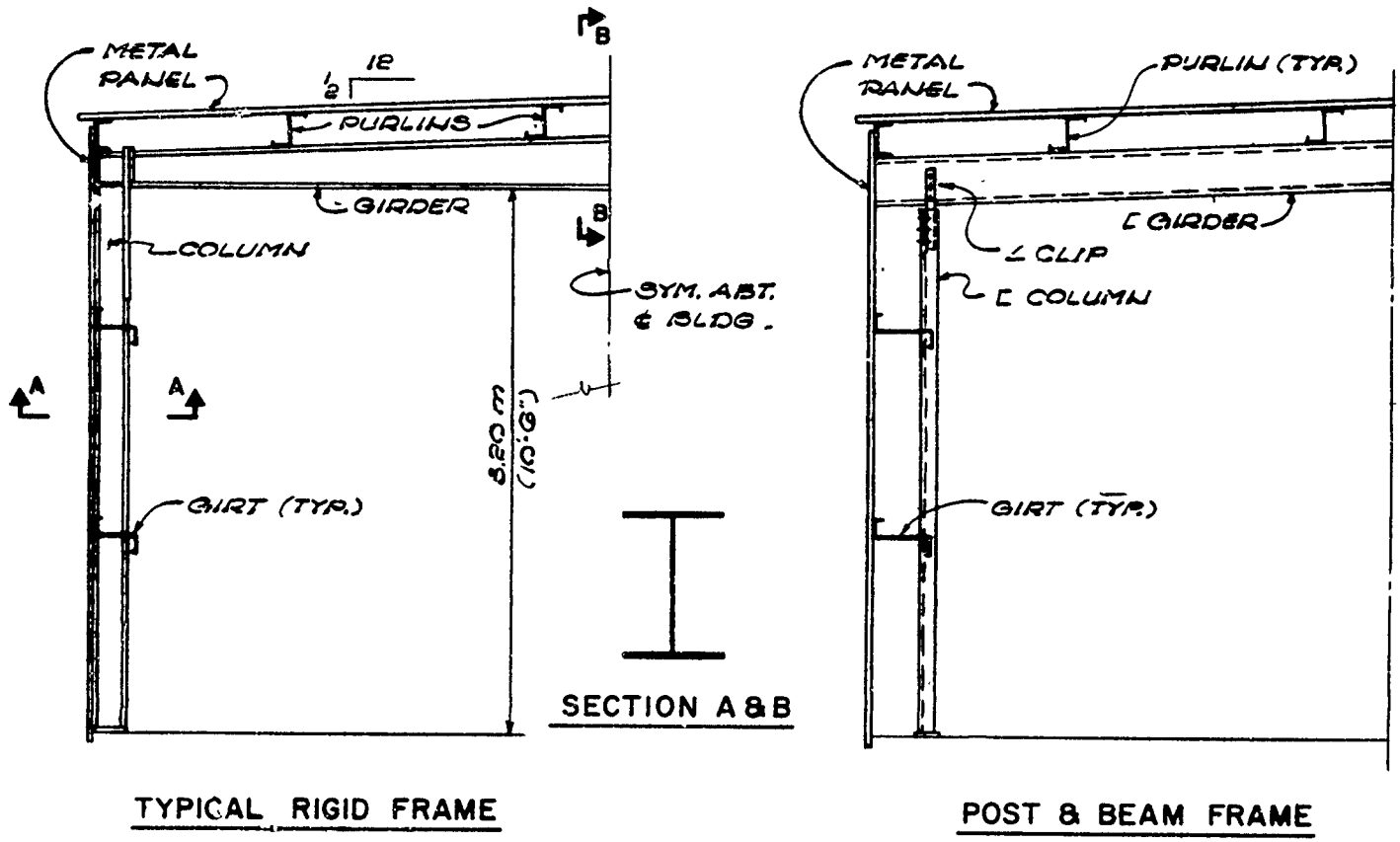

Fig 5 Typical rigid and post and beam frames

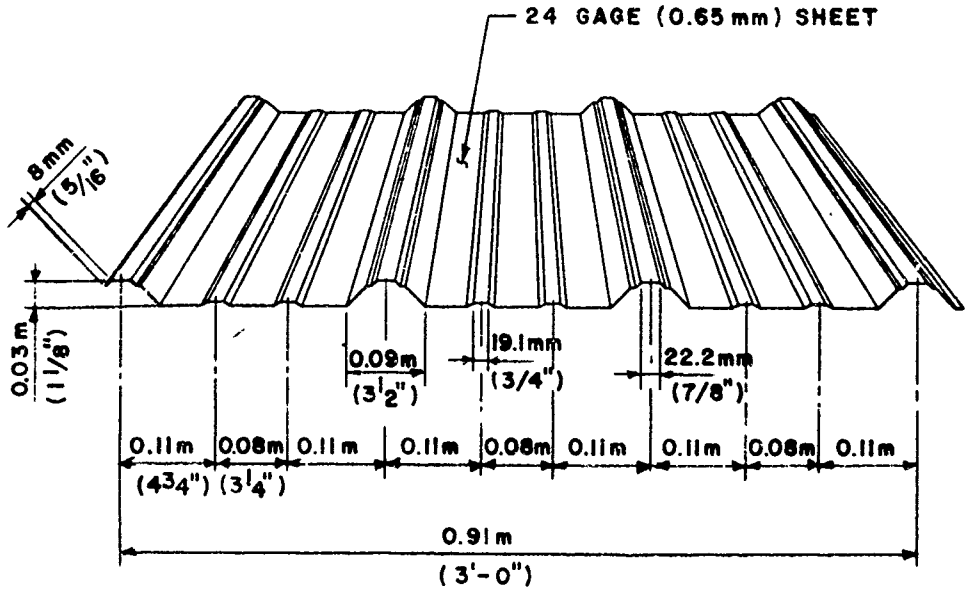

Fig 6 Wall and roof panel profile

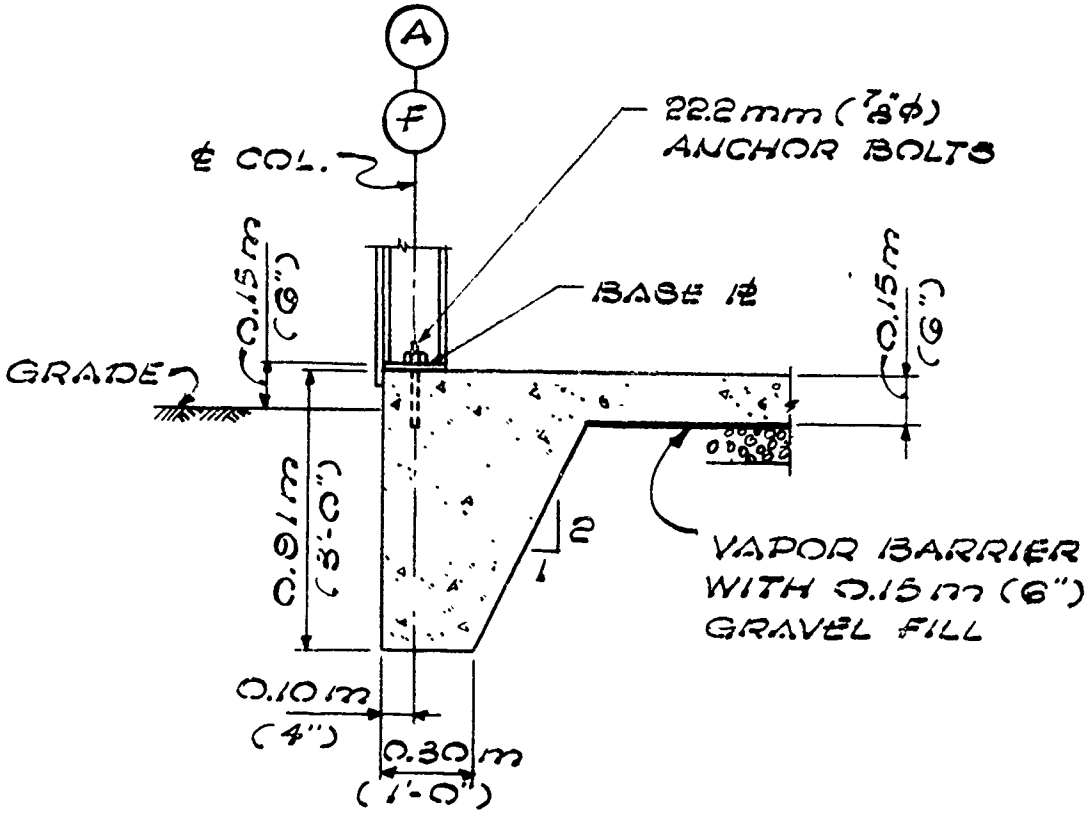

Fig 7 Typical foundation section

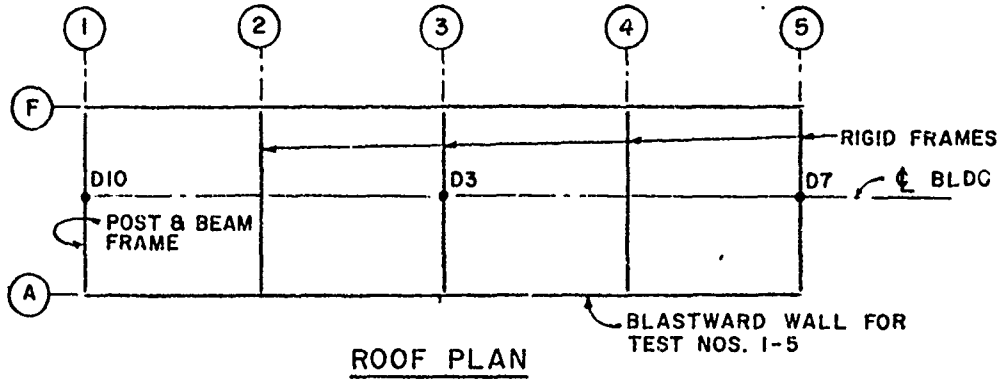

ROOF PLAN

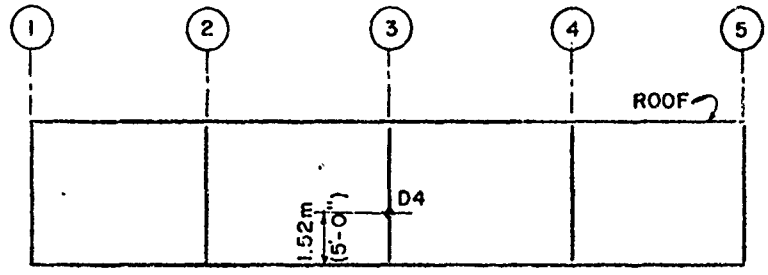

ELEVATION - LEEWARD WALL

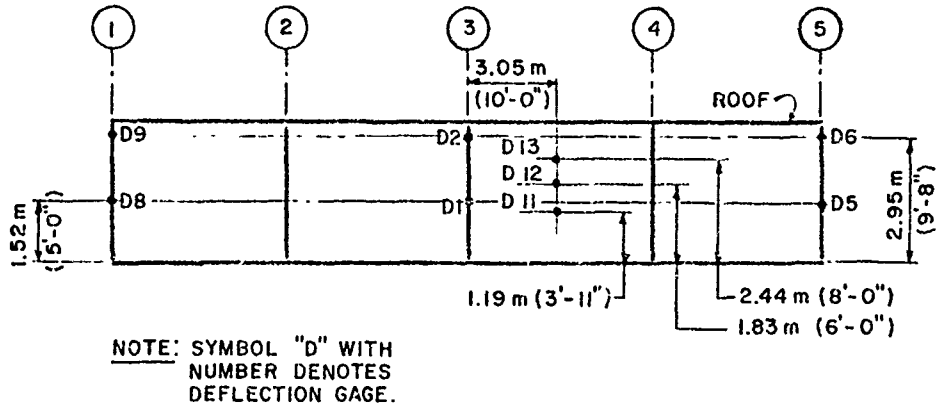

NOTE: SYMBOL "D" WITH NUMBER DENOTES DEFLECTION GAGE.

ELEVATION - BLASTWARD WALL

Fig 8 Locations of deflection gages on test structure

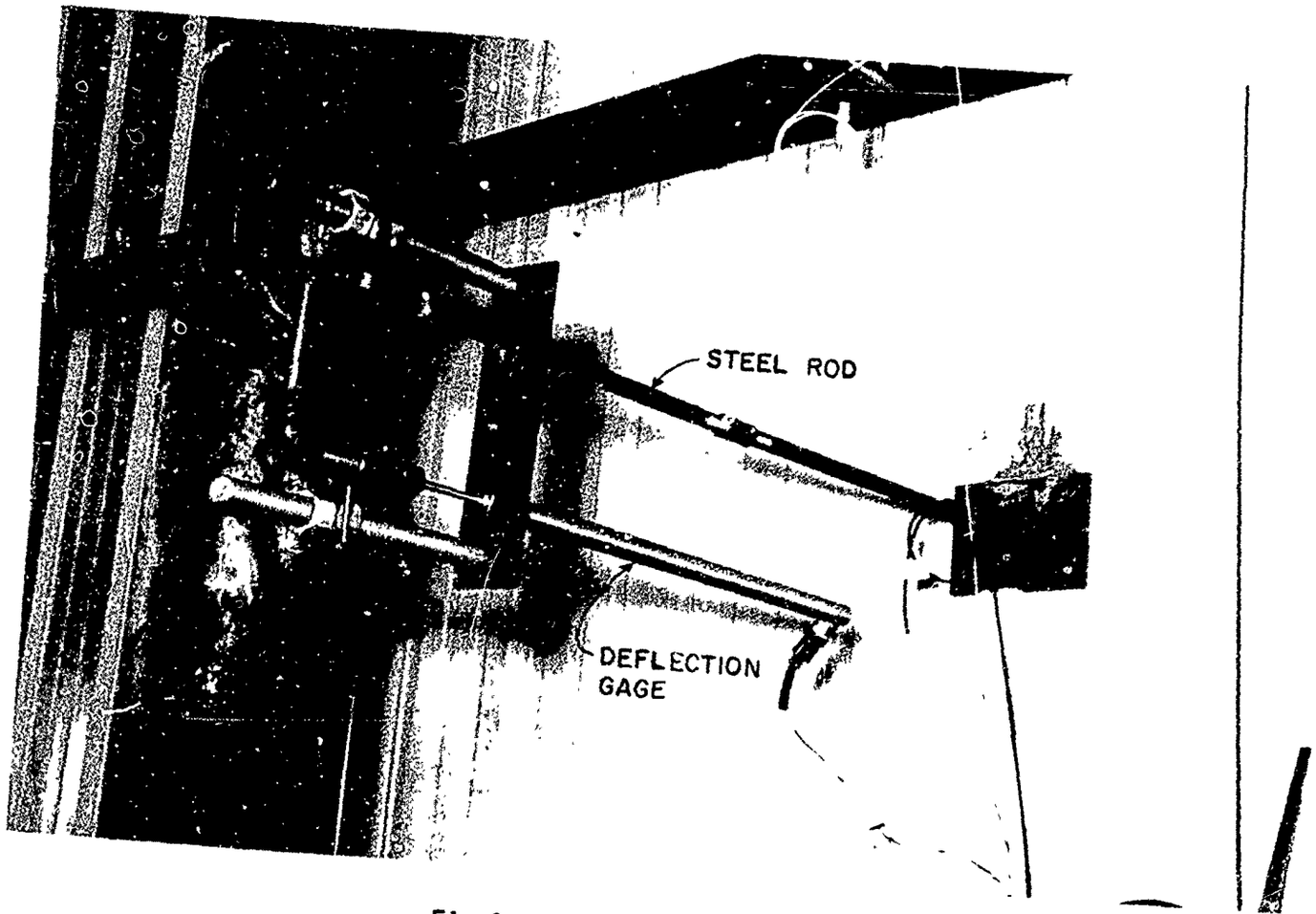

Fig 9 Typical deflection gage mount

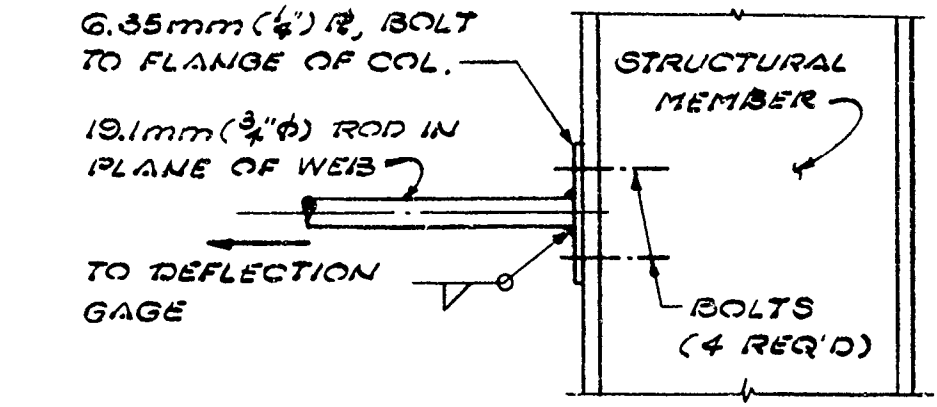

a) TYP. ATTACHMENT FOR HORIZONTAL GAGE

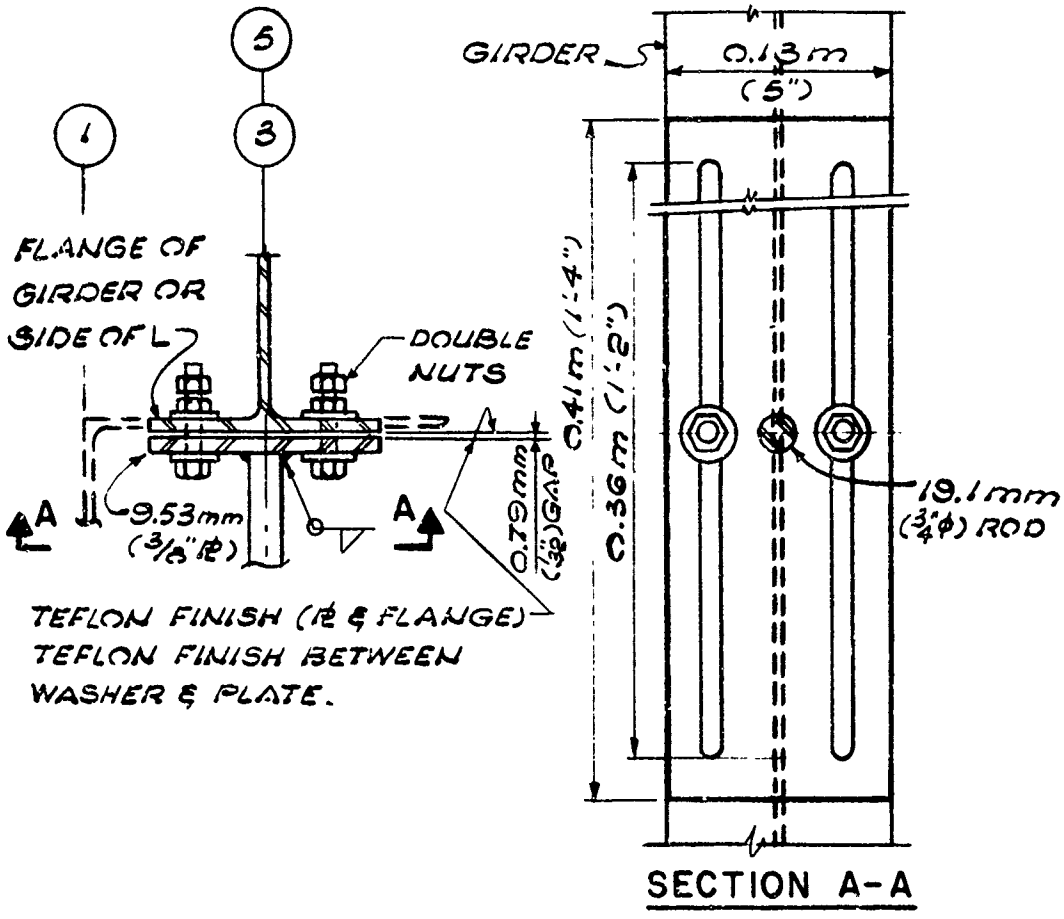

b) TYP. ATTACHMENT FOR VERTICAL GAGE

Fig 10 Deflection gage attachment details

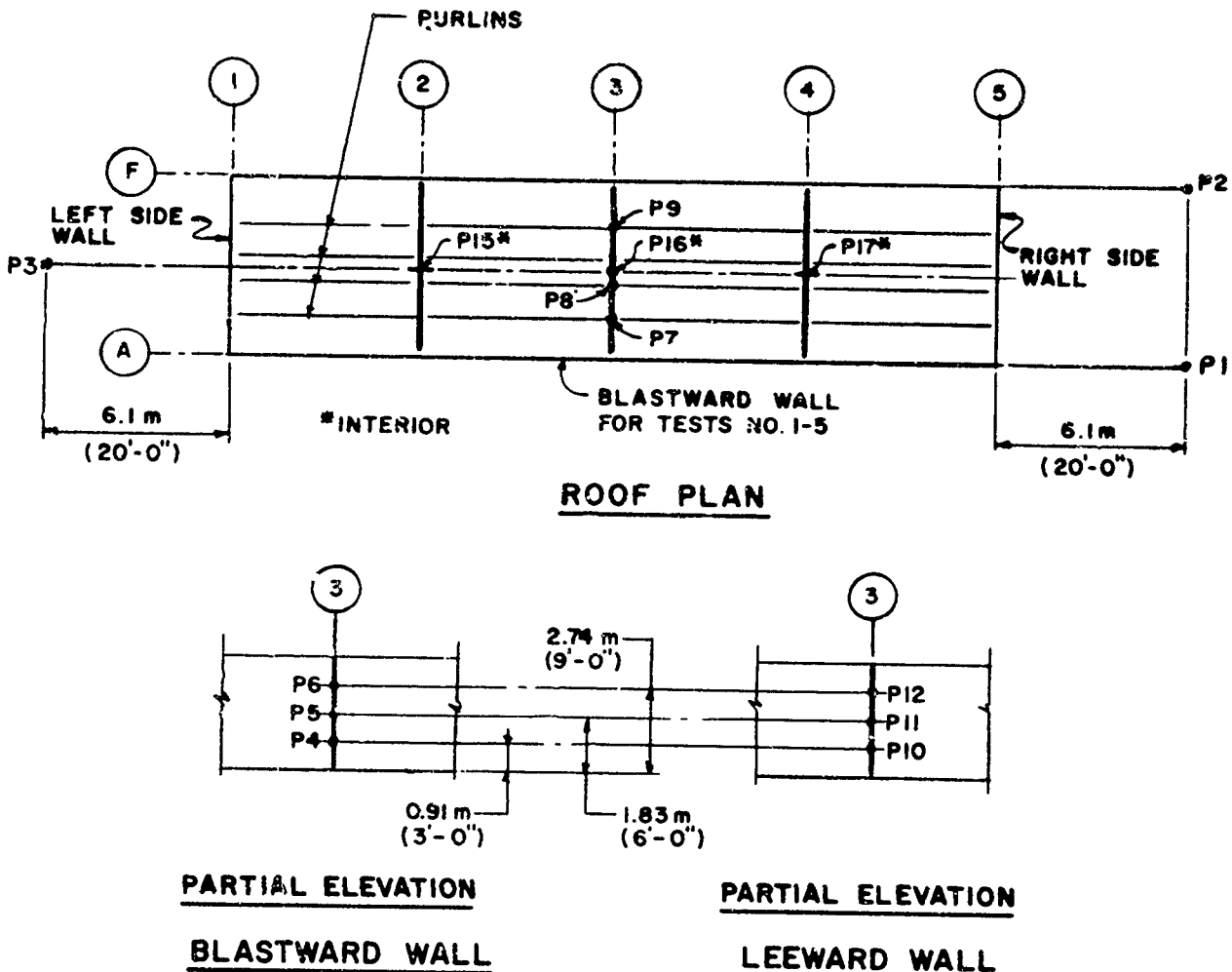

Fig 11 Locations of pressure gages on roof and front and rear walls of test structure

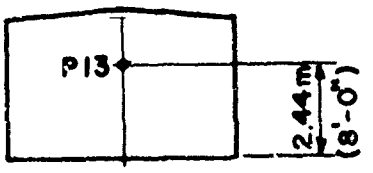

RIGHT SIDE

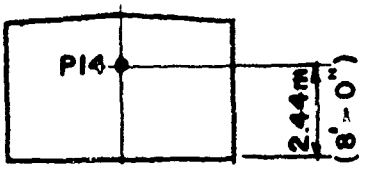

LEFT SIDE

SIDEWALL ELEVATIONS

Fig 12 Locations of pressure gages on side walls of test structure

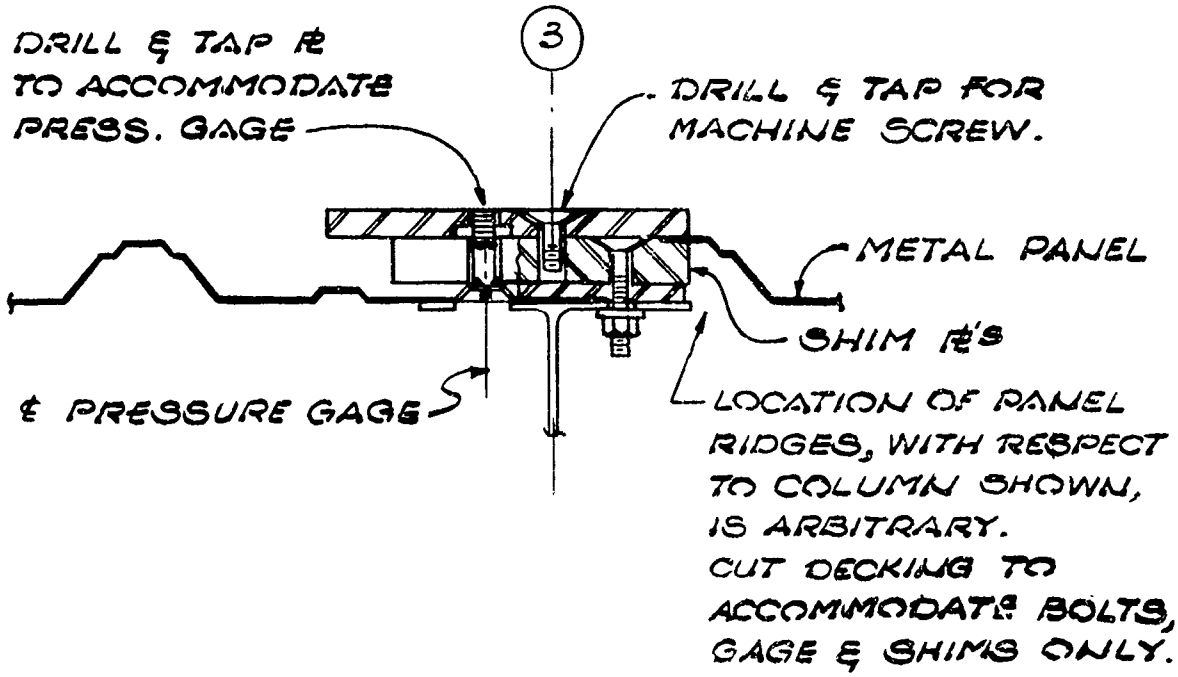

Fig 13 Typical pressure gage attachment detail

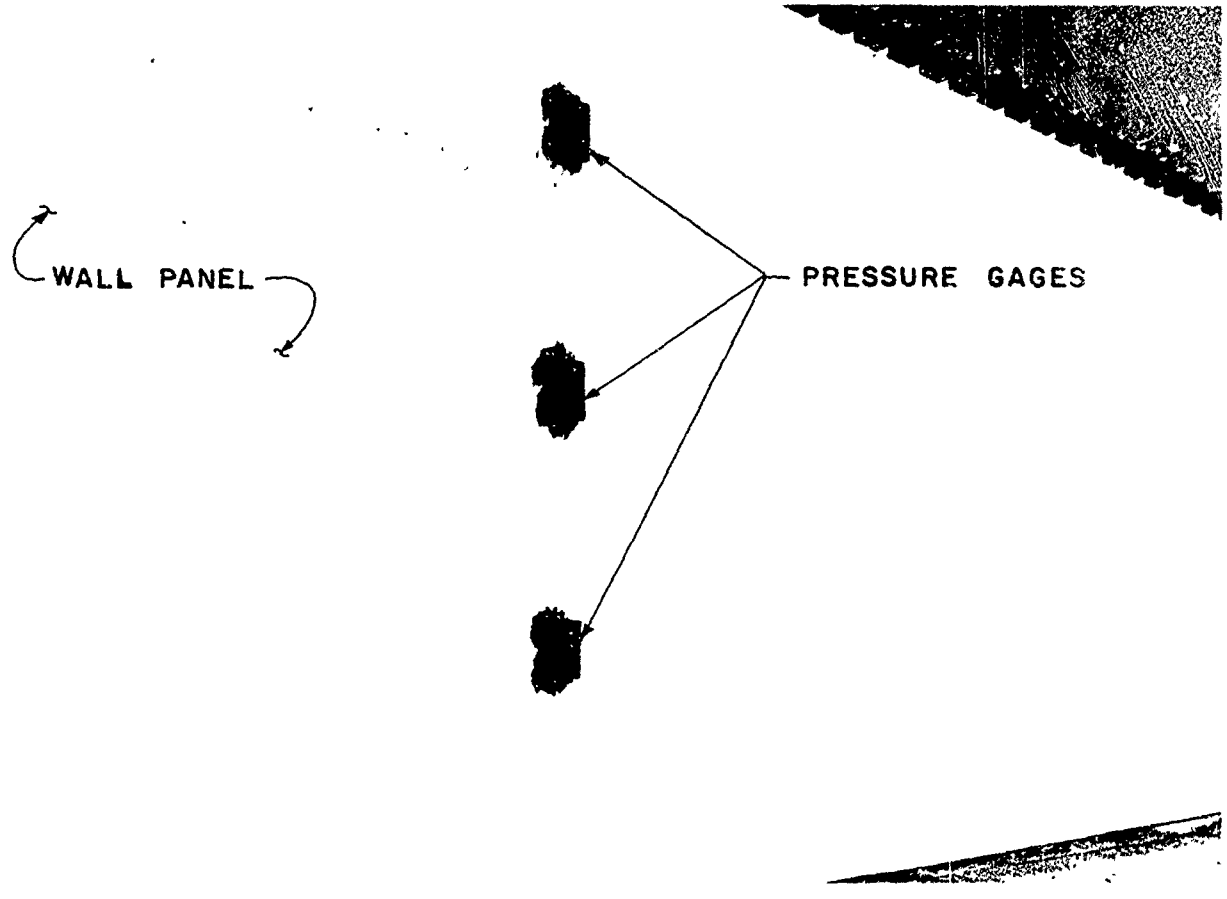

Fig 14 Exterior wall pressure gages

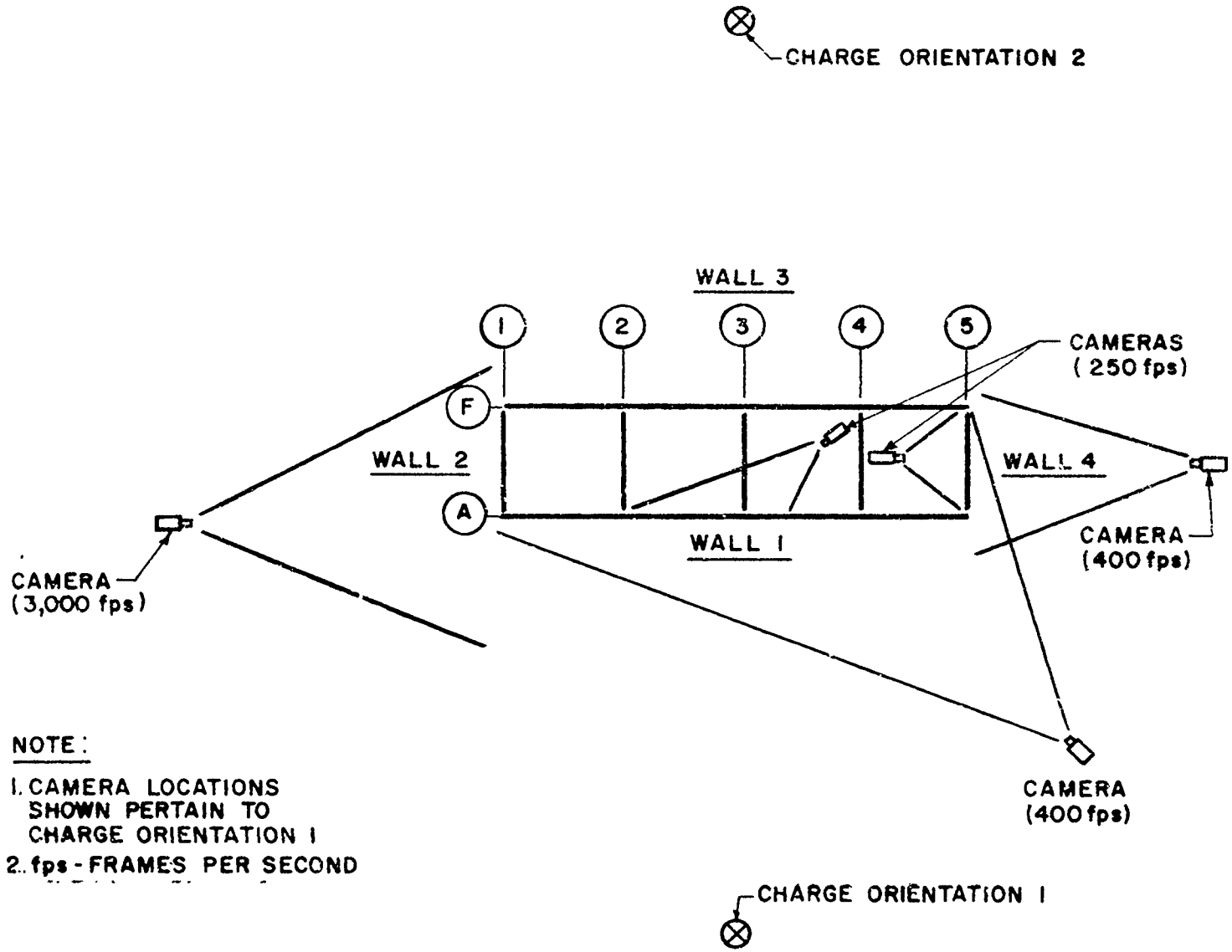

Fig 15 Orientation of explosive charge and camera coverage

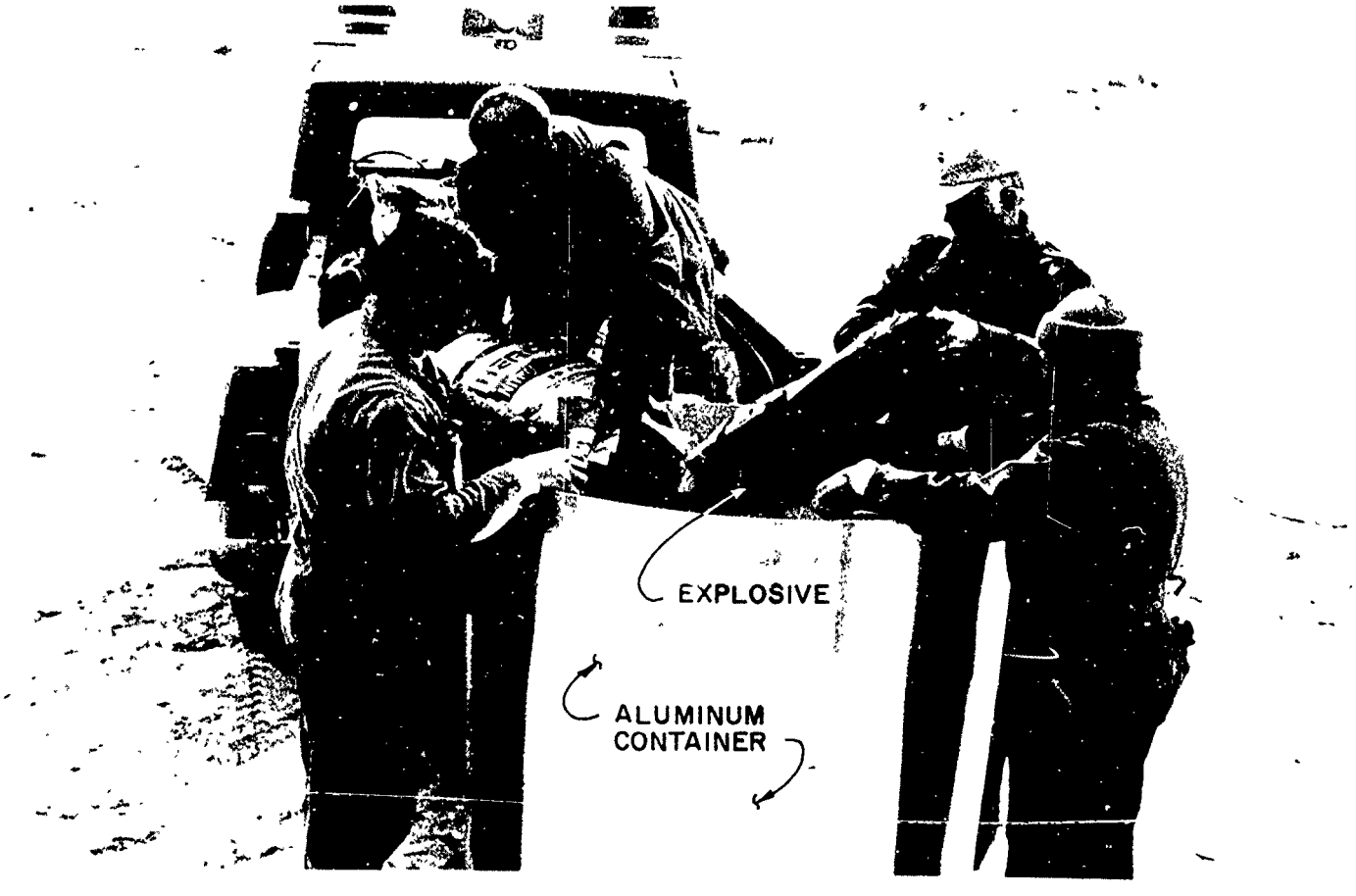

Fig 16 Preparation of explosive charge

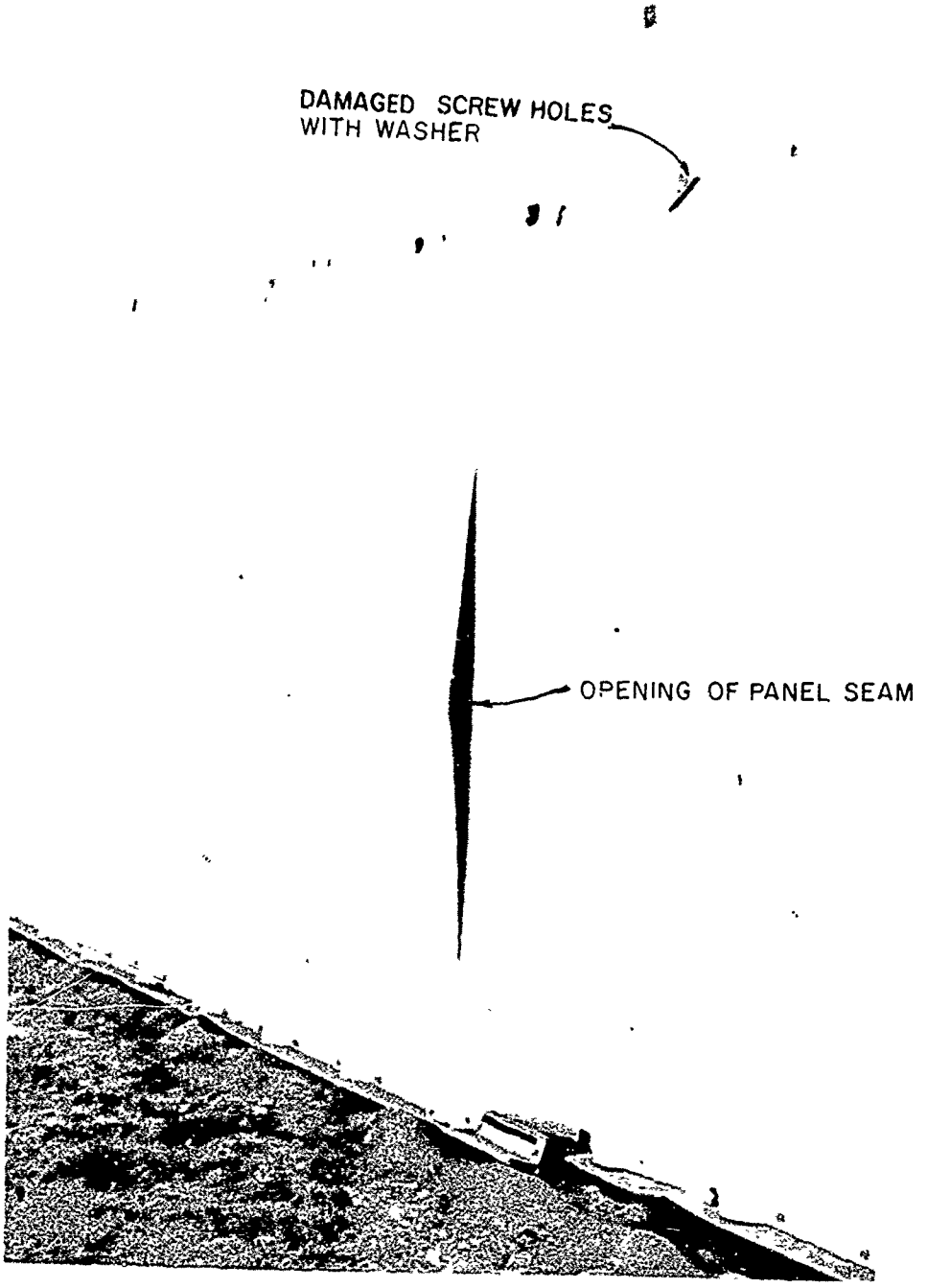

Fig 17 Permanent gaps in wall panel seams

Fig 18 Pulling away of panel anchorage

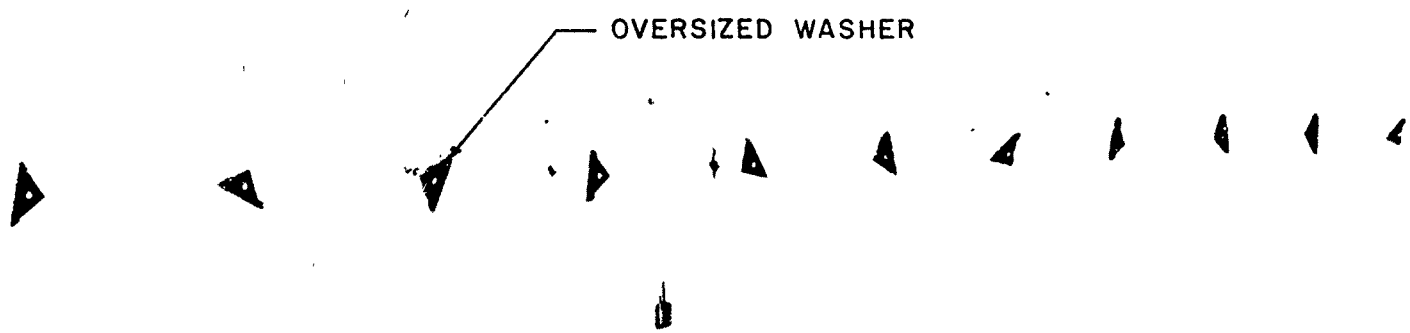

Fig 19 Oversized washers for panel attachment screws

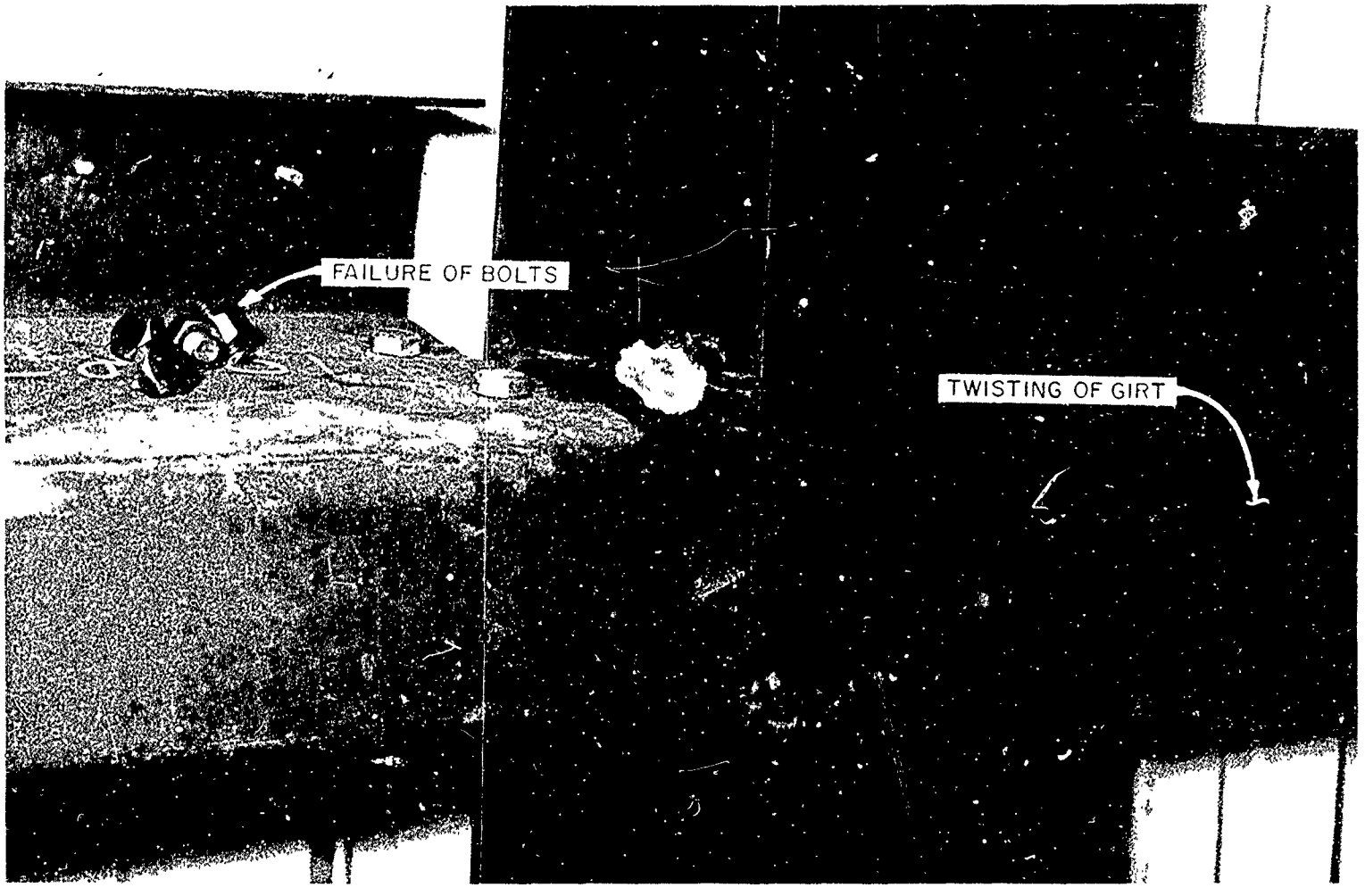

Fig 20 Damage to girt and connections

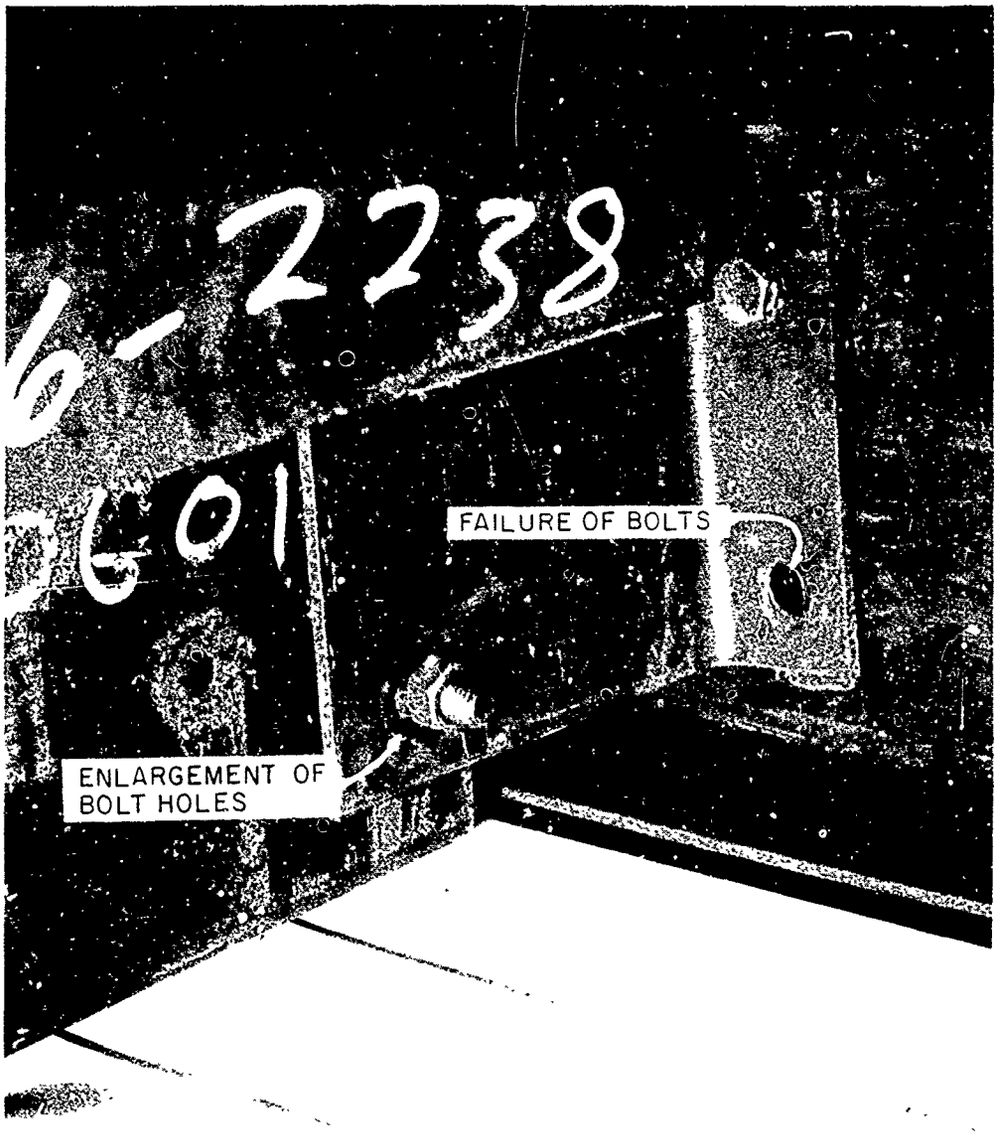

Fig 21 Enlargement of bolt holes in girt clip angle

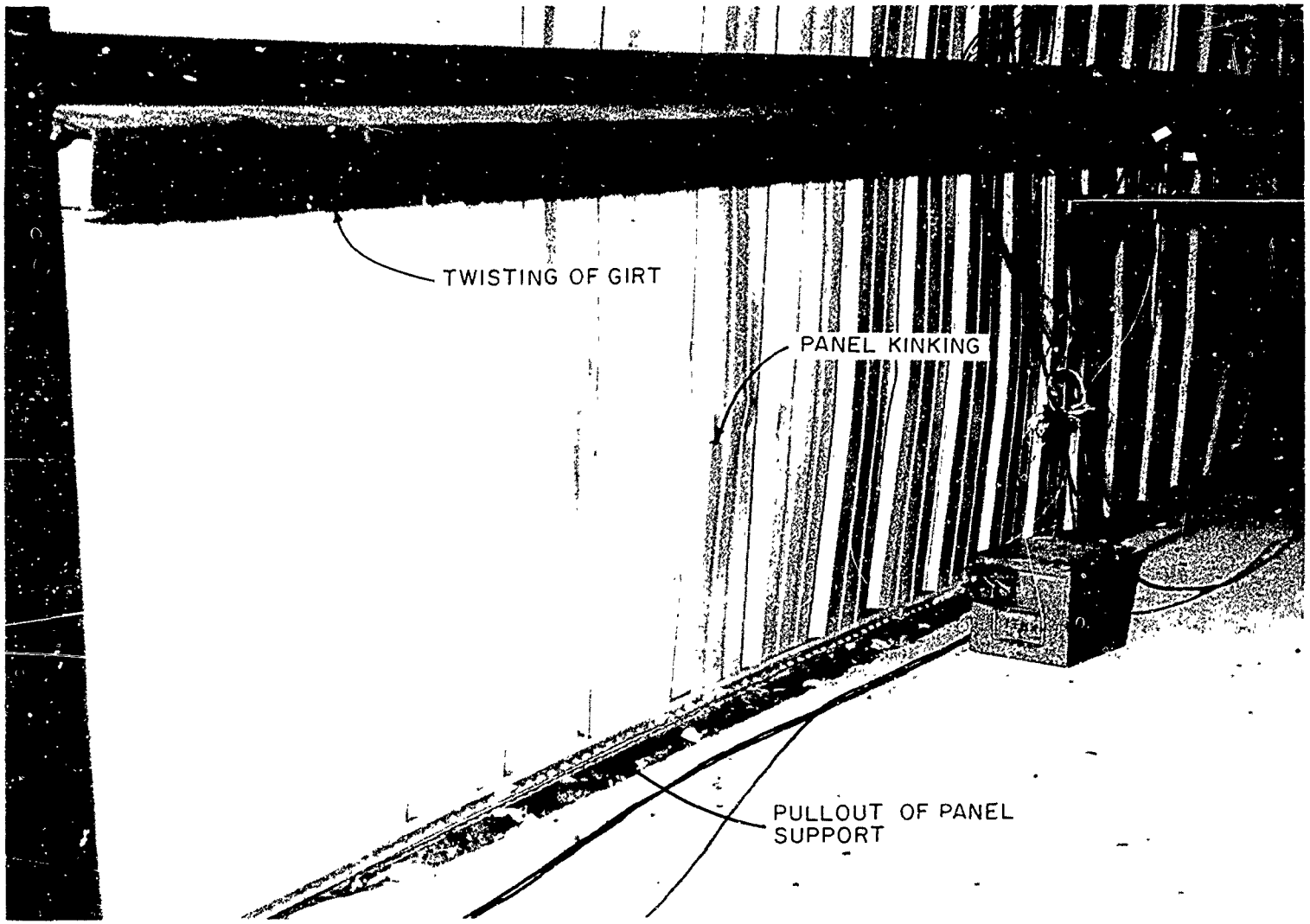

Fig 22 Blastward wall damage in Test No. 5

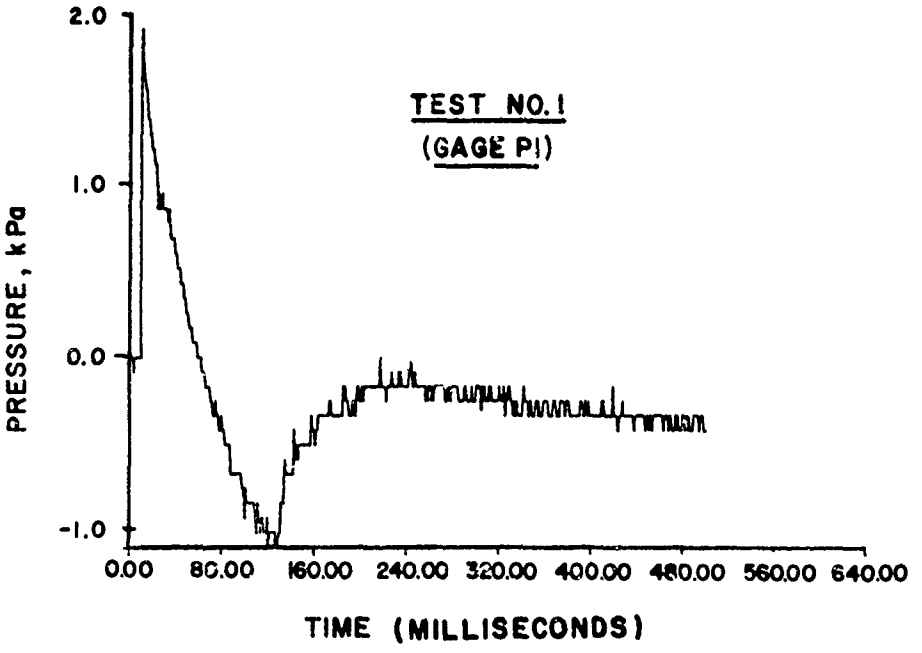

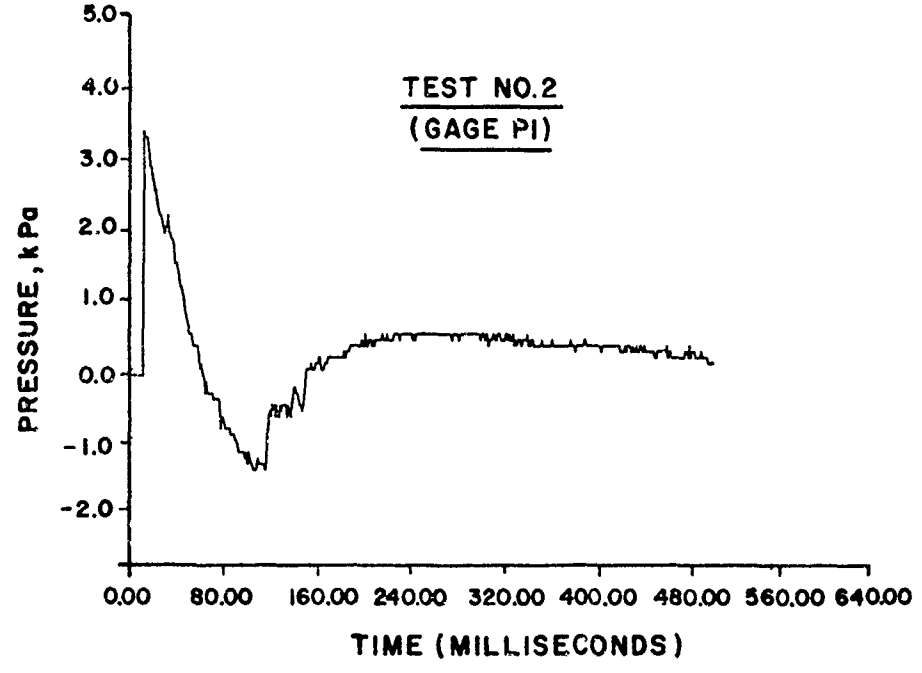

Fig 23 Measured free-field pressures for Tests Nos. 1 and 2

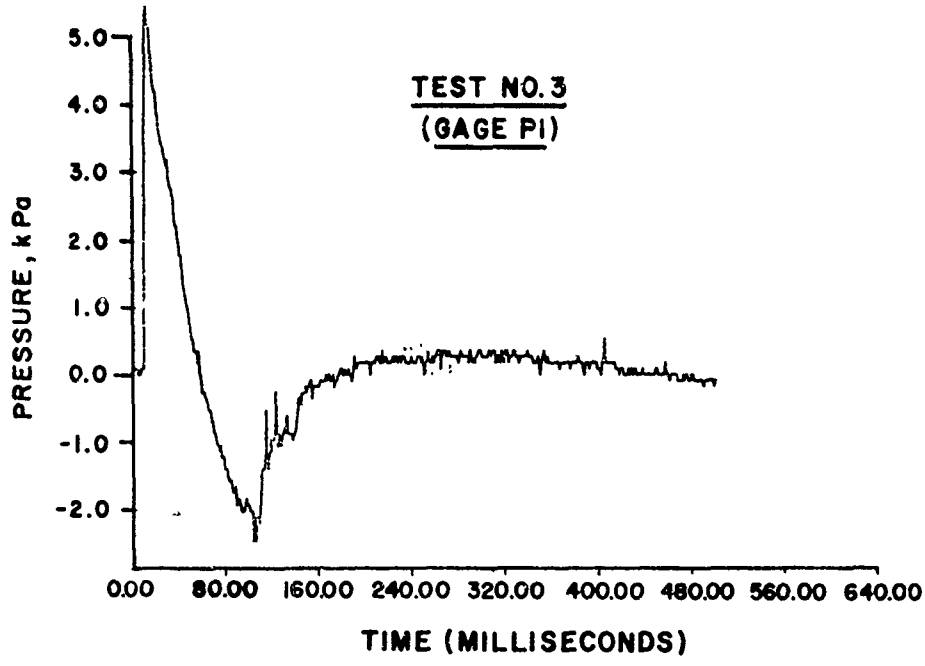

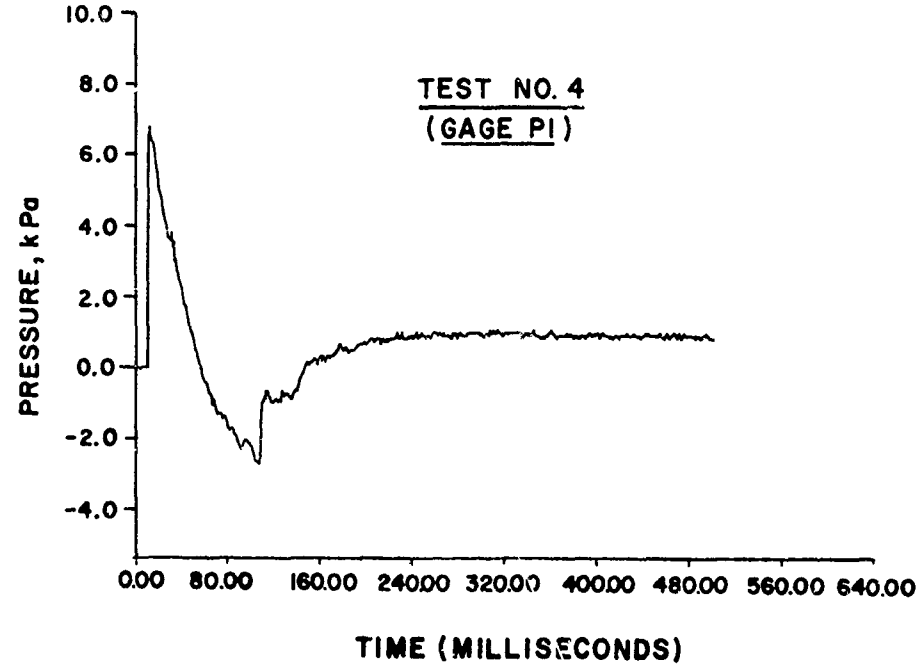

Fig 24 Measured free-field pressures for Tests Nos. 3 and 4

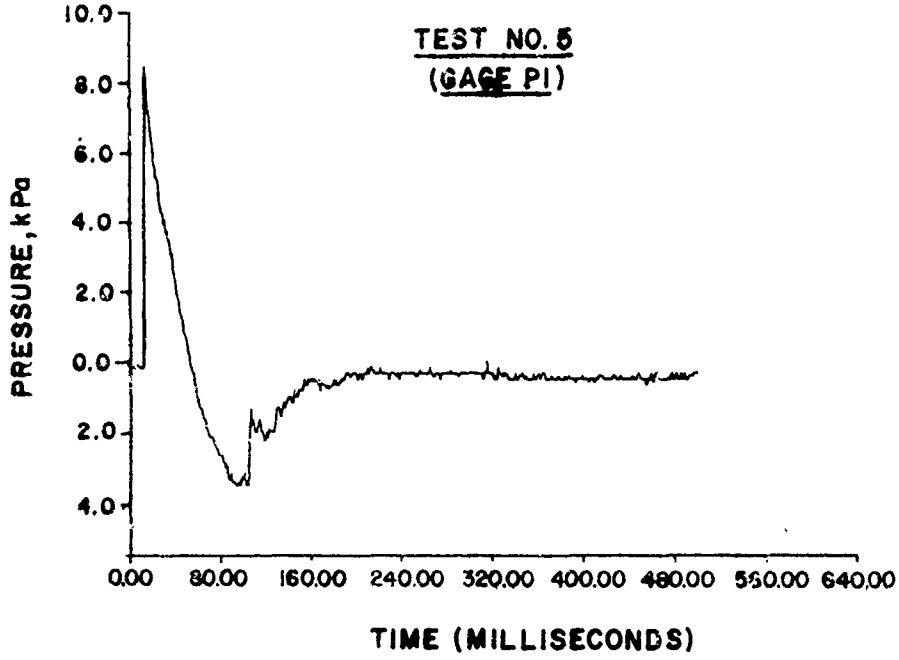

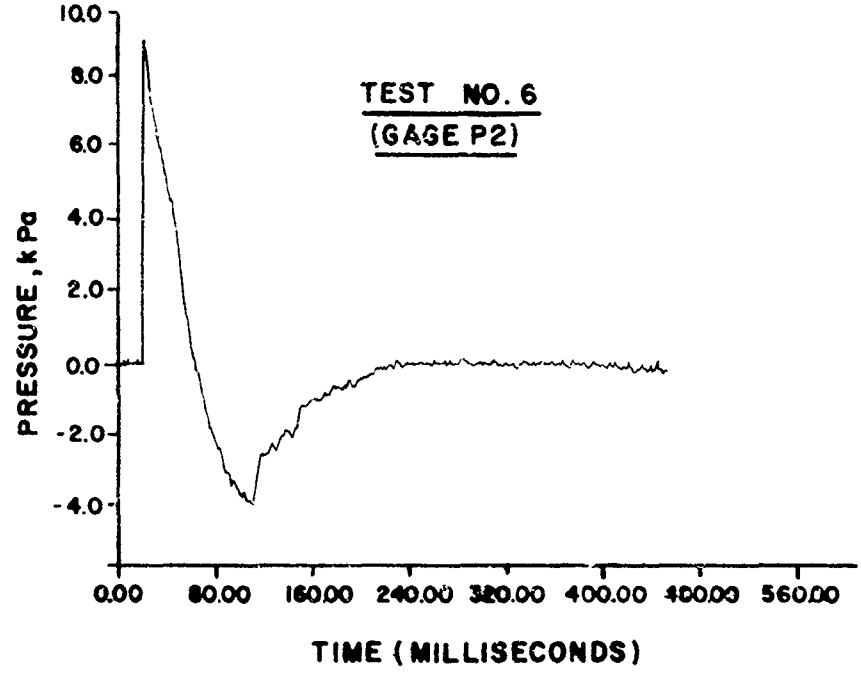

Fig 25 Measured free-field pressures for Tests Nos. 5 and 6

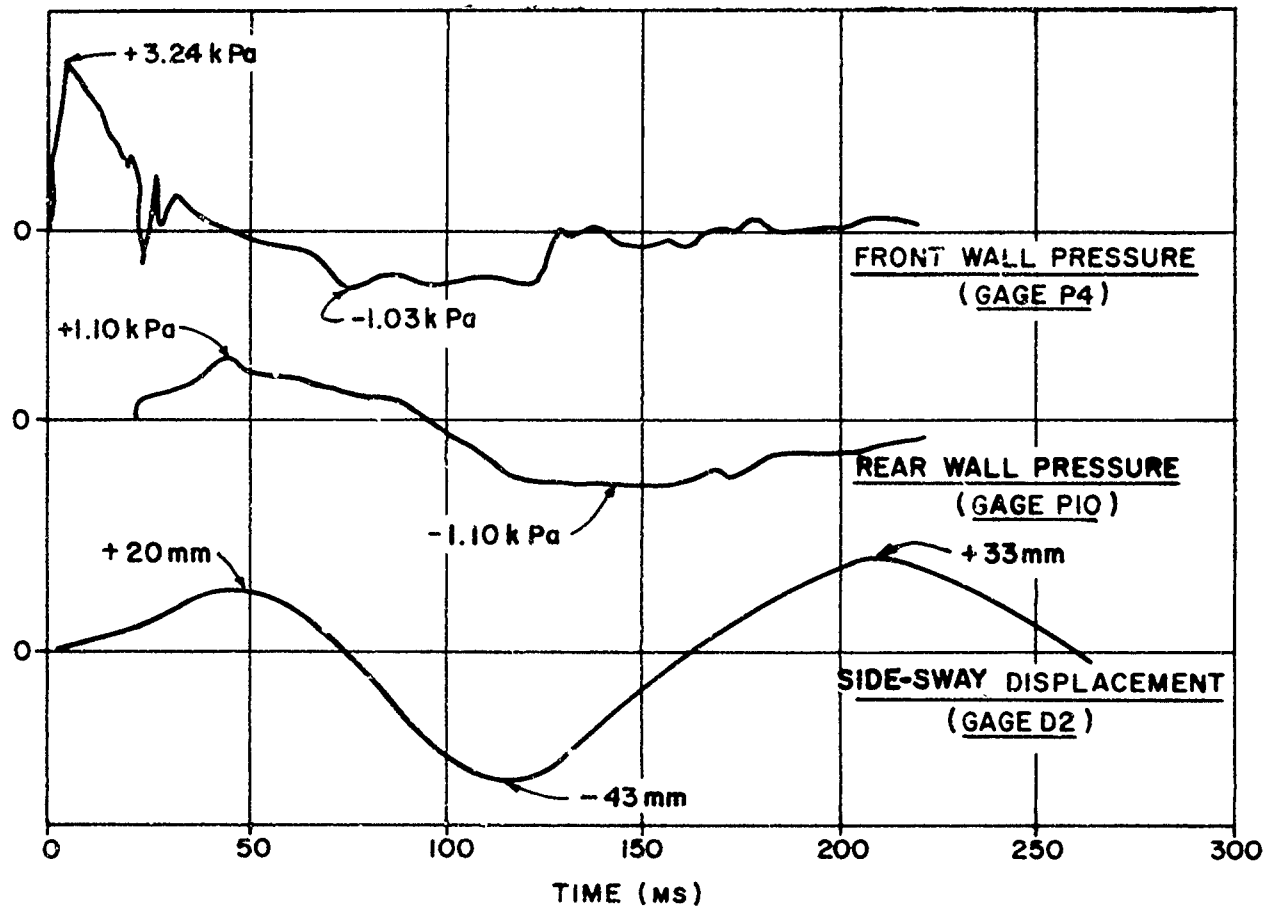

Fig 26 Measured building pressures and side-sway displacement for Test No. 1

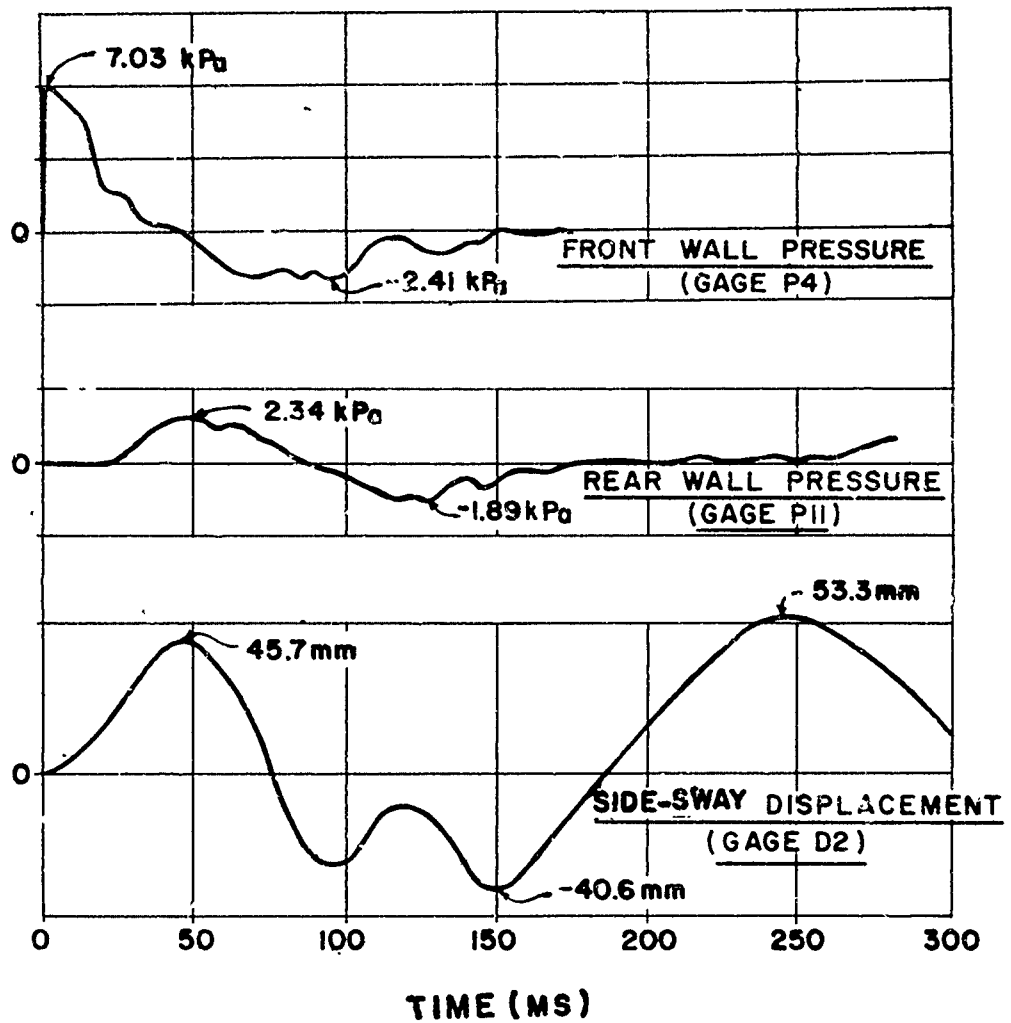

Fig 27 Measured building pressures and side-sway displacement for Test No. 2

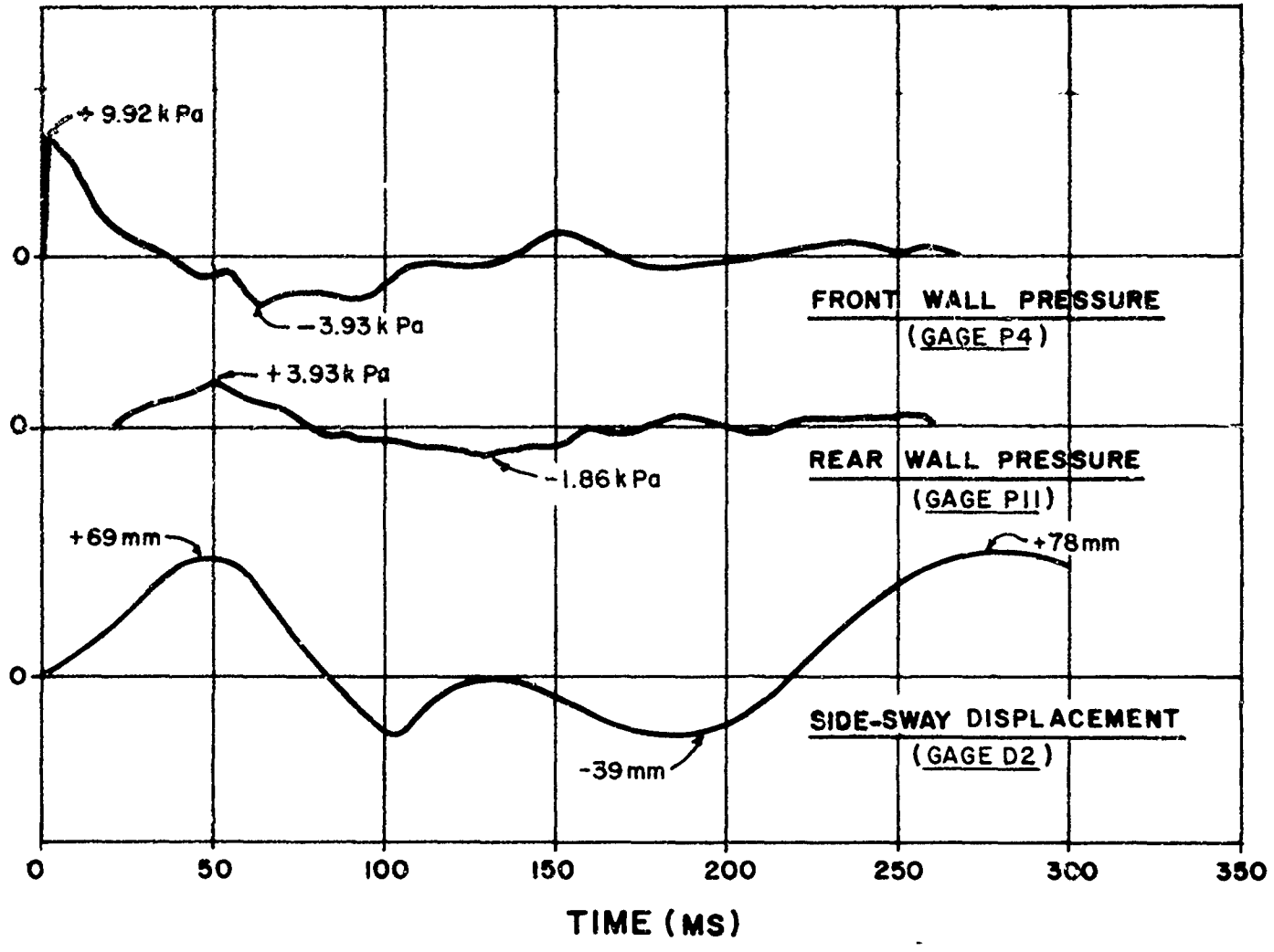

Fig 28 Measured building pressures and side-sway displacement for Test No. 3

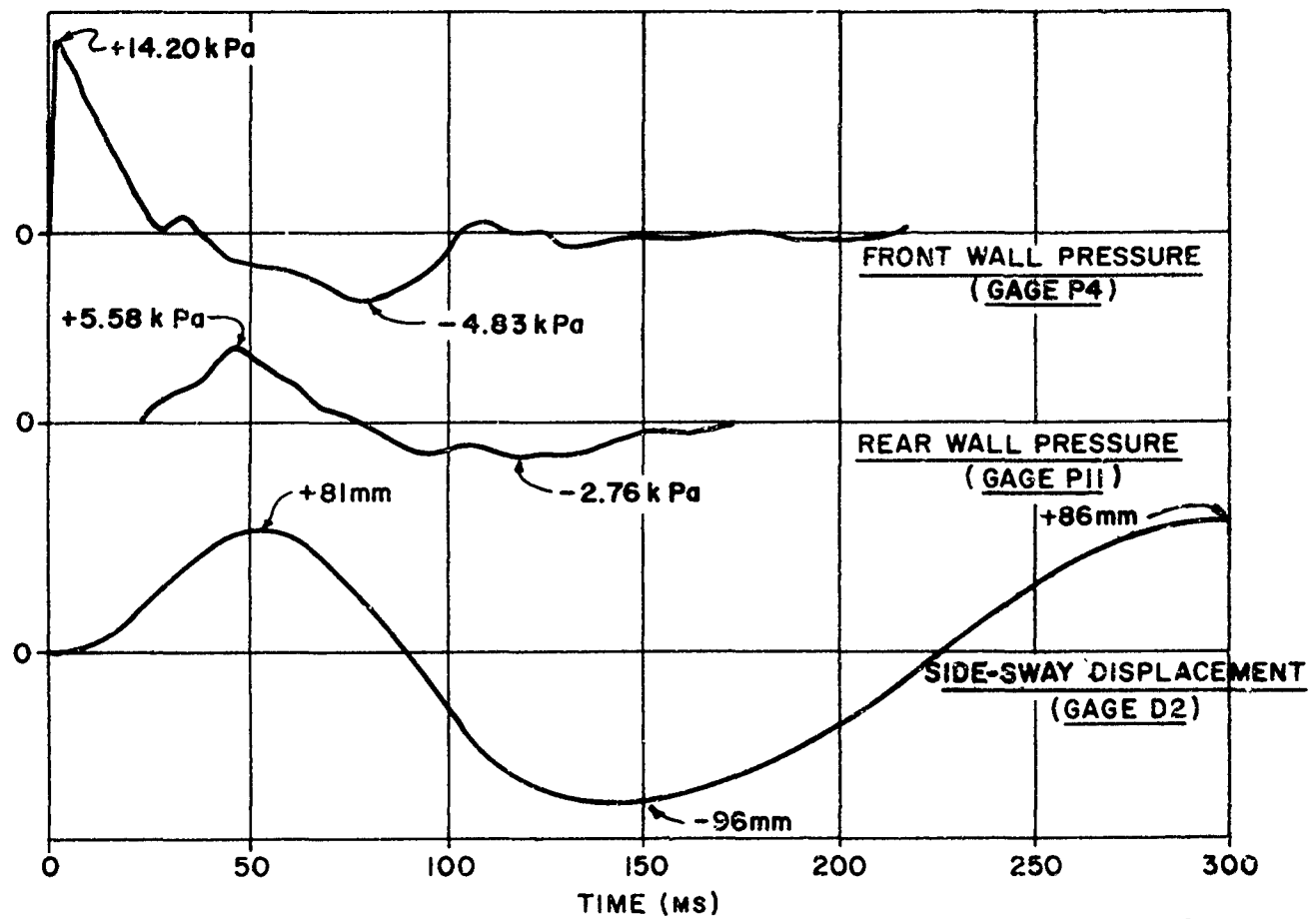

Fig 29 Measured building pressures and side-sway displacement for Test No. 4

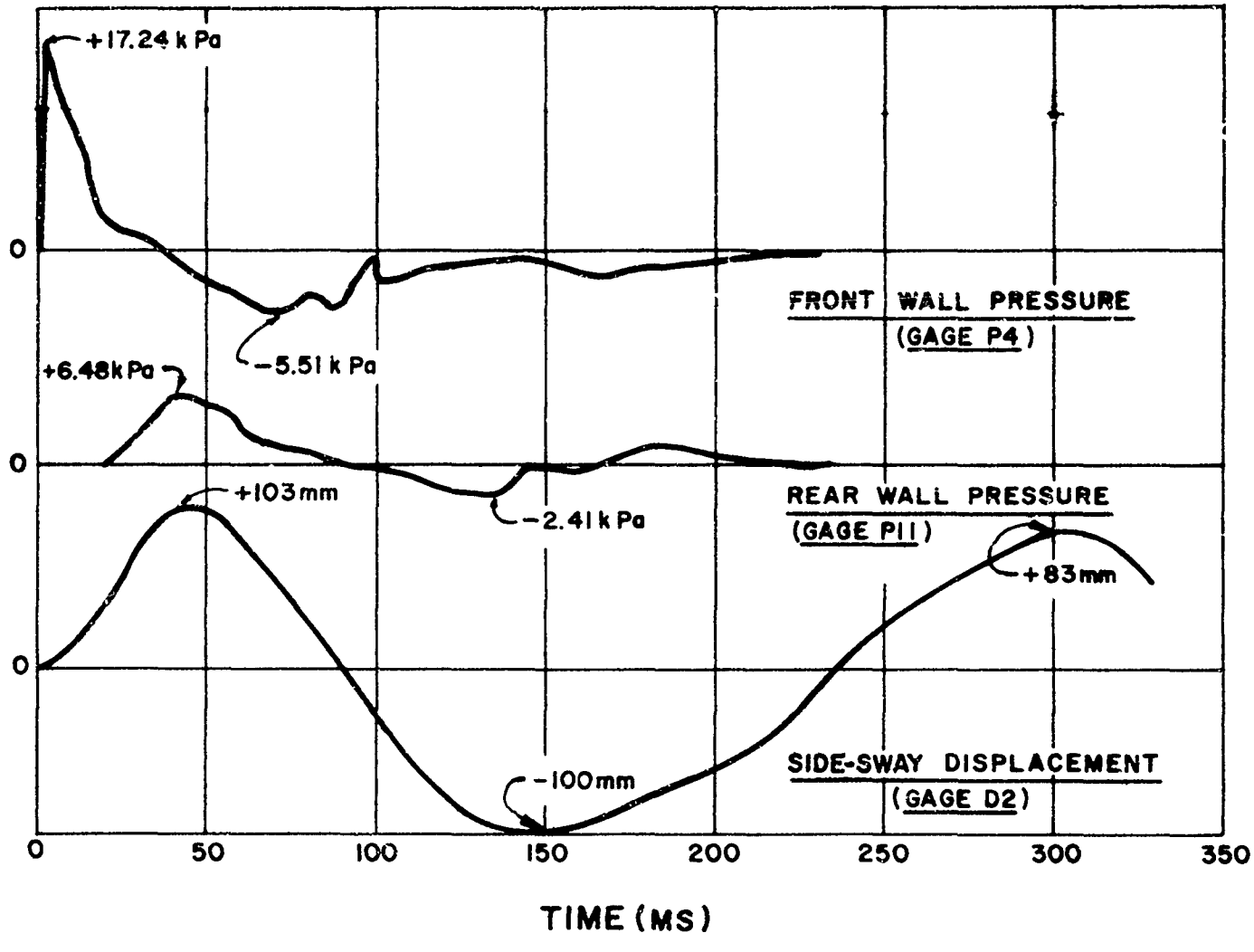

Fig 30 Measured building pressures and side-sway displacement for Test No. 5

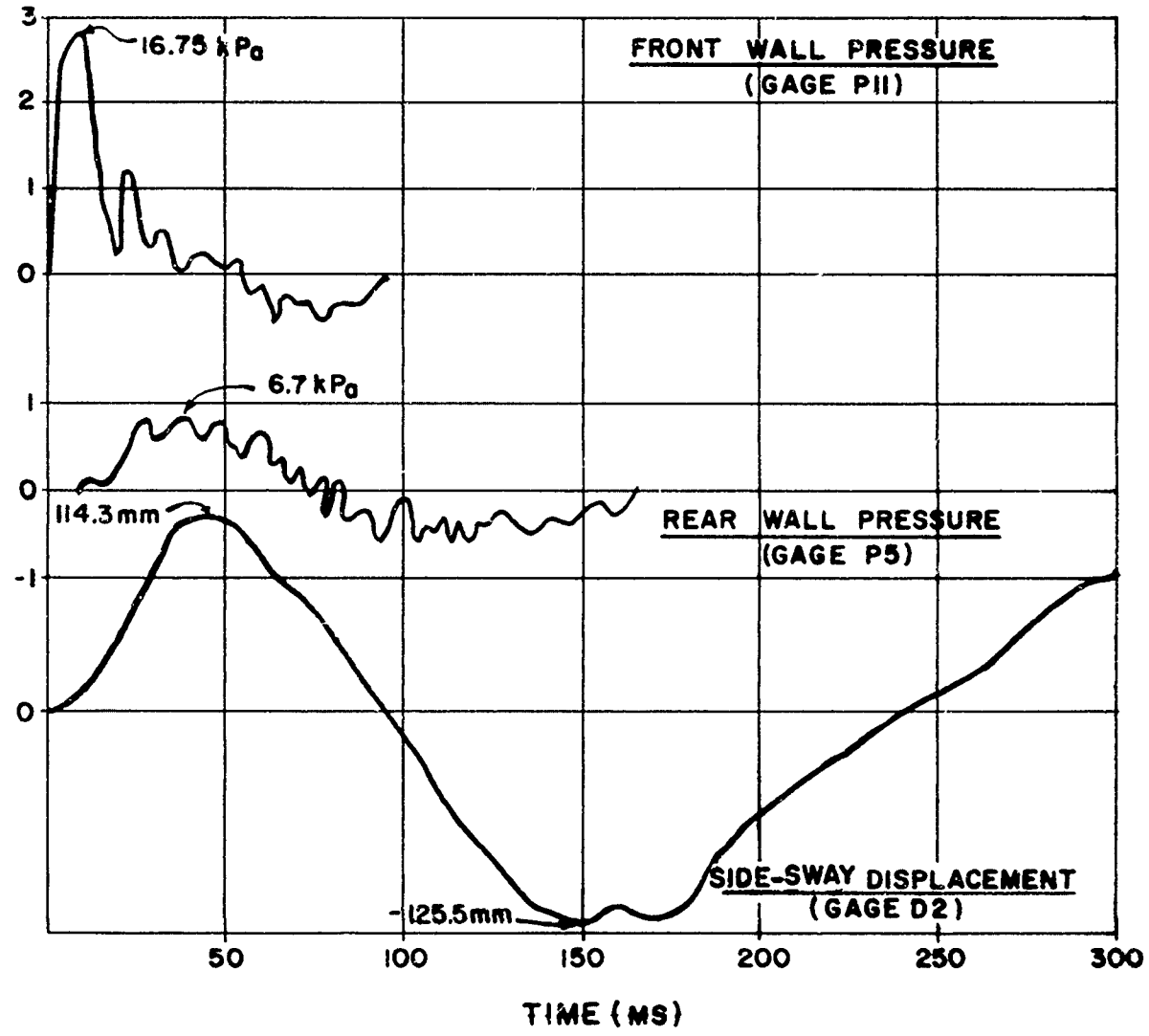

Fig 31 Measured building pressures and side-sway displacement for Test No. 6

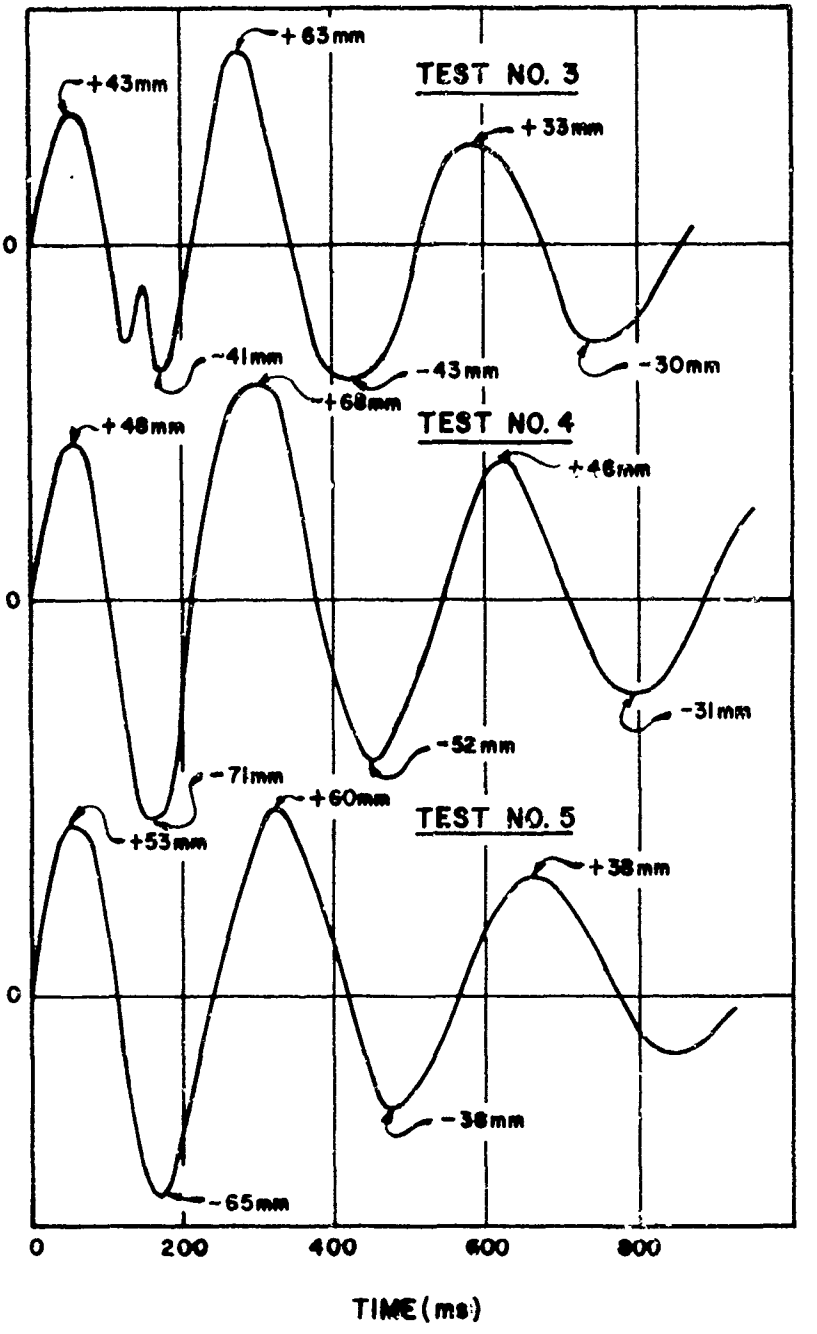

Fig 32 Measured side-sway displacements (Deflection Gage D6) for rigid end frame

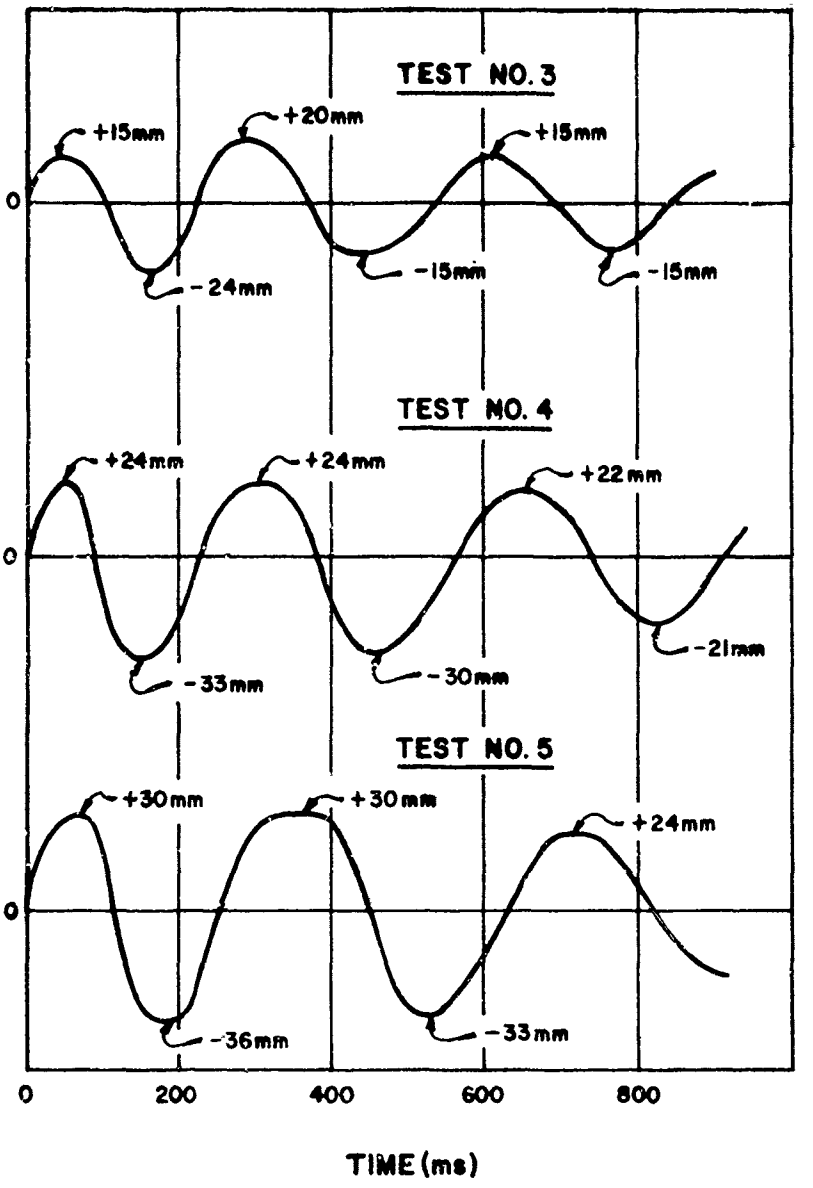

Fig 33 Measured side-sway displacements (Deflection Gage D9) for post and beam end frame

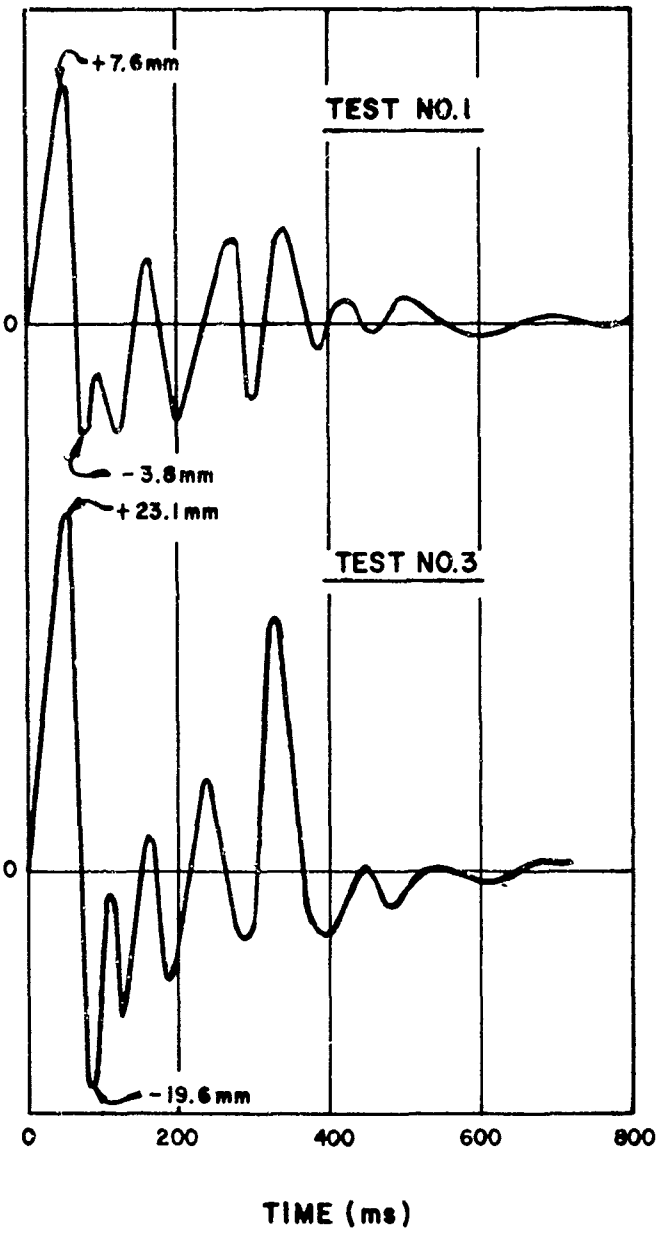

Fig 34 Measured vertical displacements (Deflection Gage D3) at mid-span of center frame girder

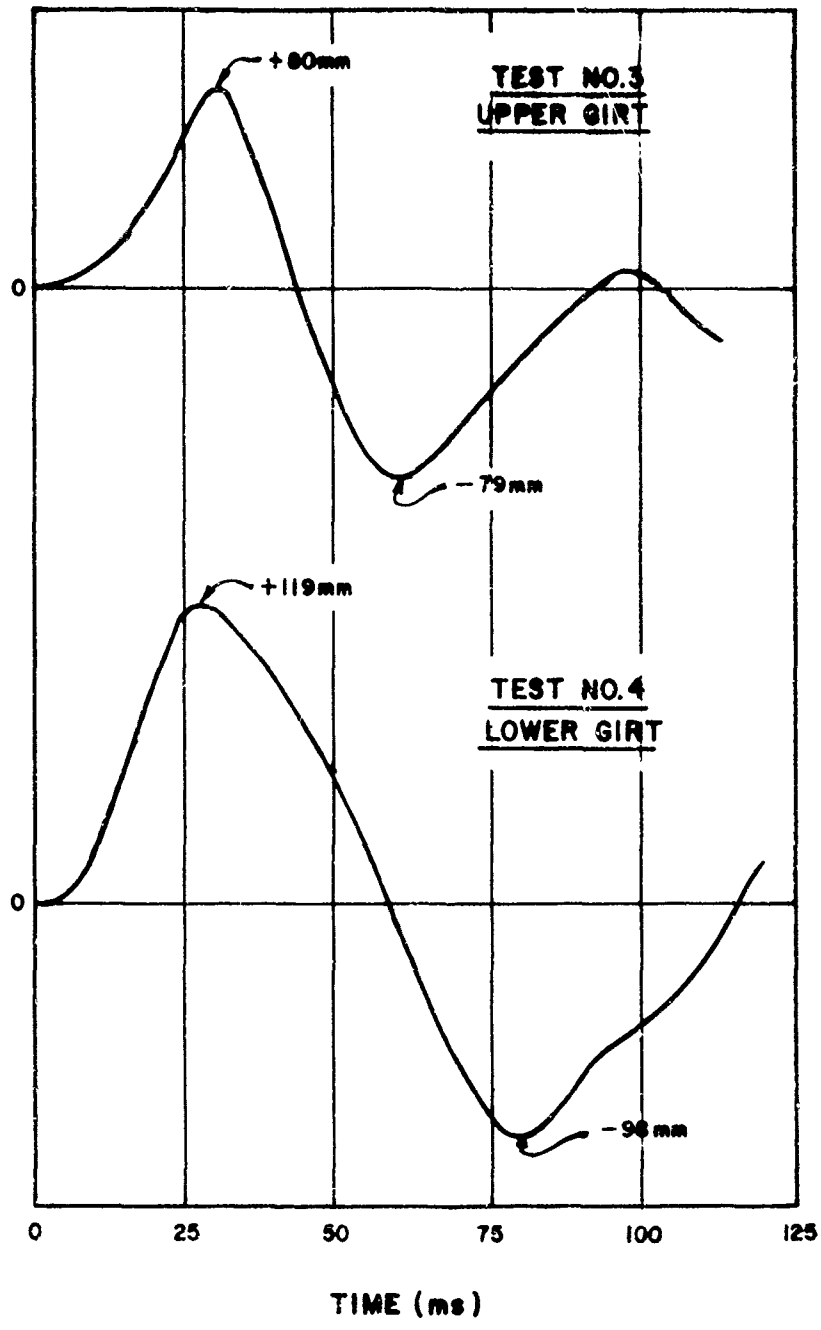

Fig 35 Measured girt displacements

FORM PD 404

PITTSBURGH TESTING LABORATORY

2838 SOUTH WEST TEMPLE
SALT LAKE CITY, UTAH 84115

ORDER NO. SLC-2616
FILE NO.
LABORATORY NO.
CUSTOMER NO. DAAD09-77-M-108
Req'n7096-4001
May 27, 19 77

U.S. Army Dugway Proving Ground
Procurement Office, P.O. Box 545
Dugway, Utah 84022

Attn: J. A. Roybal

REPORT OF TENSILE TEST OF submitted steel bar stock and steel plate

Contract Number DAAD09-77-M-1082

MADE FOR

DESCRIPTION	ORIGINAL AREA SQ IN	YIELD POINT POUNDS	MAXIMUM LOAD POUNDS	YIELD POINT LB PER SQ IN	TENSILE STRENGTH LB PER SQ IN	ELONGATION XXXXX	ELONGATION PER CENT	REDUCTION OF AREA PER CENT	FRACTURE
Bar Stock #1 0.742" diameter	.432	24,500	33,150	56,710	76,740	Gauge 2"	45		
Bar Stock #2 0.750" diameter	.442	24,100	33,350	54,520	75,450	2"	28+	*	
Bar Stock #3 0.750" diameter	.442	25,000	33,650	56,560	76,130	2"	48		
Bar Stock #4 0.755" diameter	.400	24,350	33,450	60,880	83,650	2'	35+	*	
Bar Stock #5 0.753" diameter	.445	24,700	33,550	55,510	75,390	2"	44		
8" sample-76-2238(A)1.505"x.099"	.149	8000	11,000	53,690	73,830	2"	34		
8" sample-76-2238(B)1.505"x.081"	.122	7600	9,400	62,300	77,050	2"	31		
8" sample-76-2238(C)1.505"x.077"	.116	6450	8,050	55,600	69,400	2"	31		
3" sample-76-2238(D)1.505"x.070"	.105	6400	8,100	60,950	77,140	2"	29		
8" sample-76-2238(E)1.505"x.057"	.086	5050	6,150	58,720	71,510	2"	30		
24 gauge antique white 8" sample-67-641 1.501'x0.026"	.039	**	4,080	**	104,620	2"	*		
24 gauge 01 white 8" sample 74997 1.501"x0.025"	.038	**	3,900	**	102,630	2"	*		
18" sample 76-2238 (-1) 1.503" x 0.500"	.752	48,500	60,000	64,490	79,790	2"	40		
(-2) 1.494" x 0.501"	.748	47,300	59,650	63,240	79,750	2"	41		
(-3) 1.494" x 0.501"	.748	46,600	59,200	62,300	79,140	2"	38		
(-4) 1.488" x 0.369"	.549	27,650	40,350	50,360	73,500	2"	38		
(-5) 1.485" x 0.366"	.544	27,200	40,400	50,000	74,260	2"	37		
(-6) 1.488 x 0.368"	.548	27,900	40,700	50,910	74,270	2"	37		

Fig 36 Tensile test laboratory report: Sheet 1 of 2

FORM PO 806

PITTSBURGH TESTING LABORATORY

2999 SOUTH WEST TEMPLE
SALT LAKE CITY, UTAH 84115

ORDER NO. SLC-2616
FILE NO.
LABORATORY NO.
CUSTOMER NO.

U.S. Army Dugway Proving Ground

May 27, 19 77

REPORT OF TENSILE TEST OF submitted steel bar stock and steel plate

Contract Number DAAD09-77-M-1082

MADE FOR

DESCRIPTION	ORIGINAL AREA SQ. IN.	YIELD POINT POUNDS	MAXIMUM LOAD POUNDS	YIELD POINT LB PER SQ IN.	TENSILE STRENGTH LB PER SQ IN.	ELONGATION XXXXX	ELONGATION PER CENT	REDUCTION OF AREA PER CENT	FRACTURE
18" sample 76-2238 (7) 1.506" x 0.255"	.384	24,800	32,800	64,580	85,420	2" Gauge	33		
(8) 1.507" x 0.255"	.384	27,000	34,300	70,310	89,320	2"	36		
(9) 1.507" x 0.255"	.384	24,900	32,600	64,840	84,900	2"	35		
(10) 1.507" x 0.182"	.274	15,700	20,050	57,300	73,180	2"	34		
(11) 1.513" x 0.182"	.275	14,650	19,700	53,270	71,640	2"	39		
(12) 1.505"x 0.182"	.274	14,900	19,700	54,380	71,900	2"	37		
(13) 1.507" x 0.182"	.274	14,400	20,100	52,550	73,360	2"	36		
(14) 1.506" x 0.182"	.274	15,350	20,000	56,020	73,000	2"	35		
(15) 1.512" x 0.182"	.275	14,800	20,100	53,820	73,090	2"	31		
(16) 1.513" x 0.188"	.284	13,800	19,900	48,590	70,070	2"	38		
(17) 1.506" x 0.188"	.283	13,500	20,500	47,700	72,440	2"	39		
(18) 1.514" x 0.188"	.285	13,800	19,900	48,420	69,820	2"	39		
(19) 1.506" x 0.108"	.163	9,500	11,500	58,260 **	70,550 *	2"	38		

* failed outside of gauge marks

** yield point could not be determined

PITTSBURGH TESTING LABORATORY

James L. Munnerlyn

James L. Munnerlyn, Manager
Salt Lake City District

gn

Fig 37 Tensile test laboratory report: Sheet 2 of 2

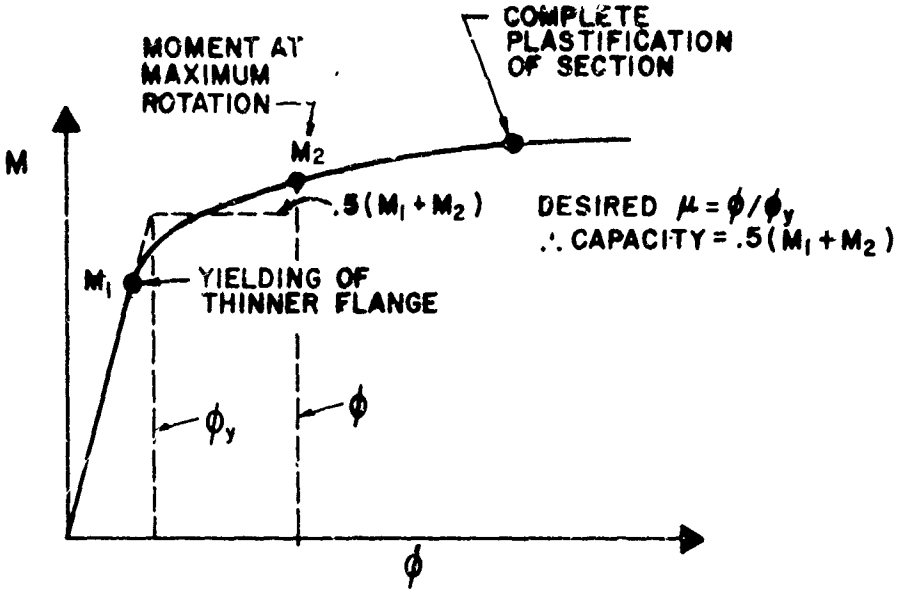

a) BUILT-UP SECTION WITH FLANGES OF DIFFERING THICKNESS & YIELD STRENGTH

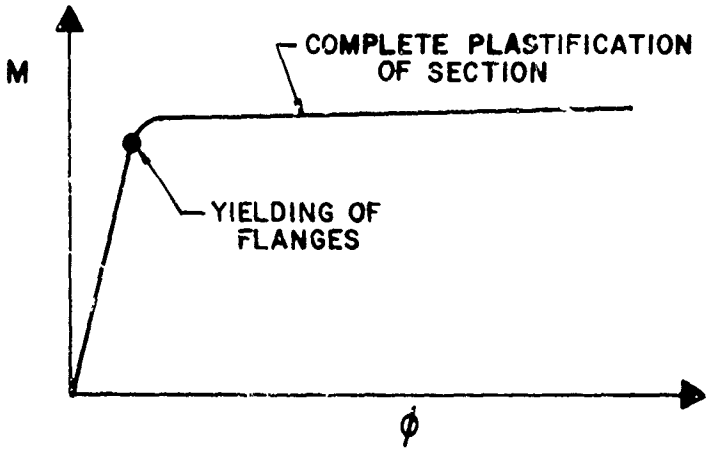

b) TYPICAL HOT-ROLLED SECTION

Fig 38 Moment (M) - Curvature (ø) diagrams for built-up and hot-rolled members

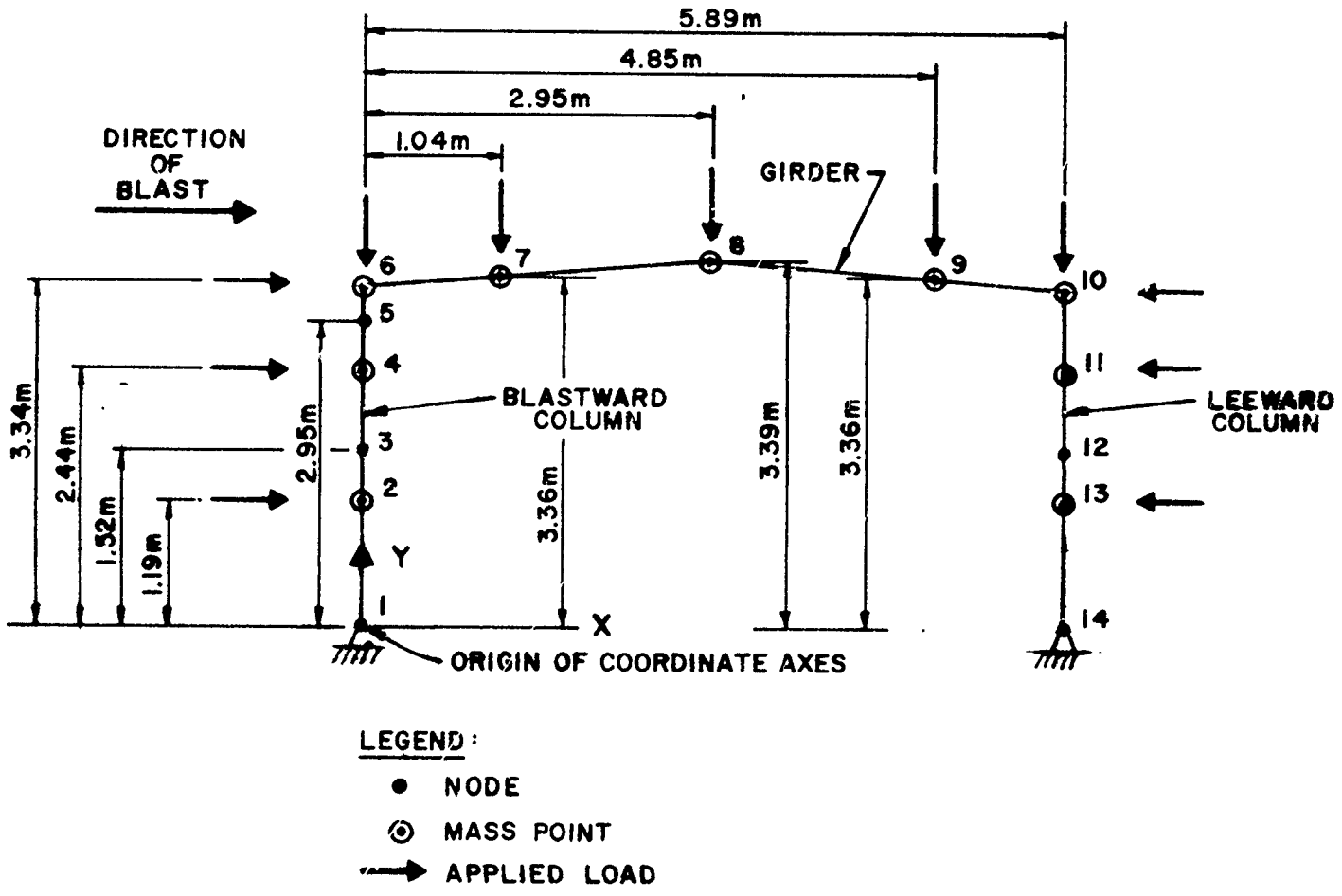

Fig 39 Typical basic frame model

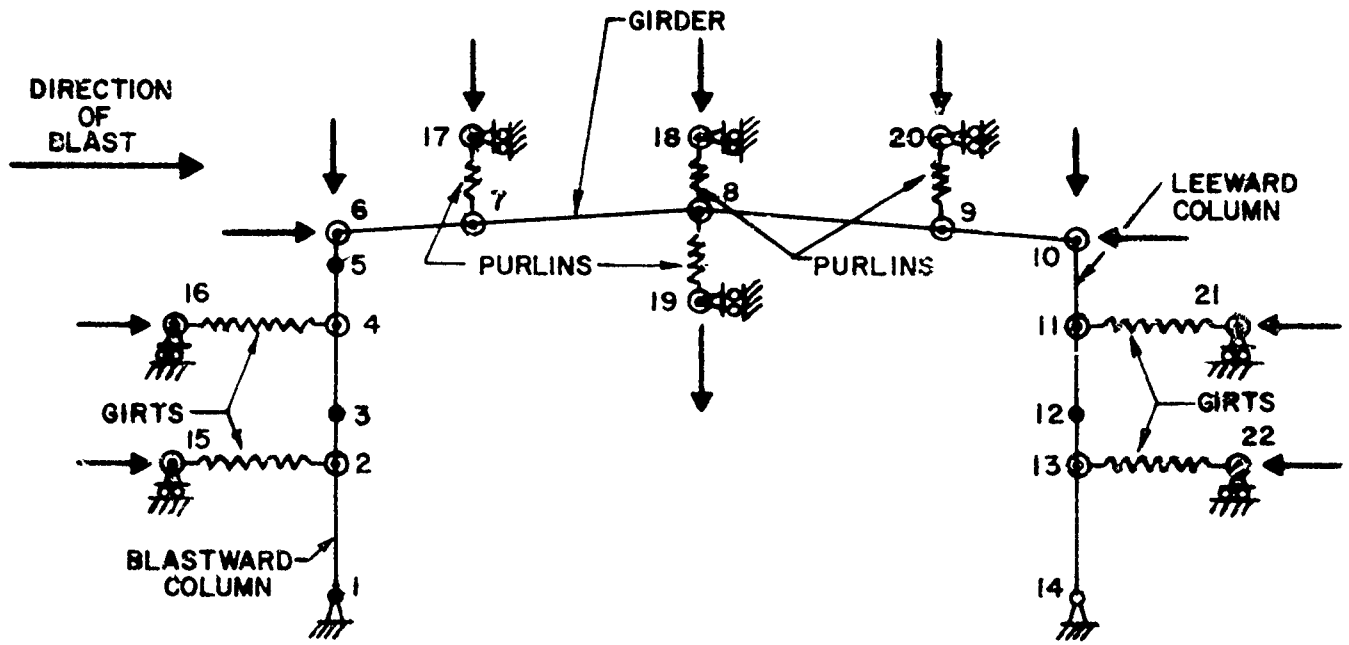

NOTE: FOR NODE DIMENSIONS
& LEGEND, SEE FIGURE 39

Fig 40 Basic frame model including purlins and girts

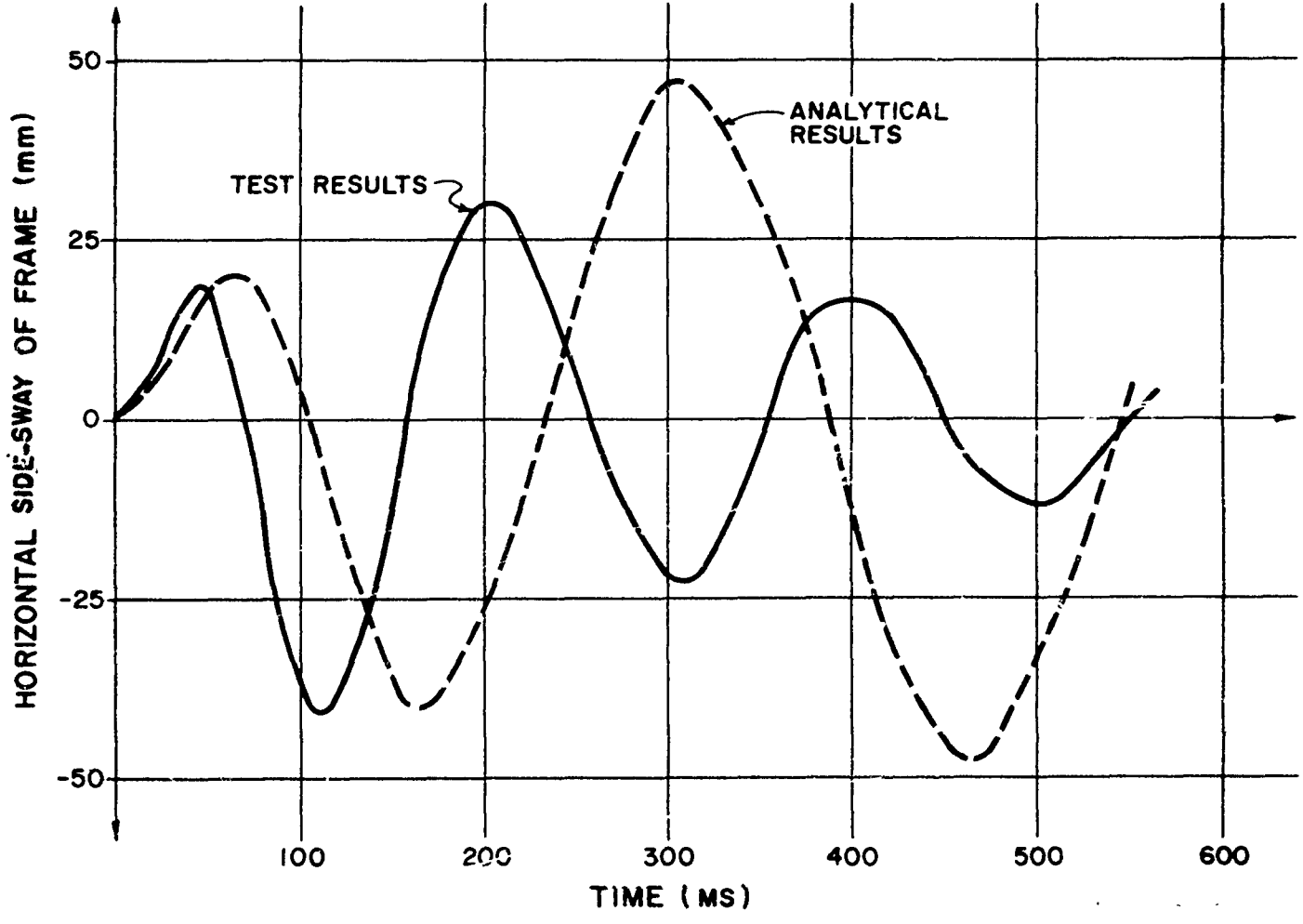

Fig 41 Center frame side-sway displacement, test and analytical results - Test No. 1

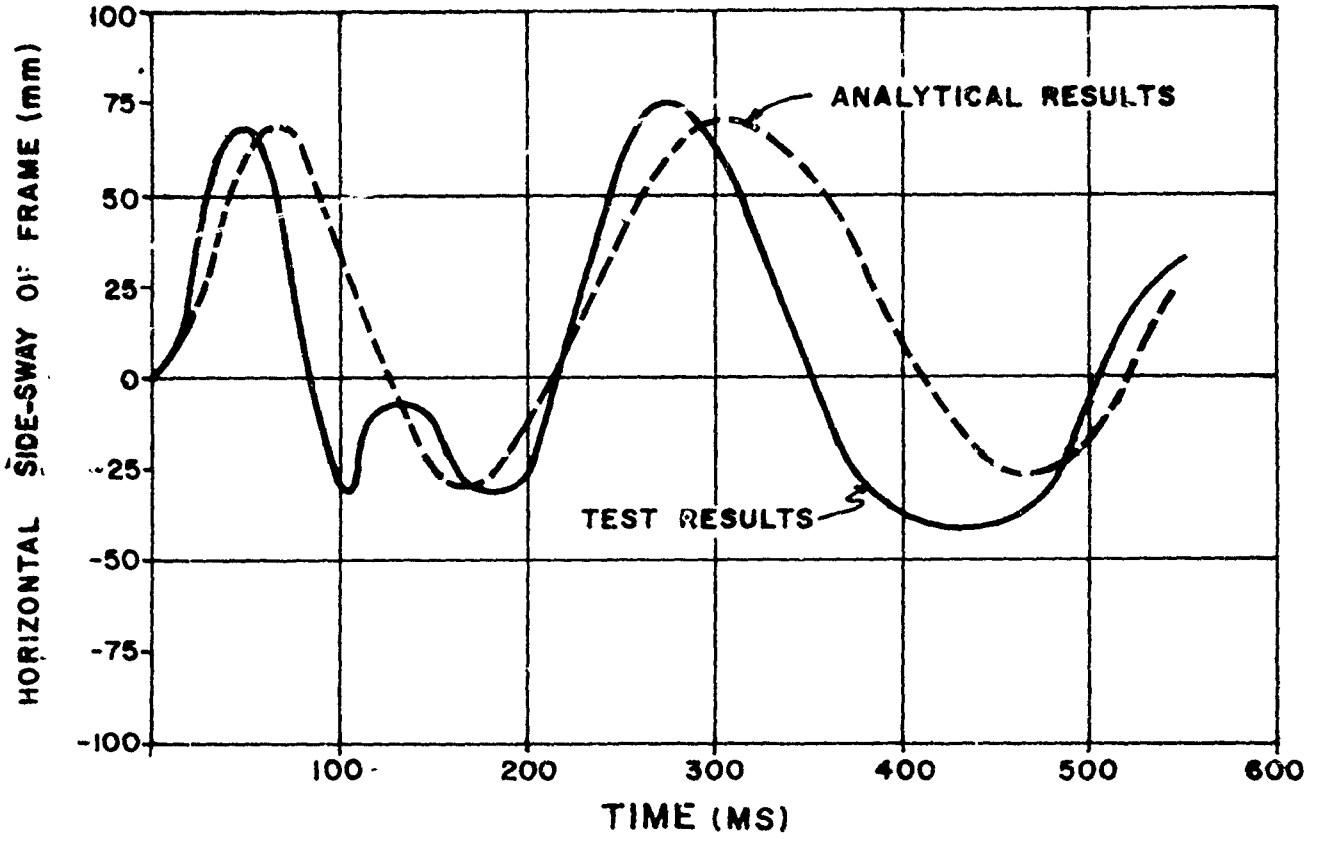

Fig 42 Center frame side-sway displacement, test and analytical results - Test No. 3

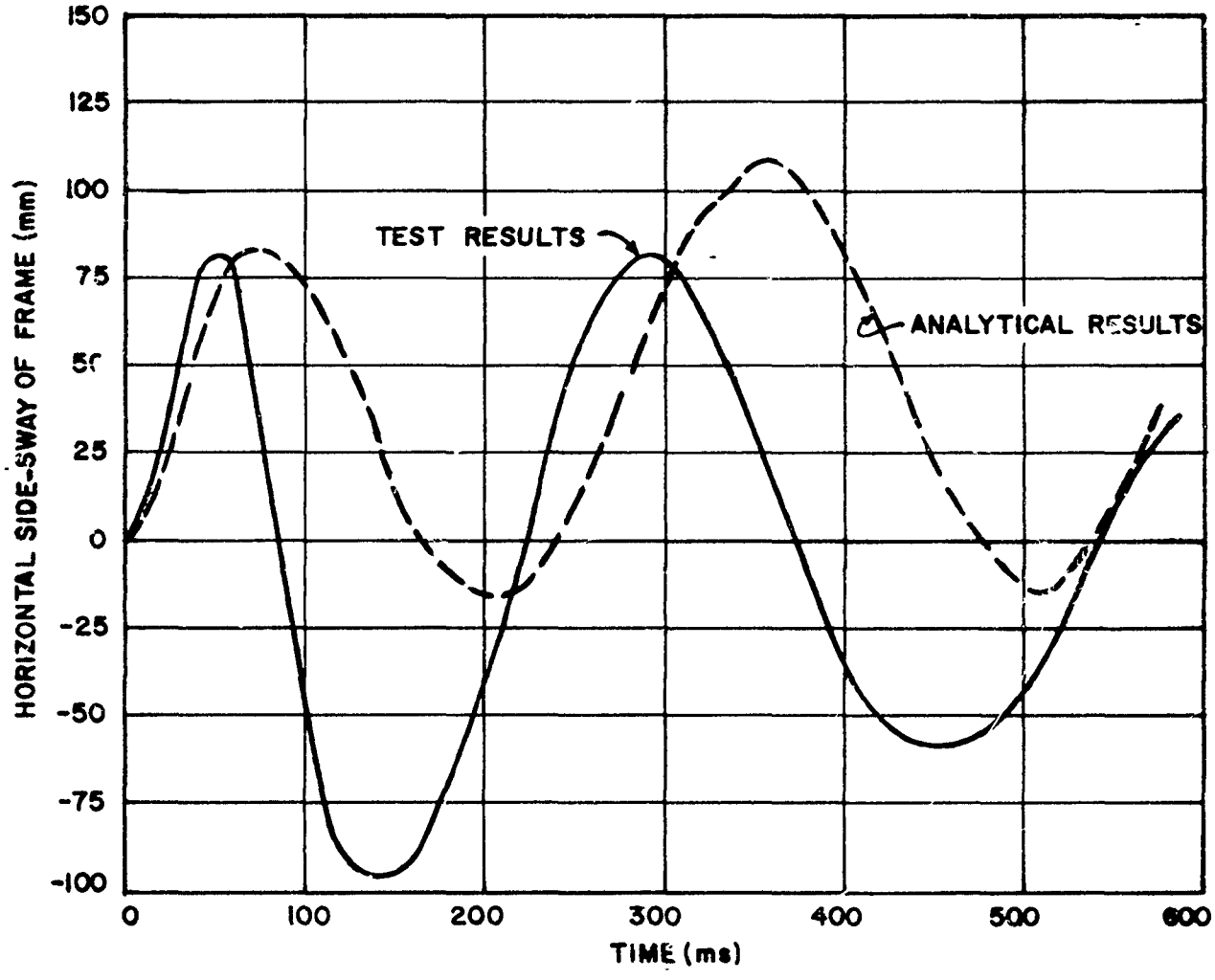

Fig 43 Center frame side-sway displacement, test and analytical results - Test No 4

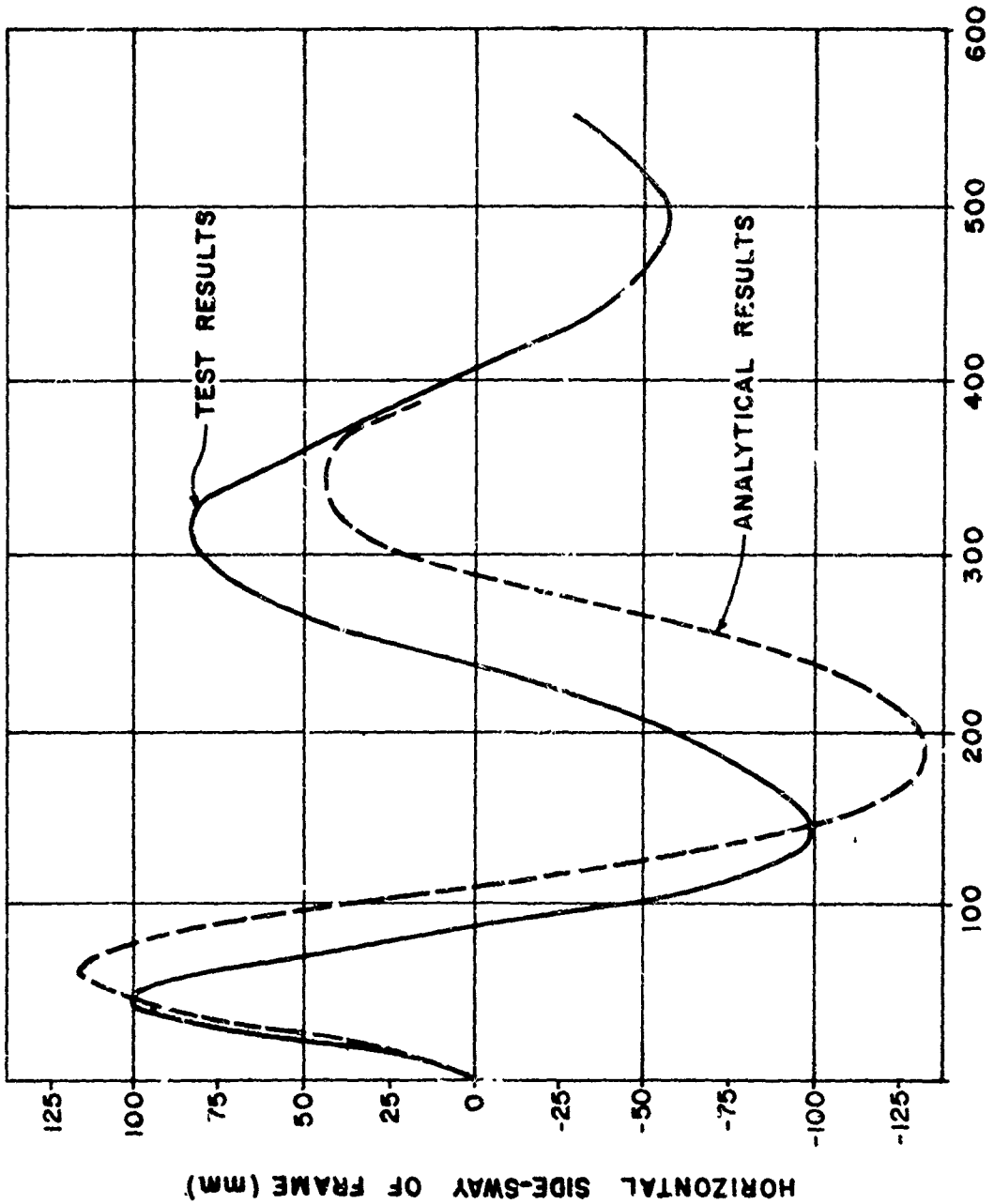

Fig 44 Center frame side-sway displacement, test and analytical results - Test No. 5

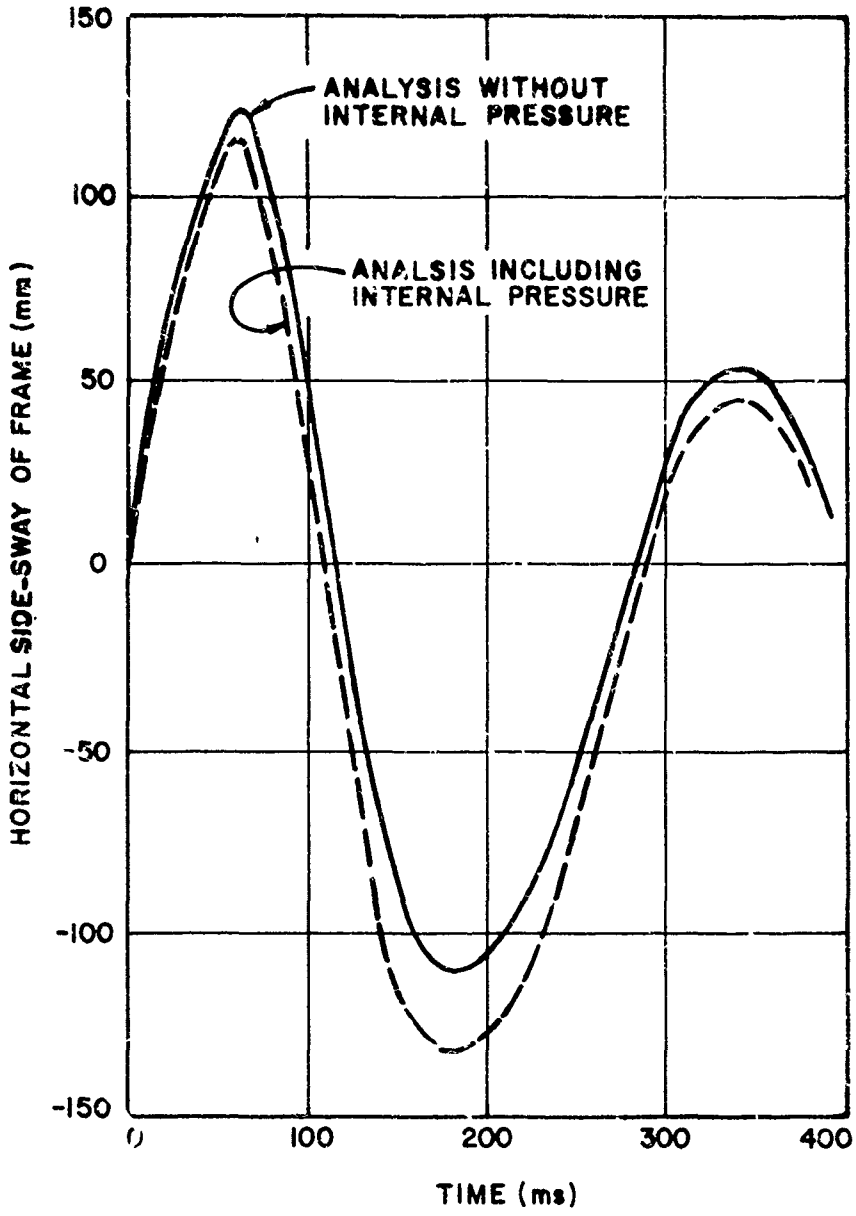

Fig 45 Center frame side-sway displacement, analytical results with and without internal pressure effects - Test No. 5

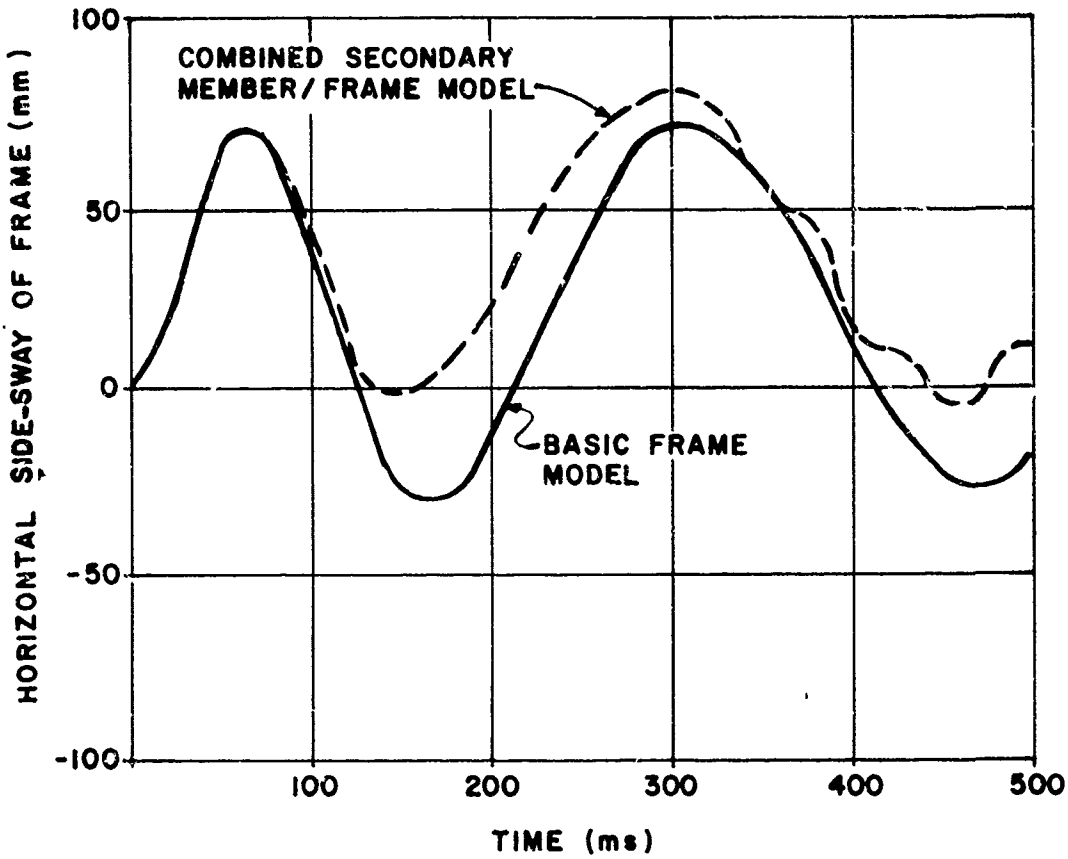

Fig 46 Center frame side-sway displacement, effect of secondary member/frame interaction - Test No. 3

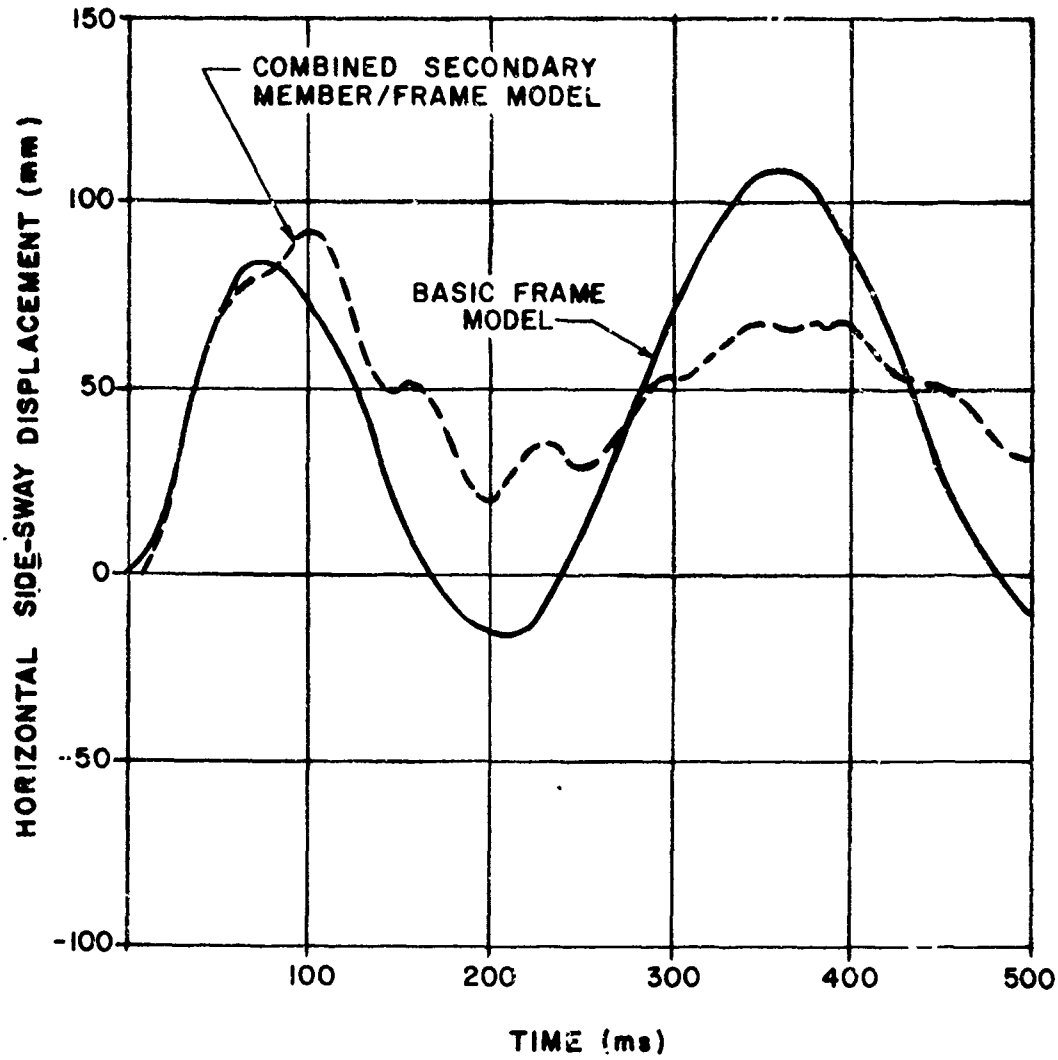

Fig 47 Center frame side-sway displacement, effect of secondary member/frame interaction - Test No. 4

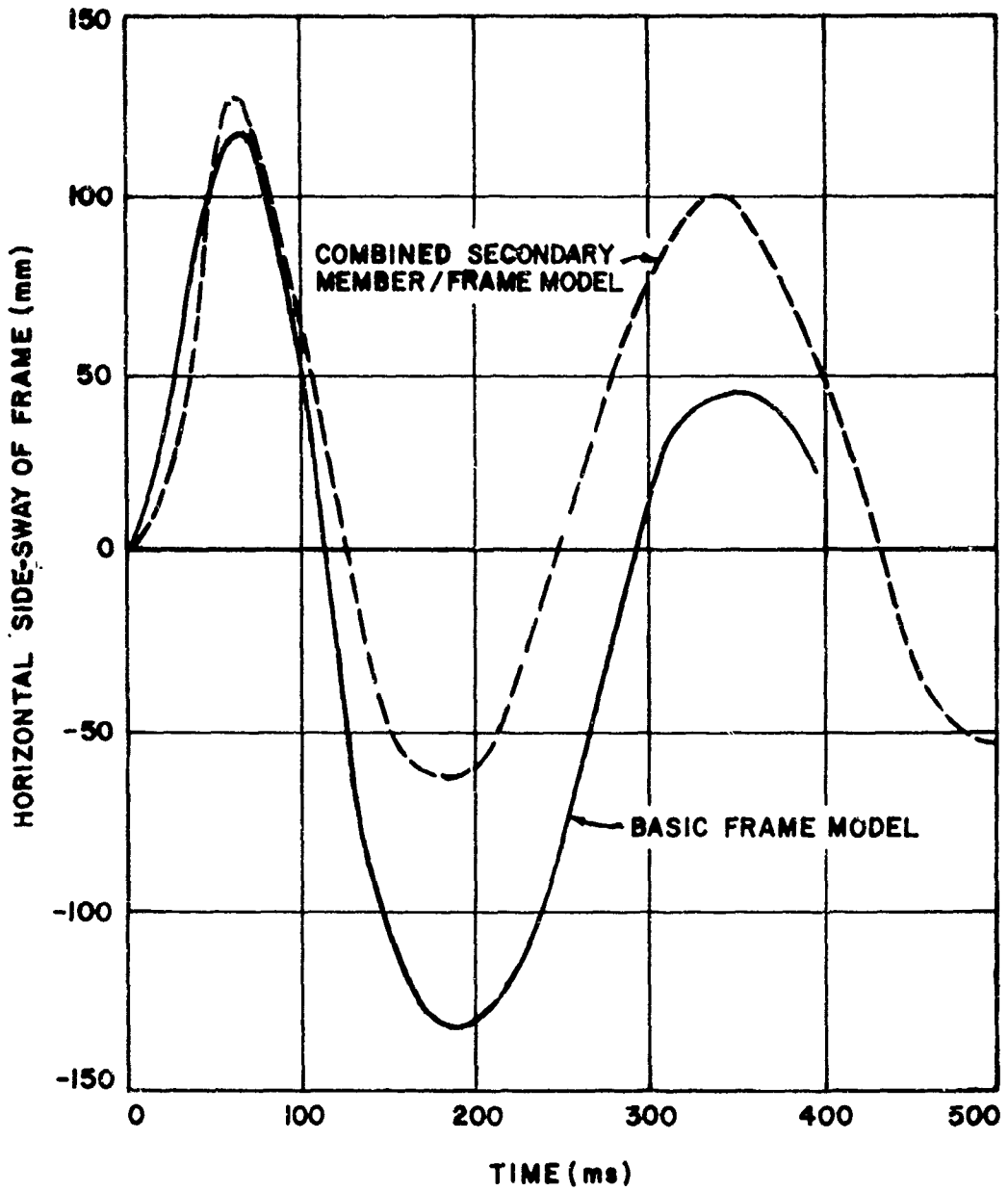

Fig 48 Center frame side-sway displacement, effect of secondary member/frame interaction - Test No. 5

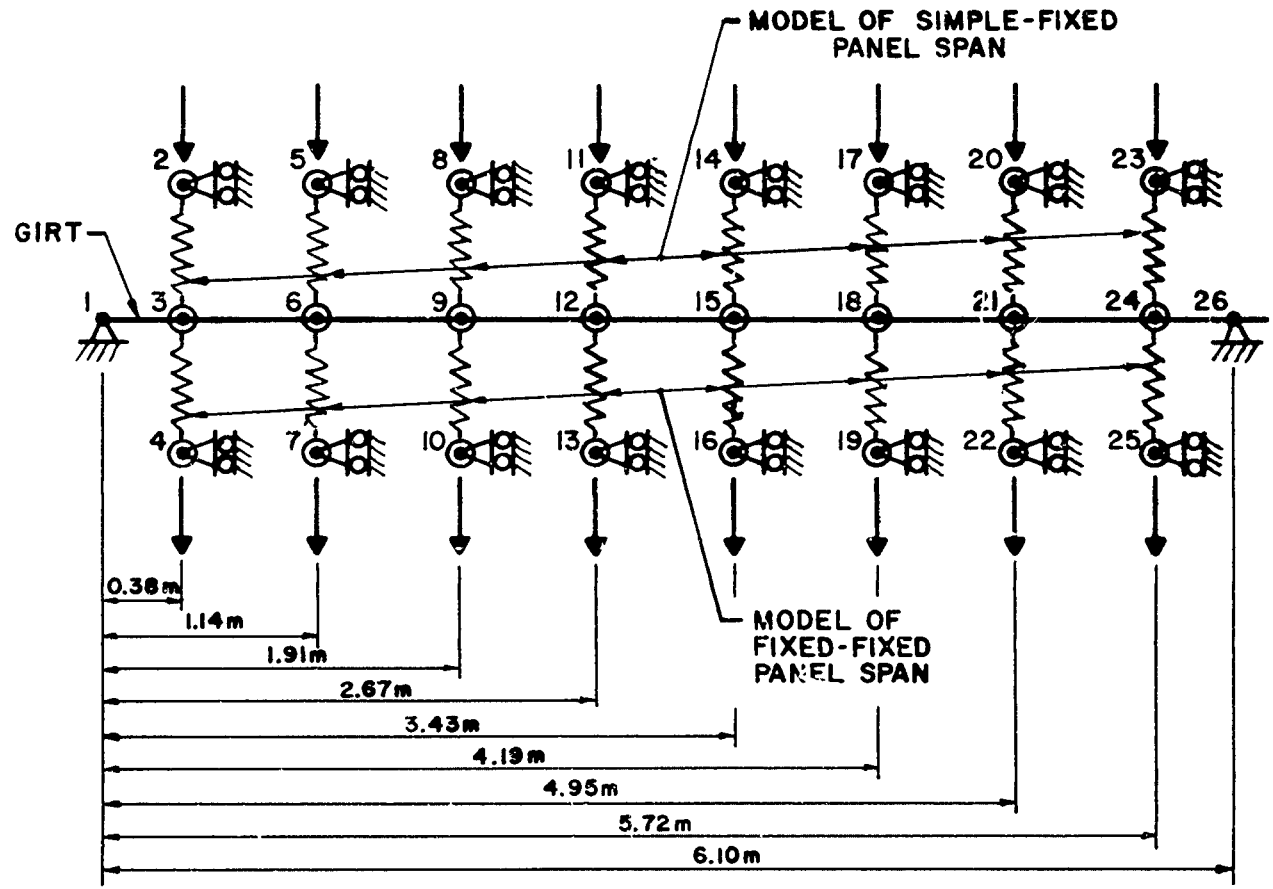

Fig 49 Combined wall panel/girt interaction model

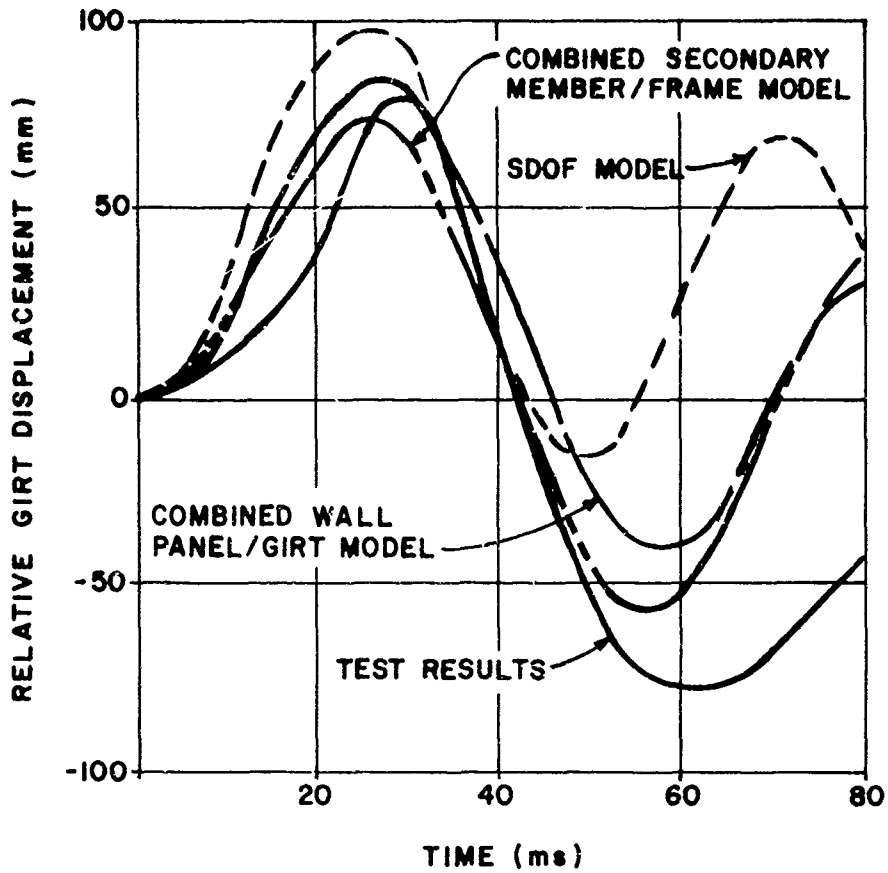

Fig 50 Relative girt displacements, upper girt; test and analytical results - Test No. 3

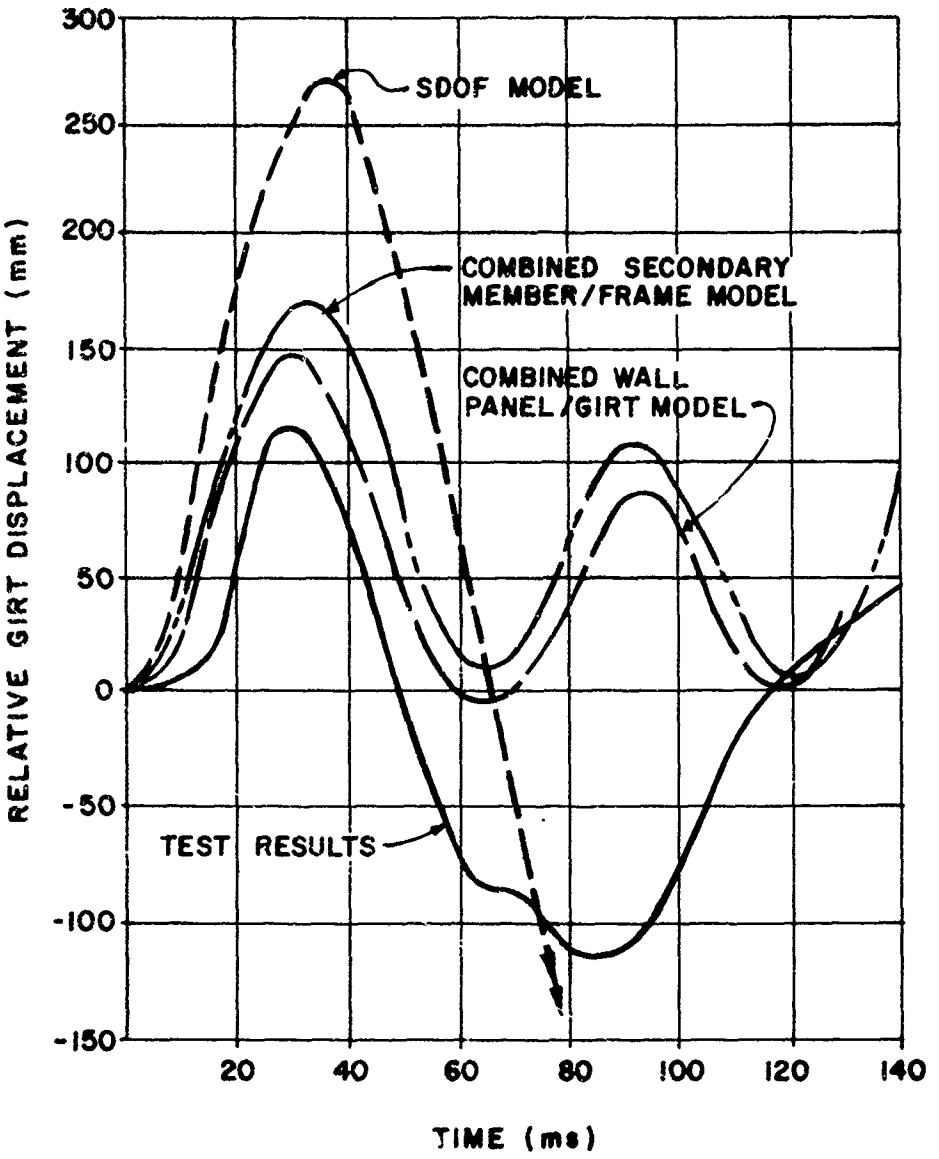

Fig 51 Relative girt displacements, upper girt; test and analytical results - Test No. 4

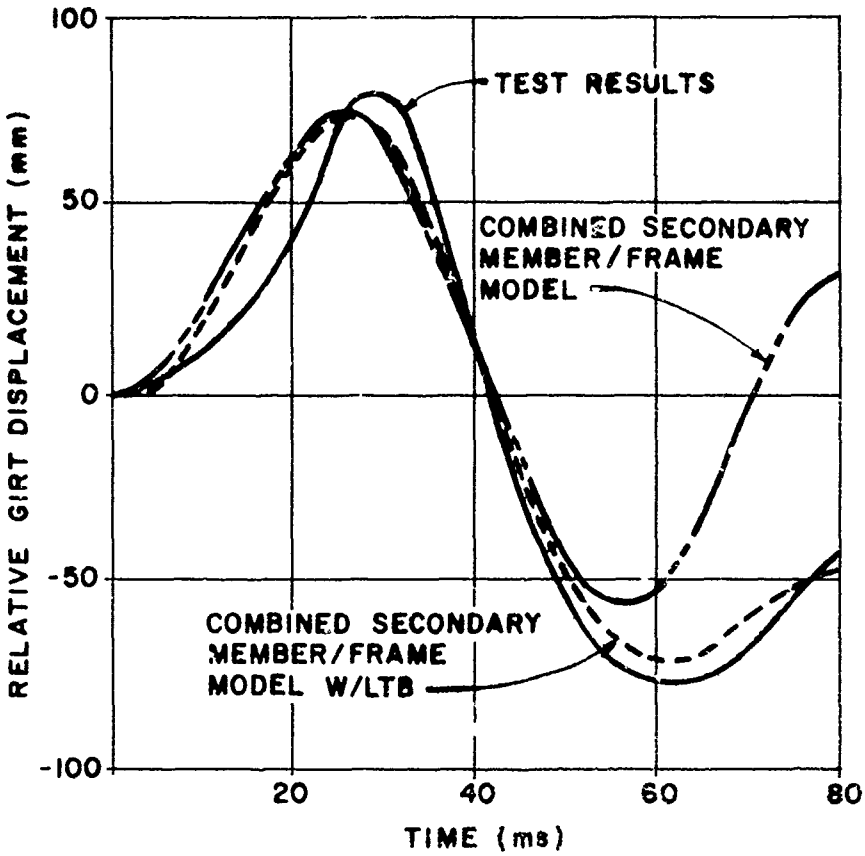

Fig 52 Effects of Lateral Torsional Buckling (LTB) on girt rebound response - Test No. 3

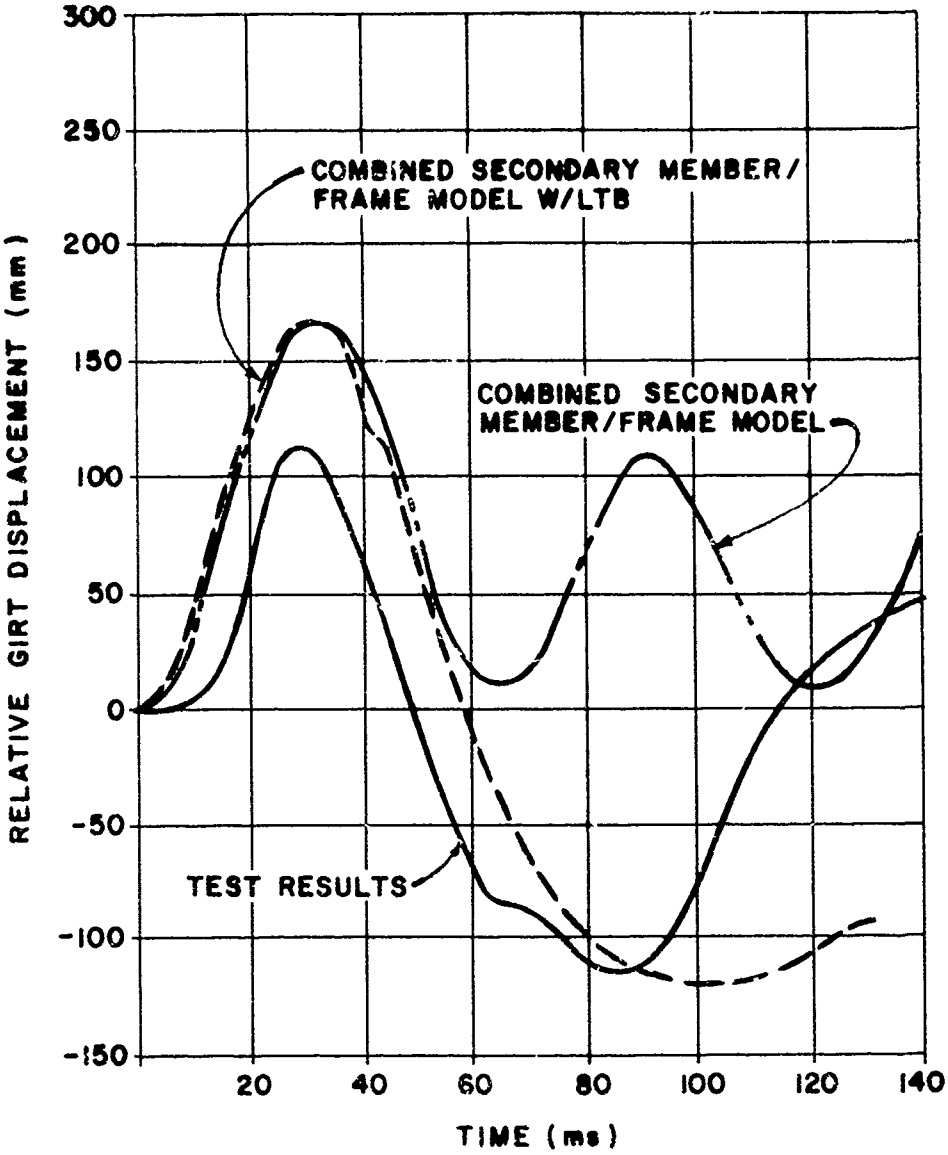

Fig 53 Effects of Lateral Torsional Buckling (LTB) on girt rebound response - Test No. 4

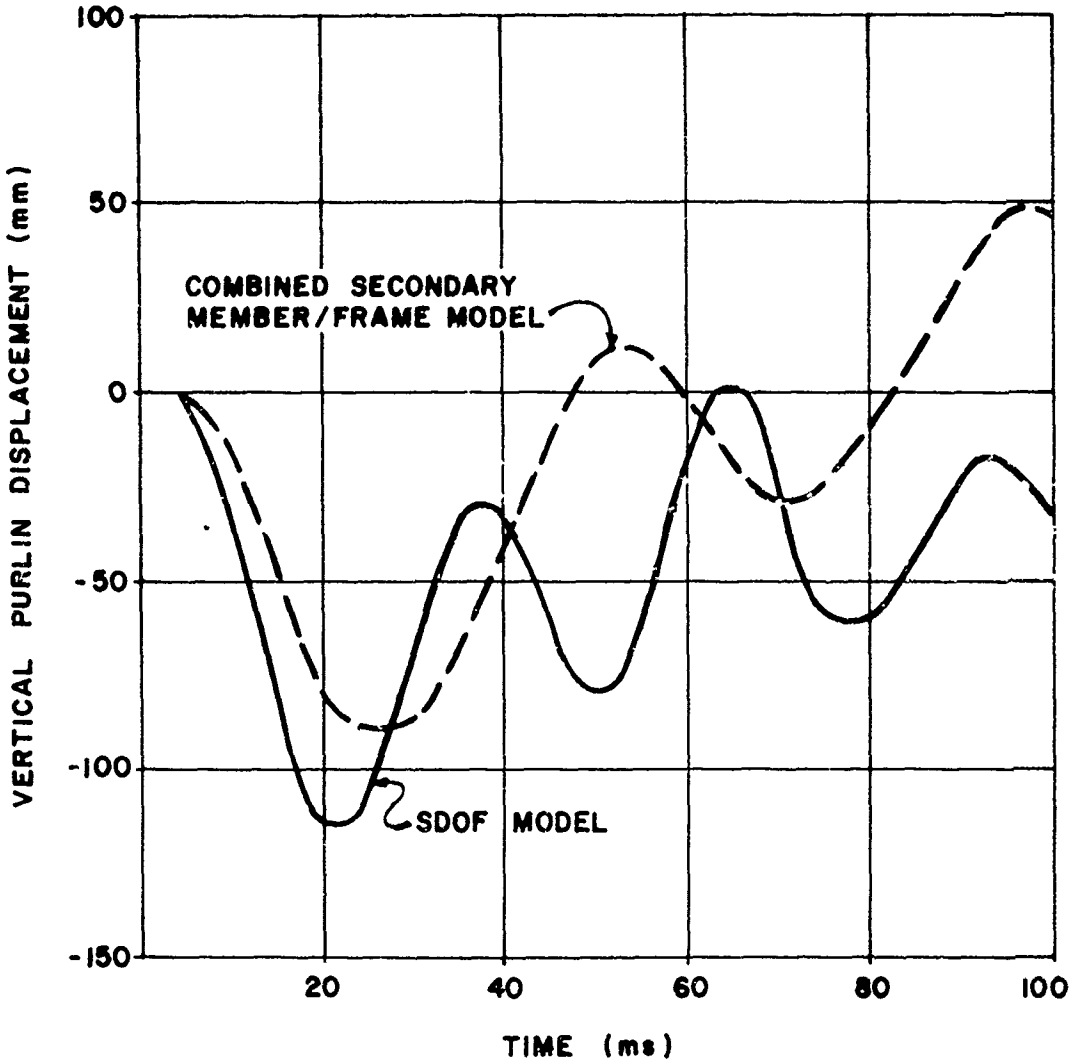

Fig 54 Purlin response; analytical results - Test No. 3

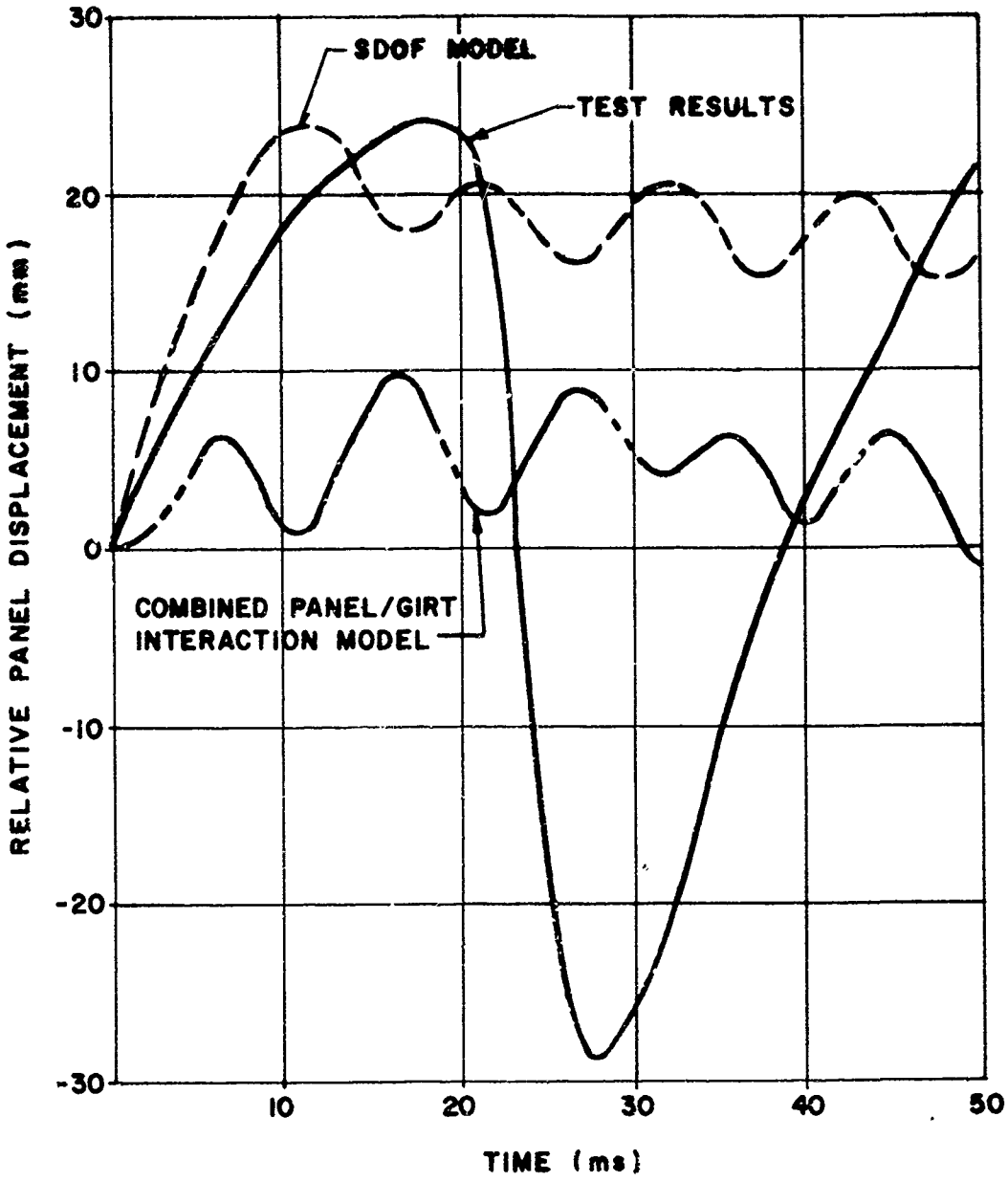

Fig 55 Panel response; test and analytical results - Test No. 3

APPENDIX A

BLAST LOADS

APPENDIX A

BLAST LOADS

General

This appendix presents recommended blast loads to be used in conjunction with free-field incident overpressures of approximately 70 kPa ($\approx$10 psi) or less. Presented are recommended free-field blast wave parameters and blast loads acting on the various surfaces of aboveground structures similar to those utilized for the tests described in this report.

Free-Field Blast Wave Parameters

Free-field blast wave parameters versus distance for hemispherical surface detonations are presented in Figures A.1 and A.2. Both of these figures are the same except that the values of Figure A.1 are expressed in the metric system and those of Figure A.2 are expressed in the United States System. The values for overpressure, impulse, positive phase duration and arrival time of the free-field incident blast wave and the shock velocity were obtained from Reference 6. All other blast wave parameters were obtained from Reference 7. The blast pressures obtained from Reference 7 were related to the incident pressures of Reference 6; whereas the impulse, durations and other parameters of Reference 7 were related to corresponding incident wave parameters given in Reference 6.

Pressure-Time Variation

Frame analyses similar to those presented in this report will, in certain circumstances, require a more accurate definition of the variation of the pressure as a function of time. This variation is usually referred to as the "P-T curve" of the blast wave. The exact form of the curve is still unknown; but a close approximation can be made using assumed functions as follows:

Positive Phase P-T Curves

For the positive phase of a blast wave, it is suggested that a close approximation of the P-T curve can be obtained by using the following relationship:

$$P_s = P_{so} (1 - t_s/t_o)e^{-\alpha(t_s/t_o)} \qquad (1)$$

where:

P_s = Pressure at time t_s

P_{so} = Peak incident pressure

t_s = Positive phase time of interest

t_o = Positive phase duration

α = Constant which determines the form of the P-T curve.

The values of α can be expressed as a function of a constant k, which, in turn, is defined as:

$$k = i_s/P_{so}t_o \qquad (2)$$

where i_s, P_{so} and t_o are obtained from either Figure A.1 or A.2. The numerical relationship between k and α is listed below:

k	0.70	0.60	0.50	0.40	0.30	0.20	0.10
α	-.93	-.52	0	0.71	1.77	3.67	8.87

To simplify the solution, normalized plots of the positive phase P-T curves as a function of values of k are presented in Figure A.3a. For the pressure ranges considered in this Appendix, these normalized curves are applicable to both incident and reflected pressures.

Negative Phase P-T Curves

The negative pressure curve can roughly be compared with a cubical parabola:

$$P_s^- = P_{so}^-(6.75t_s^-/t_o^-)(1 - t_s^-/t_o^-)^2 \qquad (3)$$

where:

P_s^- = Negative pressure at time t_s^-

P_{so}^- = Peak incident negative pressure

t_s^- = Negative phase time of interest

t_o^- = Negative phase duration

However, this curve gives a single definite value of k^-; i.e., k^- = 0.5625. According to Reference 7, this value is assumed to be valid for scaled distances greater than 6.5 $m/kg^{1/3}$ (15.2 $ft/lb^{1/3}$). A plot of Equation 3 is given in Figure A.3b. For values of k^- not equal to 0.5625, the suggested curve should be adjusted such that the area under it equals the negative phase impulse. The value of k^- is defined as follows:

$$k^- = i_s^-/P_{so}^- t_o^-$$

Similar to the positive phase, to simplify the P-T curve solution, a normalized plot of the negative phase is presented in Figure A.3b. This curve is appplicable to both incident and reflected pressures for the incident pressure range of interest.

Loads on Structures

Based upon the data given in Tables A.1 through A.6 and the discussion of the pressure measurements given in the main body of the report, it would appear that the positive phase blast loads acting on the front and side walls and the roof are consistent with data given in Reference 3. However, the positive phase blast load acting on the rear wall is less than that which would be predicted by Reference 3. For incident overpressures of approximately 3.45 kPa (0.5 psi), the pressures acting on the back wall were 50 to 65 percent of the peak incident pressures. At higher incident overpressures, the back wall pressures increased to approximately 80 percent of incident pressures. It is hereby recommended that for future frame analyses, the positive phase blast loads acting on the rear wall of a structure be taken equal to 60 percent of the incident overpressure. However, for the local design of the rear wall itself, the recommendations of Reference 3 should be followed.

On the other hand, negative phase pressures acting on the rear walls of buildings do not appear to be affected. Therefore, when performing a frame analysis, the magnitude of the negative pressures acting on the rear walls should not be reduced.

Table A.1

Blast wave parameters (Test No. 1)

Gage Location	Gage No.	Positive Pressure kPa	(psi)	Pos. Phase Duration ms	Negative Pressure kPa	(psi)	Total Duration ms
Free-Field	P1	1.76	(0.26)	38	1.17	(0.17)	181
	P2	1.86	(0.27)	41	1.17	(0.17)	185
	P3	1.86	(0.27)	-	-	-	-
Blastward Wall	P4	3.24	(0.47)	45	0.83	(0.12)	129
	P5	4.20	(0.61)	44	1.79	(0.26)	184
	P6	2.13	(0.31)	45	0.90	(0.13)	156
Roof	P7	-	-	-	-	-	-
	P8	-	-	-	-	-	-
	P9	-	-	-	-	-	-
Leeward Wall	P10	1.10	(0.16)	49	1.10	(0.16)	229
	P11	0.90	(0.13)	49	1.10	(0.16)	229
	P12	-	-	-	-	-	-
Side	P13	1.31	(0.19)	54	1.10	(0.16)	230
	P14	1.72	(0.25)	54	1.03	(0.15)	190
Interior	P15	0.69	(0.10)	50	0.41	(0.06)	180
	P16	0.69	(0.10)	45	0.48	(0.07)	220
	P17	0.69	(0.10)	45	0.34	(0.05)	200

Table A.2

Blast wave parameters (Test No. 2)

Gage Location	Gage No.	Positive Pressure kPa	(psi)	Pos. Phase Duration ms	Negative Pressure kPa	(psi)	Total Duration ms
Free-Field	P1	3.45	(0.50)	64	1.38	(0.20)	160
	P2	3.59	(0.52)	56	1.72	(0.25)	200
	P3	3.86	(0.56)	60	0.76	(0.11)	-
Blastward Wall	P4	7.03	(1.02)	63	2.62	(0.38)	200
	P5	9.85	(1.43)	50	3.10	(0.45)	-
	P6	4.69	(0.68)	50	2.41	(0.35)	160
Roof	P7	-	-	-	-	-	-
	P8	-	-	-	-	-	-
	P9	-	-	-	-	-	-
Leeward Wall	P10	2.48	(0.36)	66	1.38	(0.20)	-
	P11	2.34	(0.34)	65	1.72	(0.25)	-
	P12	-	-	-	-	-	-
Side	P13	3.24	(0.47)	58	1.38	(0.20)	190
	P14	3.24	(0.47)	55	1.72	(0.25)	190
Interior	P15	1.38	(0.20)	45	0.69	(0.10)	190
	P16	1.00	(0.14)	45	0.69	(0.10)	-
	P17	-	-	-	-	-	-

Table A.3

Blast wave parameters (Test No. 3)

Gage Location	Gage No.	Positive Pressure kPa	(psi)	Pos. Phase Duration ms	Negative Pressure kPa	(psi)	Total Duration ms
Free-Field	P1	5.10	(0.74)	50	1.72	(0.25)	160
	P2	4.83	(0.70)	50	2.07	(0.30)	230
	P3	4.96	(0.72)	55	2.07	(0.30)	160
Blastward Wall	P4	9.92	(1.44)	42	3.45	(0.50)	-
	P5	14.50	(2.10)	50	3.03	(0.44)	-
	P6	7.74	(1.12)	45	2.48	(0.36)	-
Roof	P7	6.14	(0.89)	54	2.06	(0.30)	200
	P8	-	-	-	-	-	-
	P9	-	-	-	-	-	-
Leeward Wall	P10	-	-	-	-	-	-
	P11	3.93	(0.57)	50	1.72	(0.25)	165
	P12	-	-	-	-	-	-
Side	P13	4.21	(0.61)	54	2.62	(0.38)	160
	P14	5.44	(0.79)	45	2.07	(0.30)	160
Interior	P15	2.21	(0.32)	45	1.17	(0.17)	220
	P16	-	-	-	-	-	-
	P17	1.86	(0.27)	45	1.31	(0.19)	210

Table A.4

Blast wave parameters (Test No. 4)

Gage Location	Gage No.	Positive Pressure kPa	(psi)	Pos. Phase Duration ms	Negative Pressure kPa	(psi)	Total Duration ms
Free-Field	P1	6.96	(1.01)	50	2.76	(0.40)	155
	P2	6.96	(1.01)	50	2.96	(0.43)	235
	P3	7.17	(1.04)	50	2.76	(0.40)	180
Blastward Wall	P4	14.20	(2.06)	40	5.52	(0.80)	-
	P5	19.30	(2.80)	40	5.52	(0.80)	180
	P6*	9.92	(1.44)	40	3.10	(0.45)	160
Roof	P7	8.14	(1.18)	35	-	-	-
	P8	-	-	-	-	-	-
	P9	-	-	-	-	-	-
Leeward Wall	P10	-	-	-	-	-	-
	P11	5.58	(0.81)	50	2.07	(0.30)	170
	P12	-	-	-	-	-	-
Side	P13	6.48	(0.94)	50	3.79	(0.55)	150
	P14	6.20	(0.90)	50	3.10	(0.45)	180
Interior	P15	2.90	(0.42)	50	1.72	(0.25)	170
	P16	2.83	(0.41)	47	3.10	(0.45)	180
	P17	3.10	(0.45)	-	-	-	-

*Low measurements

Table A.5

Blast wave parameters (Test No. 5)

Gage Location	Gage No.	Positive Pressure kPa	(psi)	Pos. Phase Duration ms	Negative Pressure kPa	(psi)	Total Duration ms
	P1	8.62	(1.25)	-	-	-	-
Free-	P2	8.55	(1.24)	42	2.96	(0.43)	160
Field	P3	8.14	(1.18)	40	3.45	(0.50)	240
	P4	17.24	(2.50)	40	6.21	(0.90)	200
Blastward	P5	21.20	(3.08)	47	5.52	(0.80)	150
Wall	P6	-	-	-	-	-	-
	P7	9.65	(1.40)	40	2.07	(0.30)	150
Roof	P8	-	-	-	-	-	-
	P9	-	-	-	-	-	-
	P10	-	-	-	-	-	-
Leeward	P11	6.48	(0.94)	70	1.24	(0.18)	140
Wall	P12	-	-	-	-	-	-
Side	P13	8.20	(1.19)	58	5.17	(0.75)	120
	P14	7.24	(1.05)	47	2.76	(0.40)	200
	P15	3.38	(0.49)	50	2.62	(0.38)	220
Interior	P16	3.31	(0.48)	47	2.76	(0.40)	230
	P17	3.24	(0.47)	45	2.32	(0.38)	230

Table A.6

Blast wave parameters (Test No. 6)

Gage Location	Gage No.	Positive Pressure kPa	(psi)	Pos. Phase Duration ms	Negative Pressure kPa	(psi)	Total Duration ms
Free-Field	P1	8.20	(1.10)	-	-	-	-
	P2	8.96	(1.30)	-	-	-	-
	P3	9.38	(1.36)	-	-	-	-
Leeward Wall	P4	-	-	-	-	-	-
	P5*	6.69	(0.97)	-	-	-	-
	P6	-	-	-	-	-	-
Roof	P7	9.99	(1.45)	60	5.52	(0.80)	150
	P8	-	-	-	-	-	-
	P9	-	-	-	-	-	-
Blastward Wall	P10	-	-	-	-	-	-
	P11*	16.75	(2.43)	50	2.76	(0.40)	-
	P12	-	-	-	-	-	-
Side Wall	P13	-	-	-	-	-	-
	P14	7.17	(1.04)	-	-	-	-
Interior	P15	3.65	(0.53)	-	-	-	-
	P16	2.90	(0.42)	-	-	-	-
	P17	3.93	(0.73)	-	-	-	-

*Readings not available.

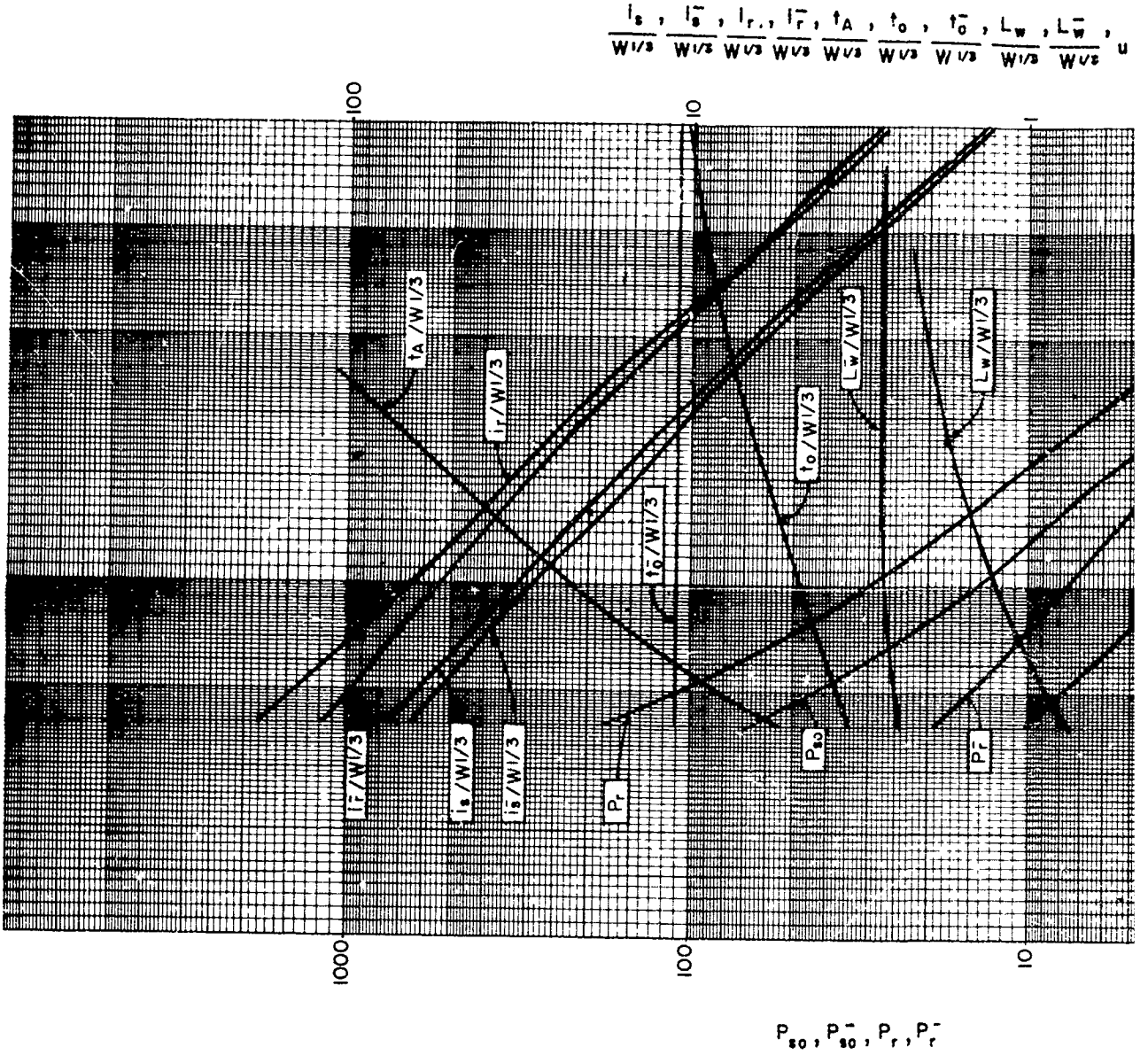

Fig A.1 Shock-wave parameters for hemispherical TNT surface explosion at sea level - SI Ur

Units

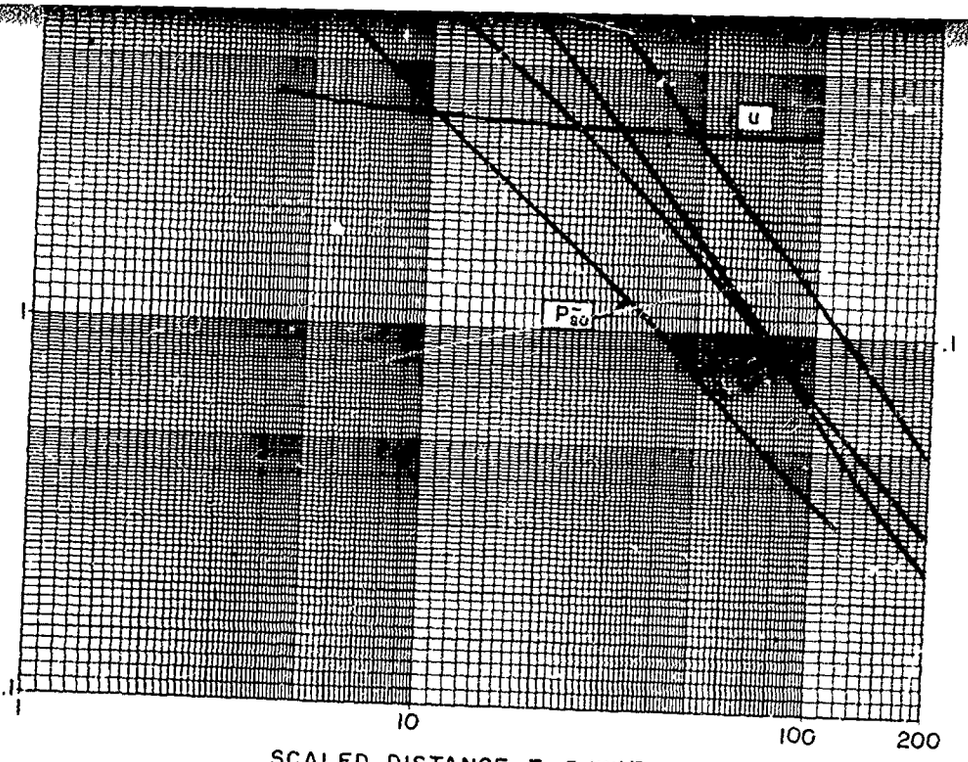

P_{so} = Peak Positive Incident Pressure, kPa
$P_{\bar{so}}$ = Peak Negative Incident Pressure, kPa
P_r = Peak Positive Normal Reflected Pressure, kPa
$P_{\bar{r}}$ = Peak Negative Normal Reflected Pressure, kPa
$i_s/W^{1/3}$ = Scaled Unit Positive Incident Impulse, kPa-ms/kg$^{1/3}$
$i_{\bar{s}}/W^{1/3}$ = Scaled Unit Negative Incident Impulse, kPa-ms/kg$^{1/3}$
$i_r/W^{1/3}$ = Scaled Unit Positive Normal Reflected Impulse, kPa-ms/kg$^{1/3}$
$i_{\bar{r}}/W^{1/3}$ = Scaled Unit Negative Normal Reflected Impulse, kPa-ms/kg$^{1/3}$
$t_a/W^{1/3}$ = Scaled Time of Arrival of Blast Wave, ms/kg$^{1/3}$

$t_o/W^{1/3}$ = Scaled Positive Duration of Positive Phase, ms/kg$^{1/3}$
$t_{\bar{o}}/W^{1/3}$ = Scaled Negative Duration of Positive Phase, ms/kg$^{1/3}$
$L_w/W^{1/3}$ = Scaled Wave Length of Positive Phase, m/kg$^{1/3}$
$L_{\bar{w}}/W^{1/3}$ = Scaled Wave Length of Negative Phase, m/kg$^{1/3}$
U = Shock Front Velocity, m/ms
u = Particle Velocity, m/ms
W = Charge Weight, kg
R = Radial Distance from Charge, m
Z = Scaled Distance, m/kg$^{1/3}$

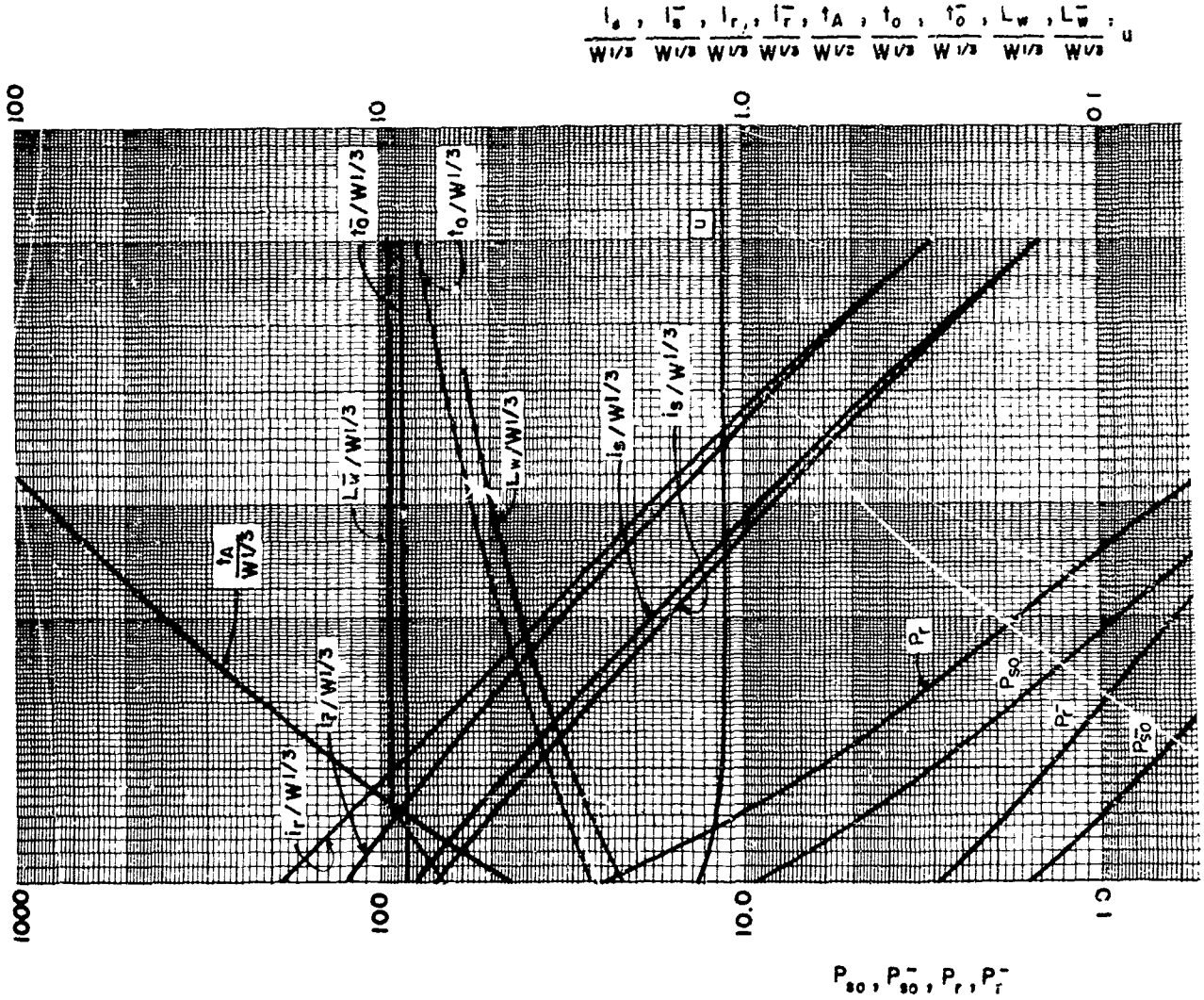

Fig A.2 Shock-wave parameters for hemispherical TNT surface explosion at sea-level - US U

P_{so} = Peak Positive Incident Pressure, psi

P_{so} = Peak Negative Incident Pressure, psi

P_r = Peak Positive Normal Reflected Pressure, psi

P_r^- = Peak Negative Normal Reflected Pressure, psi

$i_s/W^{1/3}$ = Scaled Unit Positive Incident Impulse, psi-ms/lb$^{1/3}$

$i_s^-/W^{1/3}$ = Scaled Unit Negative Incident Impulse, psi-ms/lb$^{1/3}$

$i_r/W^{1/3}$ = Scaled Unit Positive Normal Reflected Impulse, psi-ms/lb$^{1/3}$

$i_r^-/W^{1/3}$ = Scaled Unit Negative Normal Reflected Impulse, psi-ms/lb$^{1/3}$

$t_A/W^{1/3}$ = Scaled Time of Arrival of Blast Wave, ms/lb$^{1/3}$

$t_o/W^{1/3}$ = Scaled Positive Duration of Positive Phase, ms/lb$^{1/3}$

$t_o^-/W^{1/3}$ = Scaled Negative Duration of Positive Phase, ms/lb$^{1/3}$

$L_s/W^{1/3}$ = Scaled Wave Length of Positive Phase, ft/lb$^{1/3}$

$L_s^-/W^{1/3}$ = Scaled Wave Length of Negative Phase, ft/lb$^{1/3}$

U = Shock Front Velocity, ft/ms

u = Particle Velocity, ft/ms

W = Charge Weight, lbs

R = Radial Distance from Charge, ft

Z = Scaled Distance, ft/lb$^{1/3}$

S Units

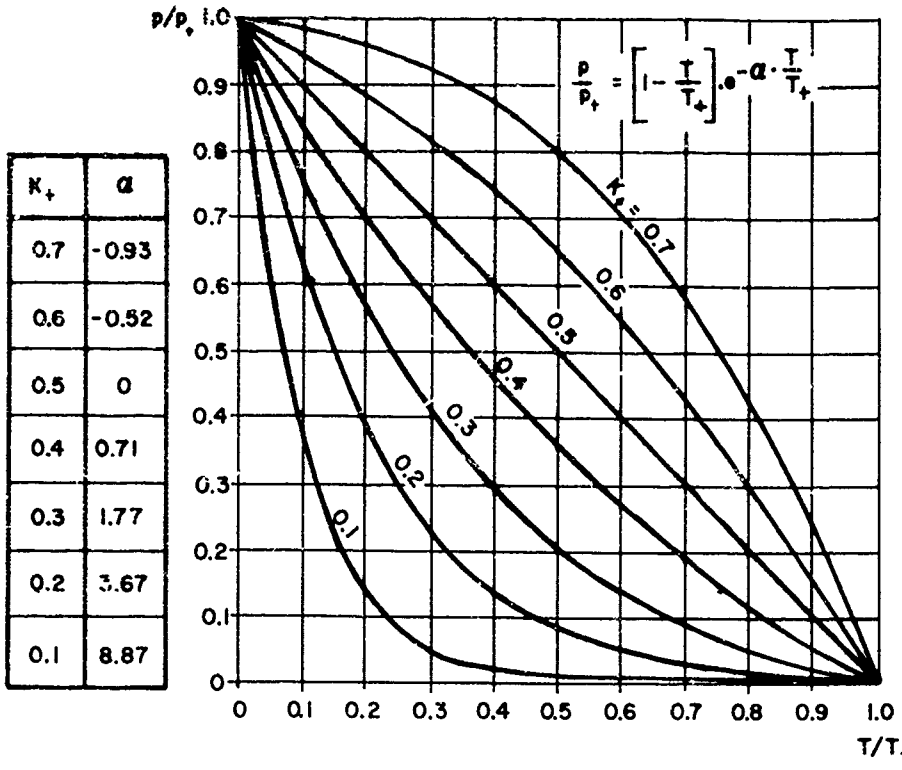

K_+	α
0.7	-0.93
0.6	-0.52
0.5	0
0.4	0.71
0.3	1.77
0.2	3.67
0.1	8.87

a) SUGGESTED p-T CURVES: POSITIVE PRESSURE PHASE

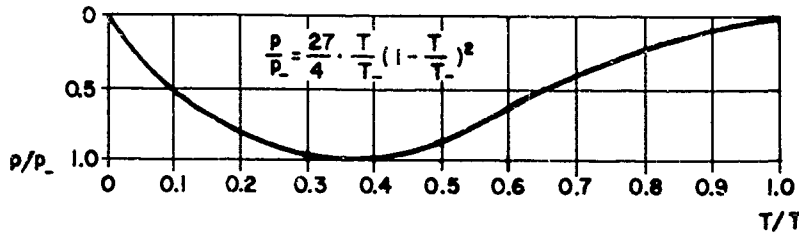

b) SUGGESTED p-T CURVE: NEGATIVE PRESSURE PHASE

Fig A.3 Suggested pressure versus time (P-t) curves

APPENDIX B

ENGINEERING DRAWINGS

APPENDIX B

ENGINEERING DRAWINGS

The following pages contain reduced-size copies of the Engineering Drawings prepared for the construction of the test structure and support framework for the instrumentation used in the dynamic tests. Drawing No. 131, Sheets Nos. 1 and 2, pertain to the structure modifications, while Drawing No. 131, Sheets Nos. 3 and 4, pertain to the type of instrumentation and supports.

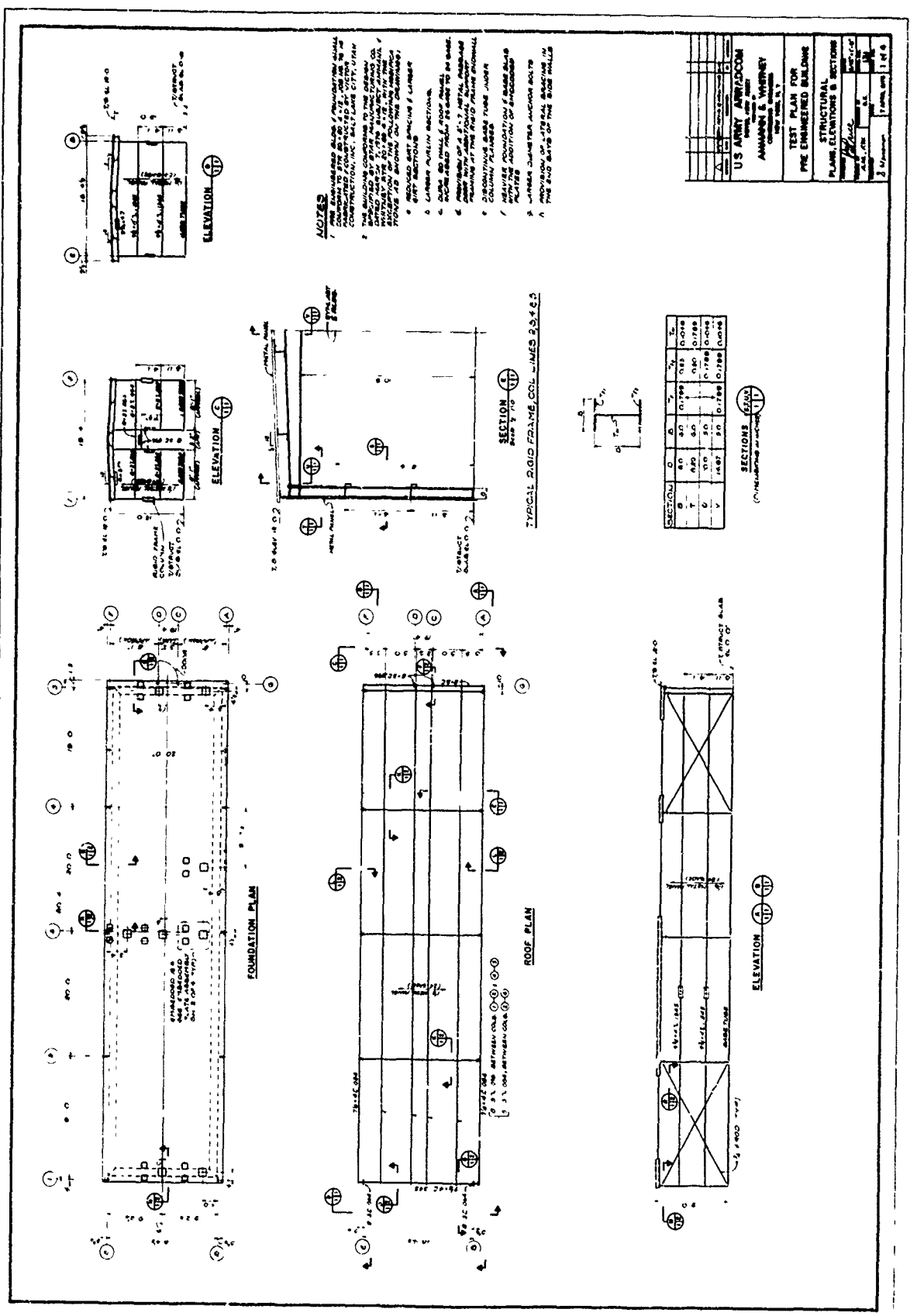

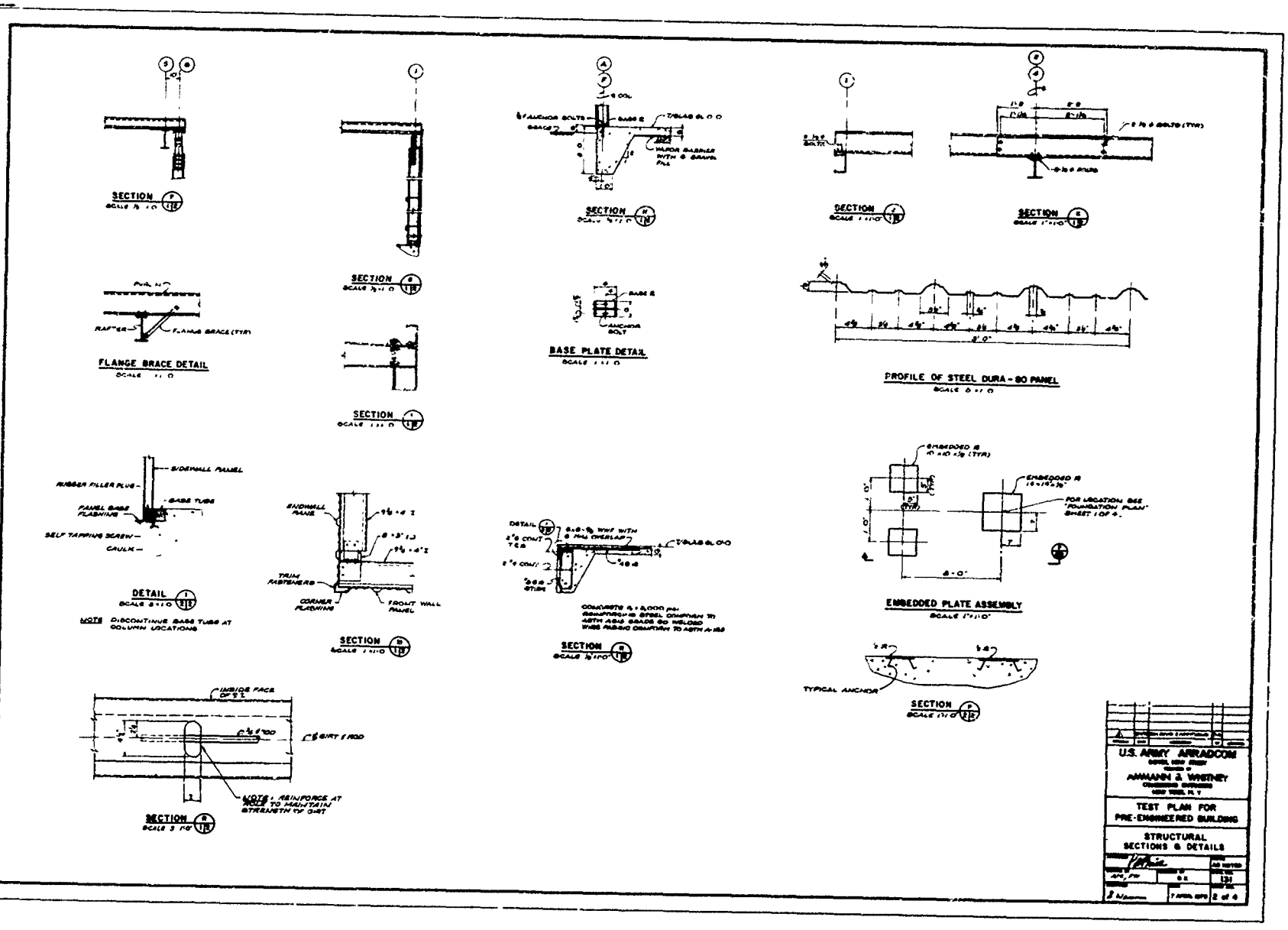

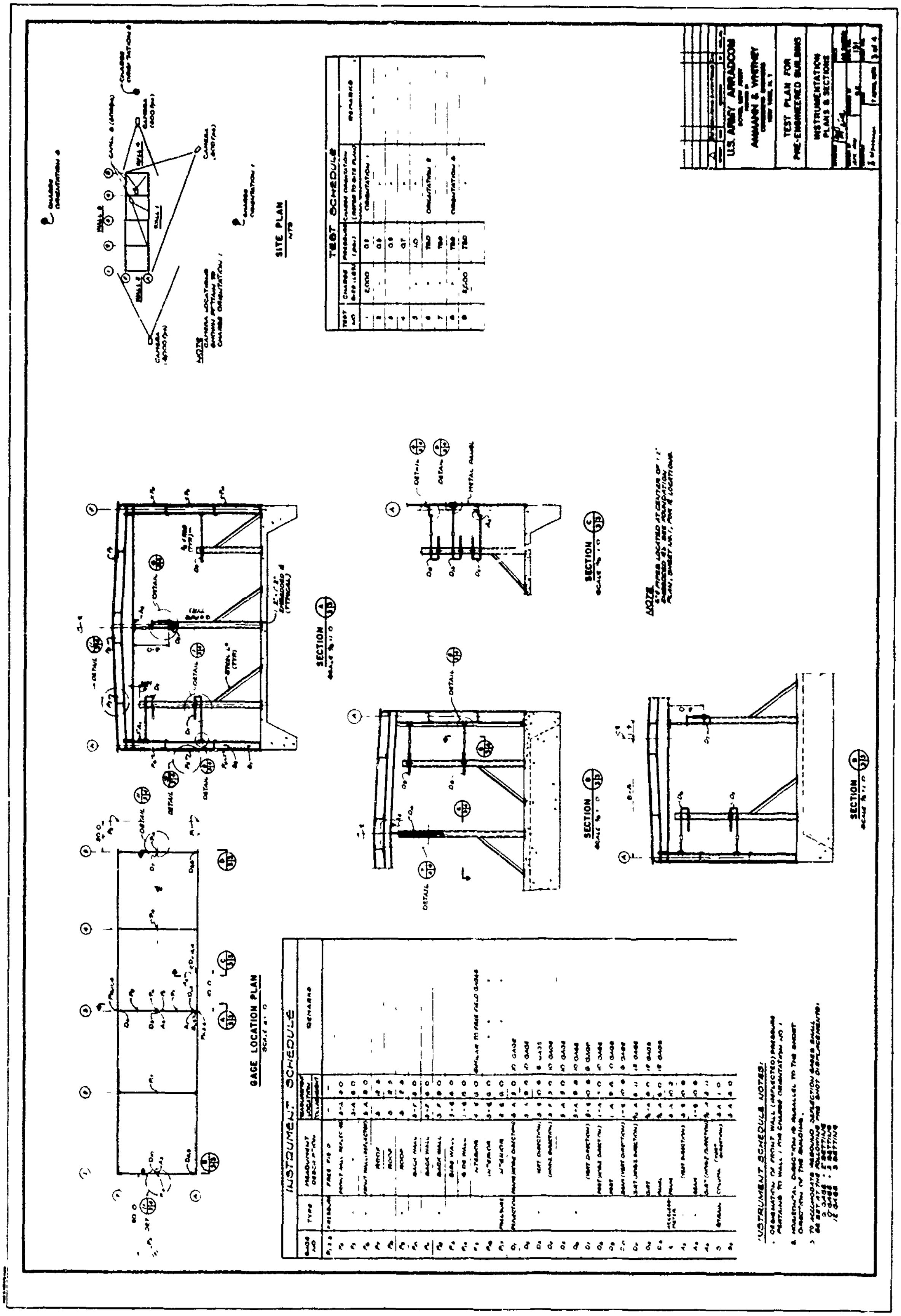

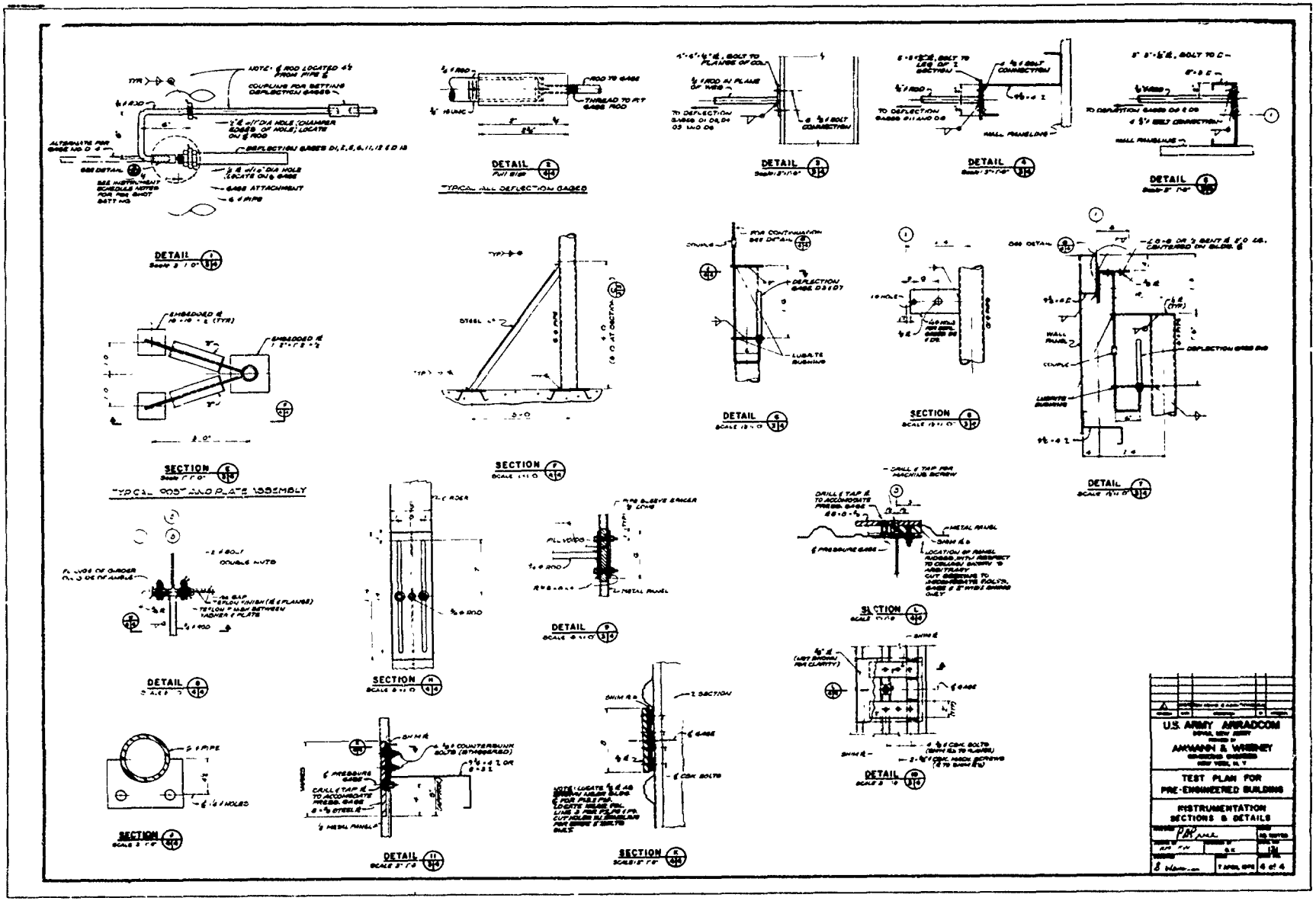

DISTRIBUTION LIST

Commander
U.S. Army Armament Research and
Development Command
ATTN: DRDAR-CG
DRDAR-LCM-E
DRDAR-LCM-S (25)
DRDAR-SF
DRDAR-TSS (5)
Dover, NJ 07801

Chairman
Dept of Defense Explosive Safety Board (2)
Room 856C, Hoffman Building I
2461 Eisenhower Avenue
Alexandria, VA 22331

Administrator
Defense Documentation Center
ATTN: Accessions Division (12)
Cameron Station
Alexandria, VA 22314

Commander
Department of the Army
Office, Chief of Research, Development
and Acquisition
ATTN: DAMA-CSM-P
Washington, DC 20310

Office, Chief of Engineers
ATTN: DAEN-MCZ
Washington, DC 20314

Commander
U.S. Army Materiel Development
and Readiness Command
ATTN: DRCSF
DRCDE
DRCRP
DRCIS
5001 Eisenhower Avenue
Alexandria, VA 22333

Commander
DARCOM Installations and Services Agency
ATTN: DRCIS-RI
Rock Island, IL 61299

Director
Industrial Base Engineering Activity
ATTN: DRXIB-MT and EN
Rock Island, IL 61299

Commander
U.S. Army Materiel Development
and Readiness Command
ATTN: DRCPM-PBM
DRCPM-PBM-T
DRCPM-PBM-L (2)
DRCPM-PBM-E (2)
DRCPM-PBM-LN-CE
Dover, NJ 07801

Commander
U.S. Army Armament Materiel
Readiness Command
ATTN: DRSAR-SF (3)
DRSAR-SC
DRSAR-EN
DRSAR-IRC
DRSAR-RD
DRSAR-IS
DRSAR-ASF
DRSAR-LEP-L
Rock Island, IL 61299

Director
DARCOM Field Safety Activity
ATTN: DRXOS-ES (2)
Charlestown, IN 47111

Commander
Volunteer Army Ammunition Plant
Chattanooga, TN 37401

Commander
Kansas Army Ammunition Plant
Parsons, KS 67357

Commander
Newport Army Ammunition Plant
Newport, IN 47966

Commander
Badger Army Ammunition Plant
Baraboo, WI 53913

Commander
Indiana Army Ammunition Plant
Charlestown, IN 47111

Commander
Holston Army Ammunition Plant
Kingsport, TN 37660

Commander
Lone Star Army Ammunition Plant
Texarkana, TX 75501

Commander
Milan Army Ammunition Plant
Milan, TN 38358

Commander
Iowa Army Ammunition Plant
Middletown, IA 52638

Commander
Joliet Army Ammunition Plant
Joliet, IL 60436

Commander
Longhorn Army Ammunition Plant
Marshall, TX 75760

Commander
Louisiana Army Ammunition Plant
Schreveport, LA 71130

Commander
Ravenna Army Ammunition Plant
Ravenna, OH 44266

Commander
Newport Army Ammunition Plant
Newport, IN 47966

Commander
Radford Army Ammunition Plant
Radford, VA 24141

Division Engineer
U.S. Army Engineer Division, Huntsville
ATTN: HNDCD
PO Box 1600, West Station
Huntsville, AL 35809

Division Engineer
U.S. Army Engineer Division, Southwestern
ATTN: SWDCD
1200 Main Street
Dallas, TX 75202

Division Engineer
U.S. Army Engineer Division, Missouri River
ATTN: MRDCD
PO Box 103,Downtown Station
Omaha, NE 68101

Division Engineer
U.S. Army Engineer Division, North Atlantic
ATTN: NADCD
90 Church Street
New York, NY 10007

Division Engineer
U.S. Army Engineer Division, South Atlantic
30 Pryor Street, S.W.
Atlanta, GA 30303

District Engineer
U.S. Army Engineer District, Norfolk
803 Front Street
Norfolk, VA 23510

District Engineer
U.S. Army Engineer District, Baltimore
PO Box 1715
Baltimore, MD 21203

District Engineer
U.S. Army Engineer District, Omaha
215 N. 17th Street
Omaha, NE 68102

District Engineer
U.S. Army Engineer District, Philadelphia
Custom House
2nd and Chestnut Street
Philadelphia, PA 19106

District Engineer
U.S. Army Engineer District, Fort Worth
PO Box 17300
Fort Worth, TX 76102

District Engineer
U.S. Army Engineer District, Kansas
601 E. 12th Street
Kansas City, MO 64106

District Engineer
U.S. Army Engineer District, Sacramento
650 Capitol Mall
Sacramento, CA 95814

District Engineer
U.S. Army Engineer District, Mobile
PO Box 2288
Mobile, AL 36628

Commander
U.S. Army Construction Engineering
Research Laboratory
Champaign, IL 61820

Commander
Dugway Proving Ground
ATTN: STEDP-MT-DA-HD (2)
Dugway, UT 84022

Civil Engineering Laboratory
Naval Construction Battalion Center
ATTN: L51
Port Hueneme, CA 93043

Commander
Naval Facilities Engineering Command
(Code 04, J. Tyrell)
200 Stovall Street
Alexandria, VA 22322

Commander
Atlantic Division
Naval Facilities Engineering Command
Norfolk, VA 23511

Commander
Chesapeake Division
Naval Facilities Engineering Command
Building S7
Washington Navy Yard
Washington, DC 20374

Commander
Northern Division
Naval Facilities Engineering Command
Building 77-L
U.S. Naval Base
Philadelphia, PA 19112

Commander
Southern Division
Naval Facilities Engineering Command
ATTN: J. Watts
PO Box 10068
Charleston, SC 29411

Commander
Western Division
Naval Facilities Engineering Command
ATTN: W. Moore
San Bruno, CA 94066

Commander
Naval Ammunition Depot
Naval Ammunition Production
Engineering Center
Crane, IN 47522

Technical Library
ATTN: DRDAR-CLJ-L
Aberdeen Proving Ground, MD 21005

Technical Library
ATTN: DRDAR-TSB-S
Aberdeen Proving Ground, MD 21010

Technical Library
ATTN: DRDAR-LCB-TL
Benet Weapons Laboratory
Watervliet, NY 12189

Ammann and Whitney (10)
2 World Trade Center
New York, NY 10048

Weapon System Concept Team/CSL
ATTN: DRDAR-ACW
Aberdeen Proving Ground, MD 21010

U.S. Army Materiel Systems Analysis Activity
ATTN: DRXSY-MP
Aberdeen Proving Ground, MD 21005